1.

Solar Energy System Design

The largest solar electric generating plant in the world produces a maximum of 354 megawatts (MW) of electricity and is located at Kramer Junction, California. This solar energy generating facility, shown below, produces electricity for the Southern California Edison power grid supplying the greater Los Angeles area. The authors' goal is to provide the necessary information to design such systems.

The solar collectors concentrate sunlight to heat a heat transfer fluid to a high temperature. The hot heat transfer fluid is then used to generate steam that drives the power conversion subsystem, producing electricity. Thermal energy storage provides heat for operation during periods without adequate sunshine.

Figure 1.1 One of nine solar electric energy generating systems at Kramer Junction, California, with a total output of 354 MWe. (photo courtesy Kramer Junction Operating Company)

Another way to generate electricity from solar energy is to use photovoltaic cells; magic slivers of silicon that converts the solar energy falling on them directly into electricity. Large scale applications of photovoltaic for power generation, either on the rooftops of houses or in large fields connected to the utility grid are promising as well to provide clean, safe and strategically sound alternatives to current methods of electricity generation.

Figure 1.2 A 2-MW utility-scale photovoltaic power system co-located with a defunct nuclear power plant near Sacramento, California. (photo courtesy of DOE/NREL, Warren Gretz)

The following chapters examine basic principles underlying the design and operation of solar energy conversion systems such as shown in Figure 1.1 and 1.2. This includes collection of solar energy, either by a thermal or photovoltaic process, and integration with energy storage and thermal-to-electric energy conversion to meet a predefined load. Study of the interaction of these subsystems yields the important guidelines for the design of optimal solar energy systems. System design tools are provided to produce optimal sizing of both collector field and storage so that optimum system designs can be produced.

Since our emphasis is on the design of entire solar energy conversion systems rather than design of its individual components, both thermal and photovoltaic systems are included. This novel approach results from recognition of the commonality of most system design considerations for both types of solar energy systems. We will not dwell on the intricacies of individual component design, but

instead encourage the designer to take experimental (or predicted) component input/output information and incorporate this into an overall system design.

The system shown in Figure 1.1 employs parabolic trough line-focus collectors. We will cover this and other types of collectors for capturing the sun's energy including flat plate, parabolic dish, central receiver and photovoltaic collectors. The purpose of a solar collector is to intercept and convert a reasonably large fraction of the available solar radiation. For solar thermal systems this energy is converted into thermal energy at some desired temperature and then, maybe, into electricity.

For photovoltaic systems as shown in Figure 1.2, intercepted solar energy is converted directly into low voltage direct current electricity. The engineering tradeoff between cost and performance of the components necessary to perform these processes has led to a wide variety of collector and system designs. Reviews of solar collector designs representative of the different concepts that have been built and tested are presented here.

The following sections serve as an overview of the solar energy system design process. They follow in a general manner, the flow of logic leading from the basic solar resource to the definition of an operating solar energy conversion system that meets a specified demand for either thermal or electrical energy.

1.1 The Solar Energy Conversion System

There are many different types of solar energy systems that will convert the solar resource into a useful form of energy. A block diagram showing three of the most basic system types is shown as Figure 1.3. In the first diagram , the solar resource is captured and converted into heat which is then supplied to a demand for thermal energy (thermal load) such as house heating, hot water heating or heat for industrial processes. This type of system may or may not include thermal storage, and usually include an auxiliary source of energy so that the demand may be met during long periods with no sunshine.

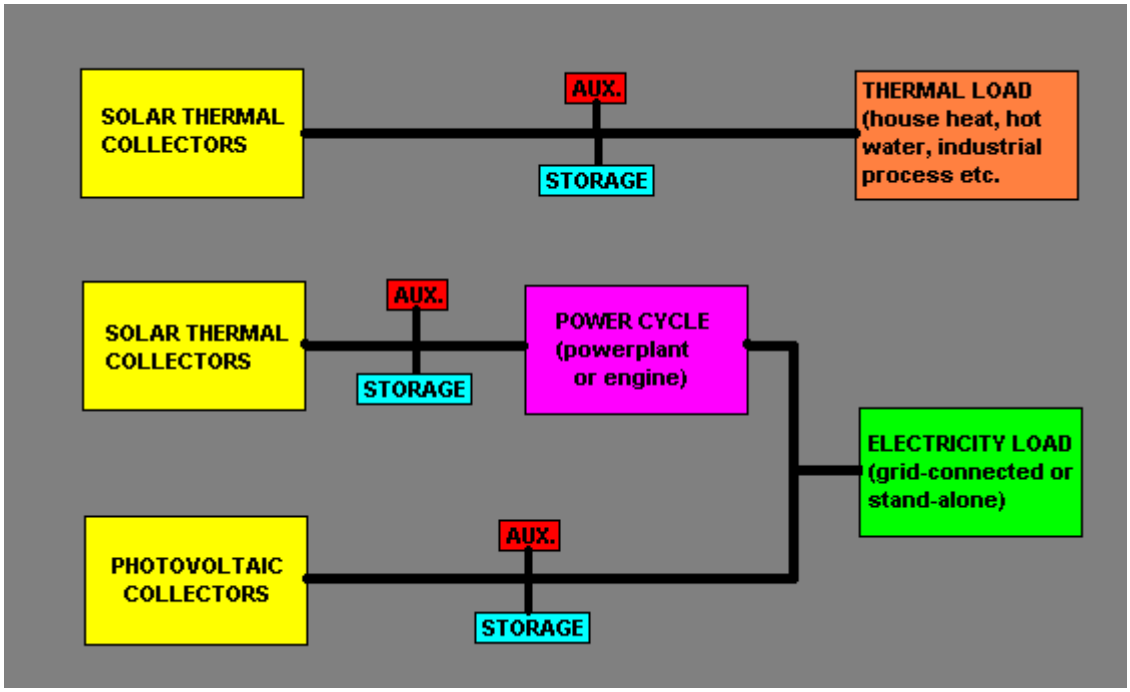

Figure 1.3 Diagram of a basic solar energy conversion systems. The AUX. box represents some auxiliary source of thermal or electrical energy.

If the demand (load) to be met is electricity (an electrical load) rather than heat, there are two common methods of converting solar energy into electricity. One method is by collecting solar energy as heat and converting it into electricity using a typical power plant or engine; the other method is by using photovoltaic cells to convert solar energy directly into electricity. Both methods are shown schematically in Figure 1.3.

In general, if solar energy conversion systems are connected to a large electrical transmission grid, no storage or auxiliary energy supply is needed. If the solar energy conversion system is to be the only source of electricity, storage and auxiliary energy supply are usually both incorporated. If the thermal route is chosen, storage of heat rather than electricity may be used to extend the operating time of the system. Auxiliary energy may either be supplied either as heat before the power conversion system, or as electricity after it. If the photovoltaic route is chosen, extra electricity may be stored, usually in storage batteries, thereby extending the operating time of the system. For auxiliary power, an external electricity source is the only choice for photovoltaic systems.

1.2 The Solar Resource

The basic resource for all solar energy systems is the sun. Knowledge of the quantity and quality of solar energy available at a specific location is of prime importance for the design of any solar energy system. Although the solar radiation (*insolation*) is relatively constant outside the earth's atmosphere, local climate influences can cause wide variations in available insolation on the earth's surface from site to site. In addition, the relative motion of the sun with respect to the earth will allow surfaces with different orientations to intercept different amounts of solar energy.

Figure 1.4 shows regions of high insolation where solar energy conversion systems will produce the maximum amount of energy from a specific collector field size. However, solar energy is available over the entire globe, and only the size of the collector field needs to be increased to provide the same amount of heat or electricity as in the shaded areas. It is the primary task of the solar energy system designer to determine the amount, quality and timing of the solar energy available at the site selected for installing a solar energy conversion system.

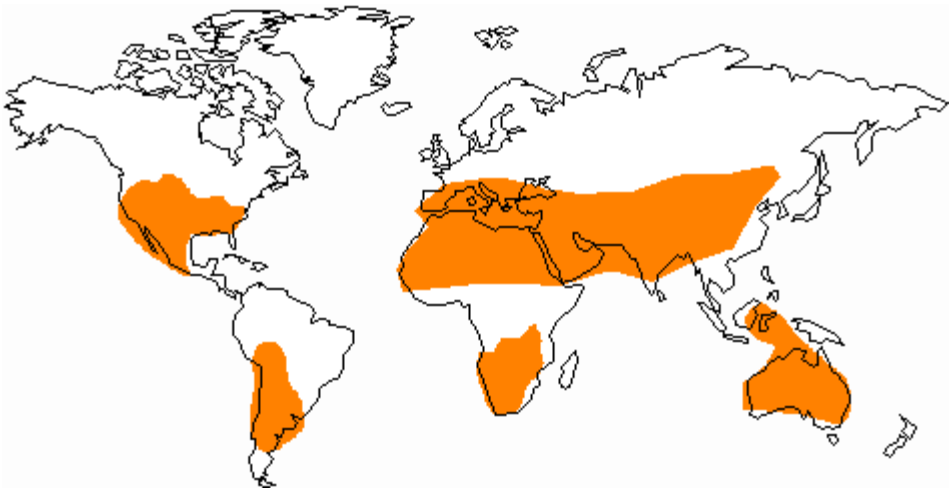

Figure 1.4 Areas of the world with high insolation.

Just outside the earth's atmosphere, the sun's energy is continuously available at the rate of 1,367 Watts on every square meter facing the sun. Due to the earth's rotation, asymmetric orbit about the sun, and the contents of its atmosphere, a large fraction of this energy does not reach the ground. In Chapter 2, we discuss the effects of the atmospheric processes that modify the incoming solar energy, how it is measured, and techniques used by designers to predict the amount of solar energy available at a particular location, both instantaneously and over a long term.

As an example of the importance of the material discussed in Chapter 2, Figure 1.5 shows the variation of insolation over a full, clear day in March at Daggett, California, a meteorological measurement site close to the Kramer Junction solar power plant described previously. The outer curve, representing the greatest rate of incident energy, shows the energy coming directly from the sun (*beam normal insolation*) and falling on a square meter of surface area which is pointed toward the sun. The peak rate of incident solar energy occurs around 12:00 noon and is 1,030 Watts per square meter. Over the full day, 10.6 kilowatt-hours of energy has fallen on every square meter of surface area as represented by the area under this curve.

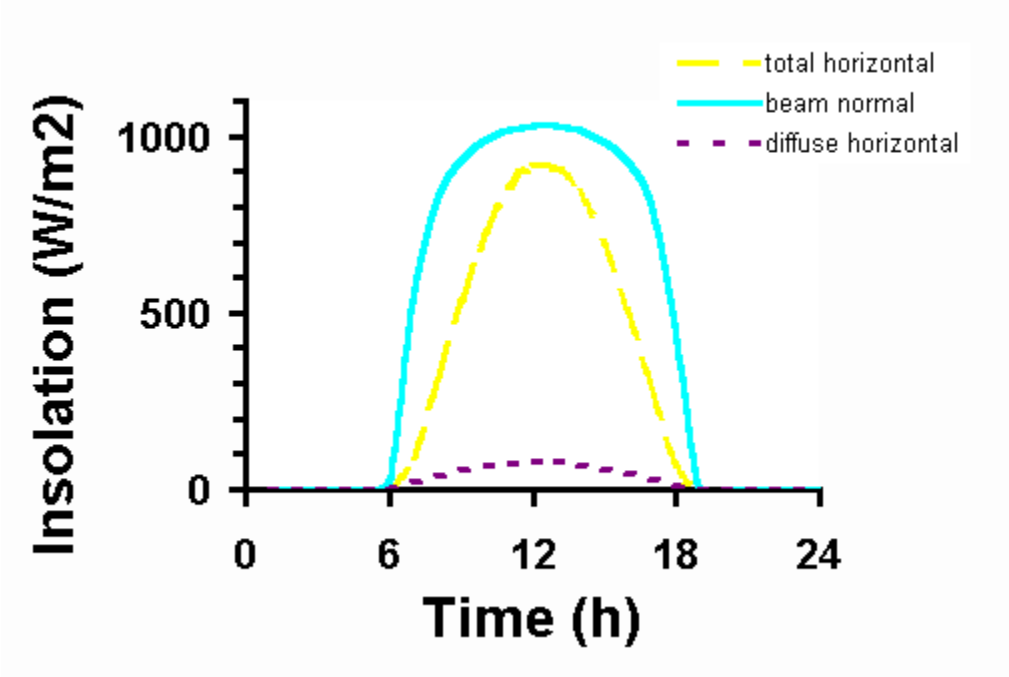

Figure 1.5 Insolation data from Daggett, California on a clear March day.

The middle curve represents the rate of solar energy falling on a horizontal surface at the same location. For reasons to be discussed later this curve includes both the energy coming directly from the sun's disc, and also that scattered by the molecules and particles in the atmosphere (*total horizontal insolation*). This scattered energy is shown as the bottom curve (*diffuse insolation*). Over the entire day, 6.7 kilowatt-hours of solar energy fall on every square meter of horizontal surface, of which 0.7 kilowatt-hours comes from all directions other than directly from the sun.

Techniques for estimating the temporal solar resource at any site on the face of the earth are presented in Chapter 2. In addition, the development and use of computerized meteorological data files is described. These data files based on long-term actual observations, form the time-dependent database of the

computerized performance computations contained within this book and, indeed, much of the solar literature.

An example of a complete set of beam normal insolation data for a given location is shown in Figure 1.6. Here we see hourly insolation data, summarized over a day, for each month of a year. With this type of data for a specific site, it is possible to predict accurately the output of a solar energy conversion system, whether it is a low temperature thermal system, a high temperature thermal system or a photovoltaic system.

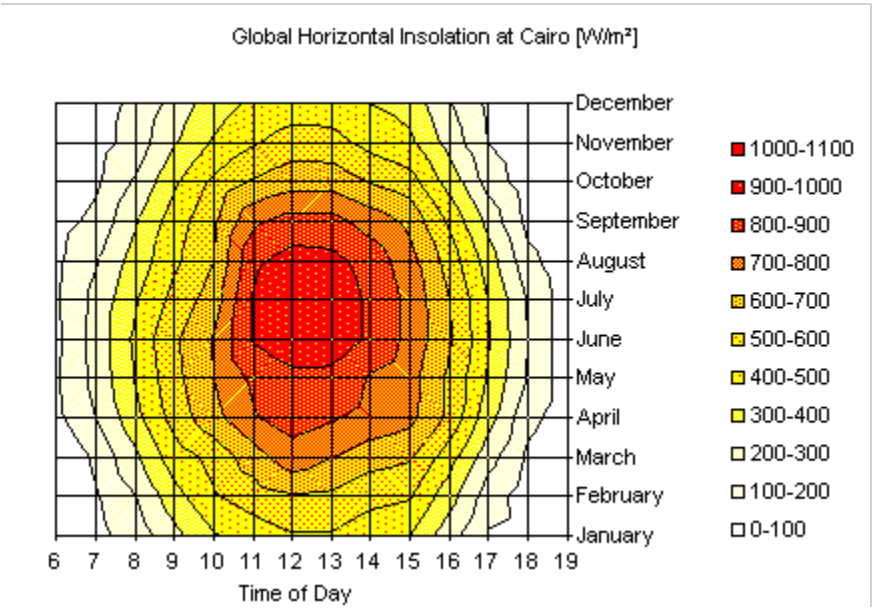

Figure 1.6 Time and date description of the global, horizontal insolation solar resource for Cairo Egypt.

In addition to estimating the amount of energy coming from the sun, the solar designer must also be able to predict the position of the sun. The sun's position must be known to predict the amount of energy falling on tilted surfaces, and to determine the direction toward which a tracking mechanism must point a collector. Chapter 3 discusses the computation of the position of the sun with respect to any given point on the face of the earth. Using only four parameters (latitude, longitude, date and local time), equations are derived to determine the location of the sun in the sky.

A characteristic fundamental to the capture of solar energy is that the amount of energy incident on a collector is reduced by a fraction equal to the cosine of the angle between the collector surface and the sun's rays. Knowing the position of the collector (or any other surface for that matter) and the position of the sun equations in Chapter 3 may be used to predict the fraction of incoming solar energy that falls on the collector. These include situations where the collector is fixed or is tracked about a single axis, no matter what the orientation.

1.3 Solar Collectors

The solar collector is the key element in a solar energy system. It is also the novel technology area that requires new understandings in order to make captured solar energy a viable energy source for the future.

The function of a solar collector is simple; it intercepts incoming insolation and changes it into a useable form of energy that can be applied to meet a specific demand. In the following text, we will develop analytical understandings of flat-plate and concentrating collectors, as used to provide heat or electricity. Each type is introduced below.

Flat-plate thermal solar collectors are the most commonly used type of solar collector. Their construction and operation are simple. A large plate of blackened material is oriented in such a manner that the solar energy that falls on the plate is absorbed and converted to thermal energy thereby heating the plate. Tubes or ducting are provided to remove heat from the plate, transferring it to a liquid or gas, and carrying it away to the load. One (or more) transparent (glass or plastic) plates are often placed in front of the absorber plate to reduce heat loss to the atmosphere. Likewise, opaque insulation is placed around the backside of the absorber plate for the same purpose. Operating temperatures up to 125^{o}C are typical.

Flat plate collectors have the advantage of absorbing not only the energy coming directly from the disc of the sun (beam normal insolation) but also the solar energy that has been diffused into the sky and that is reflected from the ground. Flat plate thermal collectors are seldom tracked to follow the sun's daily path across the sky, however their fixed mounting usually provides a tilt toward the south to minimize the angle between the sun's rays and the surface at noontime. Tilting flat-plate collectors toward the south provides a higher rate of energy at noontime and more total energy over the entire day. Figure 1.7 shows an installation of flat-plate thermal collectors.

Figure 1.7 Flat-plate thermal solar collectors for providing hot water.(photo courtesy of DOE/NREL, Warren Gretz)

Flat-plate photovoltaic collectors contain an array of individual photovoltaic cells, connected in a series/parallel circuit, and encapsulated within a sandwich structure with the front surface being glass or plastic. Solar energy falls directly upon the photovoltaic cell front surface and produces a small direct current voltage, providing electrical energy to a load. Unlike thermal collectors however, the backside of the panel is not insulated. Photovoltaic panels need to loose as much heat as possible to the atmosphere to optimize their performance.

Like flat-plate thermal collectors, flat-plate photovoltaic collectors (panels) absorb both energy coming directly from the sun's disc, and diffuse and reflected energy coming from other directions. In general, flat-plate photovoltaic panels are mounted in a fixed position and tilted toward the south to optimize noontime and daily energy production. However, it is common to see flat-plate photovoltaic panels mounted on mechanisms that track the sun about one tilted axis, thereby increasing the daily output of the panels.

Figure 1.8 Flat-plate photovoltaic collector applications.(photos courtesy of DOE/NREL, Warren Gretz)

When higher temperatures are required, concentrating solar collectors are used. Solar energy falling on a large reflective surface is reflected onto a smaller area before it is converted into heat. This is done so that the surface absorbing the concentrated energy is smaller than the surface capturing the energy and therefore can attain higher temperatures before heat loss due to radiation and convection wastes the energy that has been collected. Most concentrating collectors can only concentrate the parallel insolation coming directly from the sun's disk (beam normal insolation), and must follow (track) the sun's path across the sky. Four types of solar concentrators are in common use; parabolic troughs (as used in the Kramer Junction, California solar energy electricity generating plant shown in Figure 1.1), parabolic dishes, central receivers and Fresnel lenses. Figure 1.9 shows these concepts schematically.

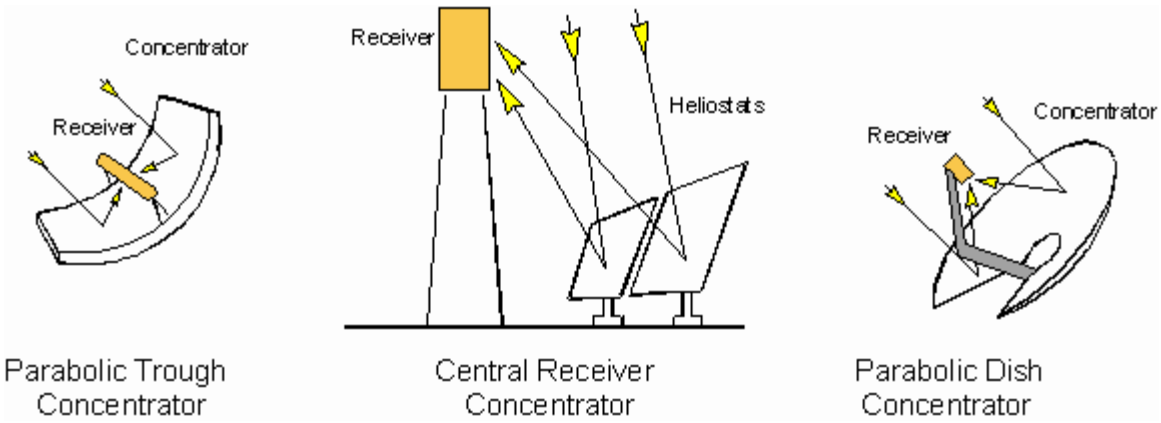

Figure 1.9 Three commonly used reflecting schemes for concentrating solar energy to attain high temperatures.

A parabolic trough concentrates incoming solar radiation onto a line running the length of the trough. A tube (receiver) carrying heat transfer fluid is placed along this line, absorbing concentrated solar radiation and heating the fluid inside. The trough must be tracked about one axis. Because the surface area of the receiver tube is small compared to the trough capture area (aperture), temperatures up to 400°C can be reached without major heat loss. Figure 1.10c shows one parabolic trough from the Kramer Junction, California field shown in Figure 1.1.

A parabolic dish concentrates the incoming solar radiation to a point. An insulated cavity containing tubes or some other heat transfer device is placed at this point absorbing the concentrated radiation and transferring it to a gas. Parabolic dishes must be tracked about two axes. Figure 1.10b shows six 9kWe parabolic dish concentrators with Stirling engines attached to the receiver at the focus.

A central receiver system consists of a large field of independently movable flat mirrors (heliostats) and a receiver located at the top of a tower. Each heliostat moves about two axes, throughout the day, to keep the sun's image reflected onto the receiver at the top of the tower. The receiver, typically a vertical bundle of tubes, is heated by the reflected insolation, thereby heating the heat transfer fluid passing through the tubes. Figure 1.10a shows the 10 MWe Solar One central receiver generating plant at Daggett, California with its adjoining steam power plant.

A Fresnel lens concentrator, such as shown in Figure 1.10d uses *refraction* rather than reflection to concentrate the solar energy incident on the lens surface to a point. Usually molded out of inexpensive plastic, these lenses are used in photovoltaic concentrators. Their use is not to increase the temperature, but to enable the use of smaller, higher efficiency photovoltaic cells. As with parabolic dishes, point-focus Fresnel lenses must track the sun about two axes.

Figure 1.10a A central receiver system. (courtesy of Sandia National Laboratories, Albuquerque)

Figure 1.10b Two-axis tracking parabolic dish collectors. (courtesy of Schlaich, Bergermann und Partner)

Figure 1.10c A single-axis tracking parabolic trough collector. (courtesy of Kramer Junction Operating Company)

Figure 1.10d A concentrating photovoltaic collector using Fresnel lenses. (courtesy of Amonix Corp.)

1.4 Need for Storage

Like with any other power plant, solar power plant *output* must satisfy the demands of the utility market. During peak demand periods, kilowatt-hour prices are high and financial incentives are high for guaranteed supply. Solar plant *input* is limited by diurnal, seasonal and weather-related insolation changes. In order to cope with these fluctuations, the solar plant input may be backed up by fossil fuels, or the solar changes may be mitigated by a buffering storage system. The choice depends on demands, system and site conditions, the relationship between storage capacity and collector area is discussed in Chapter 10.

In thermal solar power plants, thermal storage and/or fossil backup act as:

- an output management tool to prolong operation after sunset, to shift energy sales from low revenue off-peak hours to high revenue peak demand hours, and to contribute to guaranteed output

- An internal plant buffer, smoothing out insolation charges for steadying cycle operation, and for operational requirements such as blanketing steam production, component pre-heating and freeze protection.

Photovoltaic plants in general need no internal buffer, and output management can be achieved with battery or other electrochemical storage, pumped hydroelectric storage, or with diesel-generator backup. The implications of battery storage are discussed in Chapter 10.

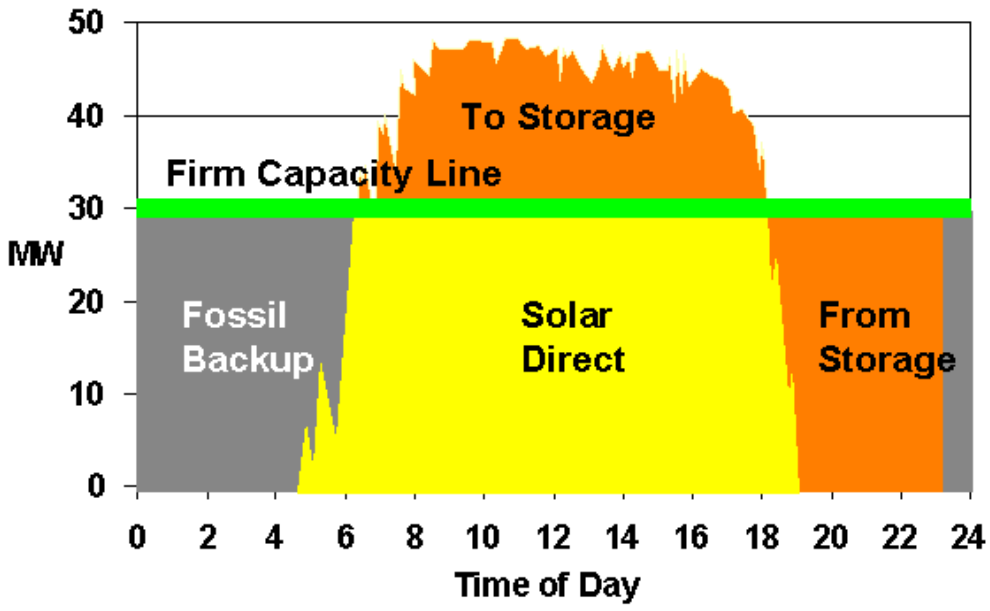

Figure 1.11 Stored solar energy provides a firm capacity of 31MW until midnight at which time fossil fuel backup us used.

1.5 Integration with Power Cycles

Because of their thermal nature, all the solar thermal technologies can be hybridized, or operated with fossil fuel as well as solar energy. Hybridization has the potential to increase the value of concentrating solar thermal technology by increasing its availability and dispatchability, decreasing its cost (by making more effective use of power generation equipment), and reducing technological risk by allowing conventional fuel use when needed.

Although an interconnected field of solar thermal collectors and thermal energy storage may be sufficient for providing high temperature heat directly to a thermal demand, a power generation subsystem must be incorporated into the system design if mechanical work or electrical power is to be an output from the system. Chapter 11 reviews the technology for power generation with particular emphasis on power generation units suitable for interfacing with solar thermal energy collection subsystems. The inclusion of power generation in a solar thermal energy design presents a challenge in selecting the appropriate design conditions. The efficiency of a power generation unit usually increases with the operating temperature of the power generation cycle, whereas the efficiency of solar collectors decreases with temperature. A tradeoff must be performed to determine the best system design point.

Figure 1.12 One of the steam cycle power cycles at the Kramer Junction solar energy generating system.(photo courtesy of DOE/NREL, Warren Gretz)

1.6 Site Qualification

Solar technologies using concentrating systems for electrical production require sufficient beam normal radiation, which is the beam radiation which comes from the sun and passes through the planet's atmosphere without deviation and refraction. Consequently, appropriate site locations are normally situated in arid to semi-arid regions. On a global scale, the solar resource in such regions is very high. More exactly, acceptable production costs of solar electricity typically occur where radiation levels exceed about 1,700 kWh/m²-yr, a radiation level found in many areas as illustrated in Figure 1.4. Appropriate regions include the southwest United States, northern Mexico, the north African desert, the Arabian peninsula, major portions of India, central and western Australia, the high plateaus of the Andean states, and northeastern Brazil. Promising site locations in Europe are found in southern Spain and several Mediterranean islands.

Figure 1.13 A View of Kuraymat (Egypt), the envisaged site for a solar thermal power plant in the Egyptian desert with cooling water from the Nile and connections to the national high voltage grid.

Solar electricity generation costs and feasibility of the project highly depend on the project site itself. A good site has to have a high annual beam insolation to obtain maximum solar electricity output. It must be reasonably flat to accommodate the solar field without prohibitive expensive earth works. It must also be close to the grid and a substation to avoid the need to build expensive electricity lines for evacuating the power. It needs sufficient water supply to cover the demand for cooling water of its steam cycle. A backup fuel must be available for granting firm power during the times when no solar energy is available. Access roads must be suitable for transporting the heavy equipment like turbine generators to the site. Skilled personnel must be available to construct and operate the plants. Chapter 13 reviews the criteria, methodology and examples of site selection and qualification for solar plants.

1.7 Economic and Environmental Considerations

The most important factor driving the solar energy system design process is whether the energy it produces is economical. Although there are factors other than economics that enter into a decision of when to use solar energy; i.e. no pollution, no greenhouse gas generation, security of the energy resource etc., design decisions are almost exclusively dominated by the 'levelized energy cost'. This or some similar economic parameter, gives the expected cost of the energy produced by the solar energy system, averaged over the lifetime of the system. In the following chapters, we will provide tools to aid in evaluating the factors that go into this calculation.

Commercial applications from a few kilowatts to hundreds of megawatts are now feasible, and plants totaling 354 MW have been in operation in California since the 1980s. Plants can function in dispatchable, grid-connected markets or in distributed, stand-alone applications. They are suitable for fossil-hybrid operation or can include cost-effective storage to meet dispatchability requirements. They can operate worldwide in regions having high beam-normal insolation, including large areas of the southwestern United States, and Central and South America, Africa, Australia, China, India, the Mediterranean region, and the Middle East, . Commercial solar plants have achieved levelized energy costs of about 12-15¢/kWh, and the potential for cost reduction are expected to ultimately lead to costs as low as 5¢/kWh.

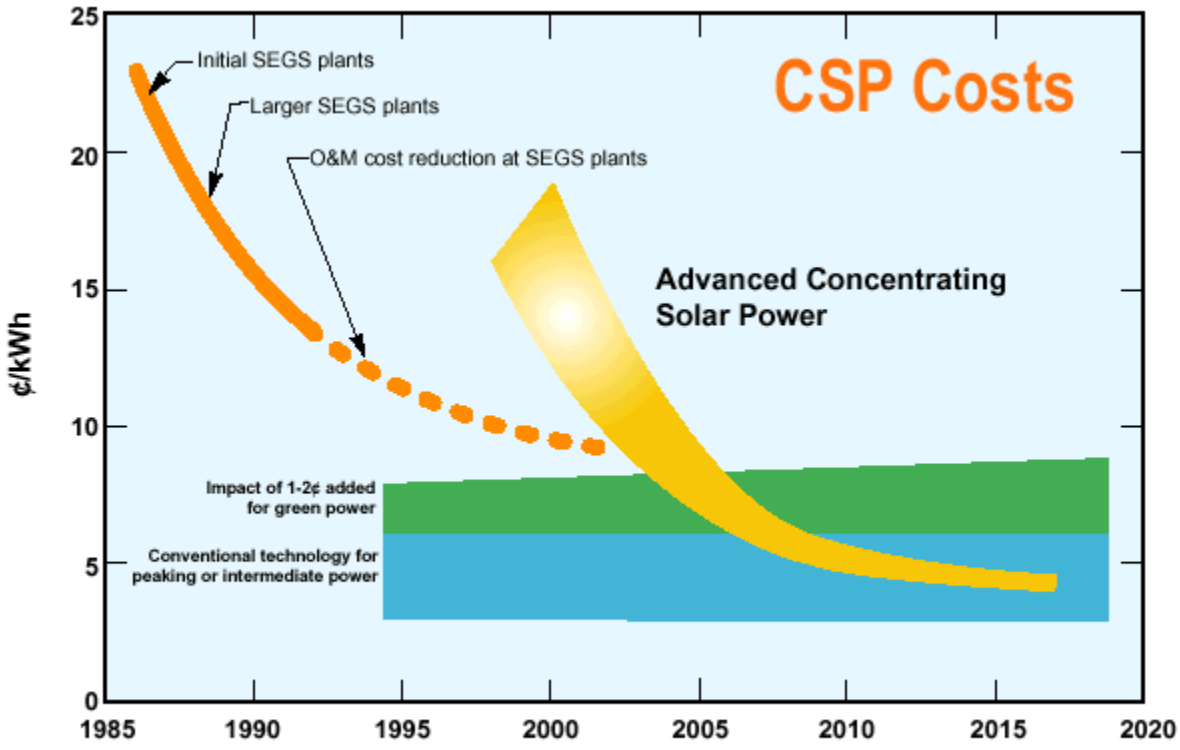

Figure 1.14 Projections of levelized electricity cost predictions for large scale solar thermal power plants. Current costs are shown in blue with a 1-2 cent/kWh addition for 'green' power shown in green.

1.8 Summary

The authors' overall objective is to illustrate the design of solar energy systems, both thermal and photovoltaic types. To do this, we examine the solar resource and the ability of various types of solar collectors to capture it effectively. Design tools are developed which integrate performance of isolated solar collectors, along with energy storage, into a larger system that delivers either electrical or thermal energy to a demand. We show as many examples as possible, both graphic and photographic of these systems and their components.

It is our hope that once the simplicity of solar energy system design is understood, engineers and manufacturers will provide new system designs that will expand the solar market worldwide and permit all to benefit from this clean, sustainable and distributed source of energy.

3. The Sun's Position

In order to understand how to collect energy from the sun, one must first be able to predict the location of the sun relative to the collection device. In this chapter we develop the necessary equations by use of a unique vector approach. This approach will be used in subsequent chapters to develop the equations for the sun's position relative to a fixed or tracking solar collector, (Chapter 4) and the special case of a sun-tracking mirror reflecting sunlight onto a fixed point (Chapter 10). Once developed, the sun position expressions of this chapter are used to demonstrate how to determine the location of shadows and the design of simple sundials. In outline form, our development looks like this:

- Earth-sun angles
  - Time
    - Standard time zones
    - Daylight savings time
    - Sidereal time
  - Hour angle 
    - Solar time
    - Equation of time
    - Time conversion
  - Declination angle 
  - Latitude angle 
- Observer-Sun Angles
  - Solar altitude, zenith and azimuth angles
  - Geometric view of sun's path
  - Daily and seasonal events
- Shadows and Sundials
  - Simple shadows
  - Sundials
- Notes on Transformation of Vector Coordinates
- Summary

Although many intermediate steps of derivation used to obtain the equations described in this chapter have been omitted, it is hoped that there are adequate comments between steps to encourage the student to perform the derivation, thereby enhancing understanding of the materials presented. Brief notes on the transformation of vector coordinates are included as Section 3.5 and a summary of sign conventions for all of the angles used in this chapter is given in Table 3.3 at the end of this chapter. Figures defining each angle and an equation to calculate it are also included.

One objective in writing this chapter has been to present adequate analytical expressions so that the solar designer is able to develop simple computer algorithms for predicting relative sun and collector positions for exact design conditions and locations. This will eliminate the need to depend on charts and tables and simplified equations.

3.1 Earth-Sun Angles

The earth revolves around the sun every 365.25 days in an elliptical orbit, with a mean earth-sun distance of 1.496 x 10^{11} m (92.9 x 10^{6} miles) defined as one astronomical unit (1 AU). This plane of this orbit is called the *ecliptic plane.* The earth's orbit reaches a maximum distance from the sun, or *aphelion, of* 1.52 $\times$ 10^{11} m (94.4 $\times$ 10^{6} miles) on about the third day of July. The minimum earth-sun distance, *the perihelion,* occurs on about January 2nd, when the earth is 1.47 $\times$ 10^{11} m (91.3 $\times$ 10^{6} miles) from the sun. Figure 3.1 depicts these variations in relation to the Northern Hemisphere seasons.

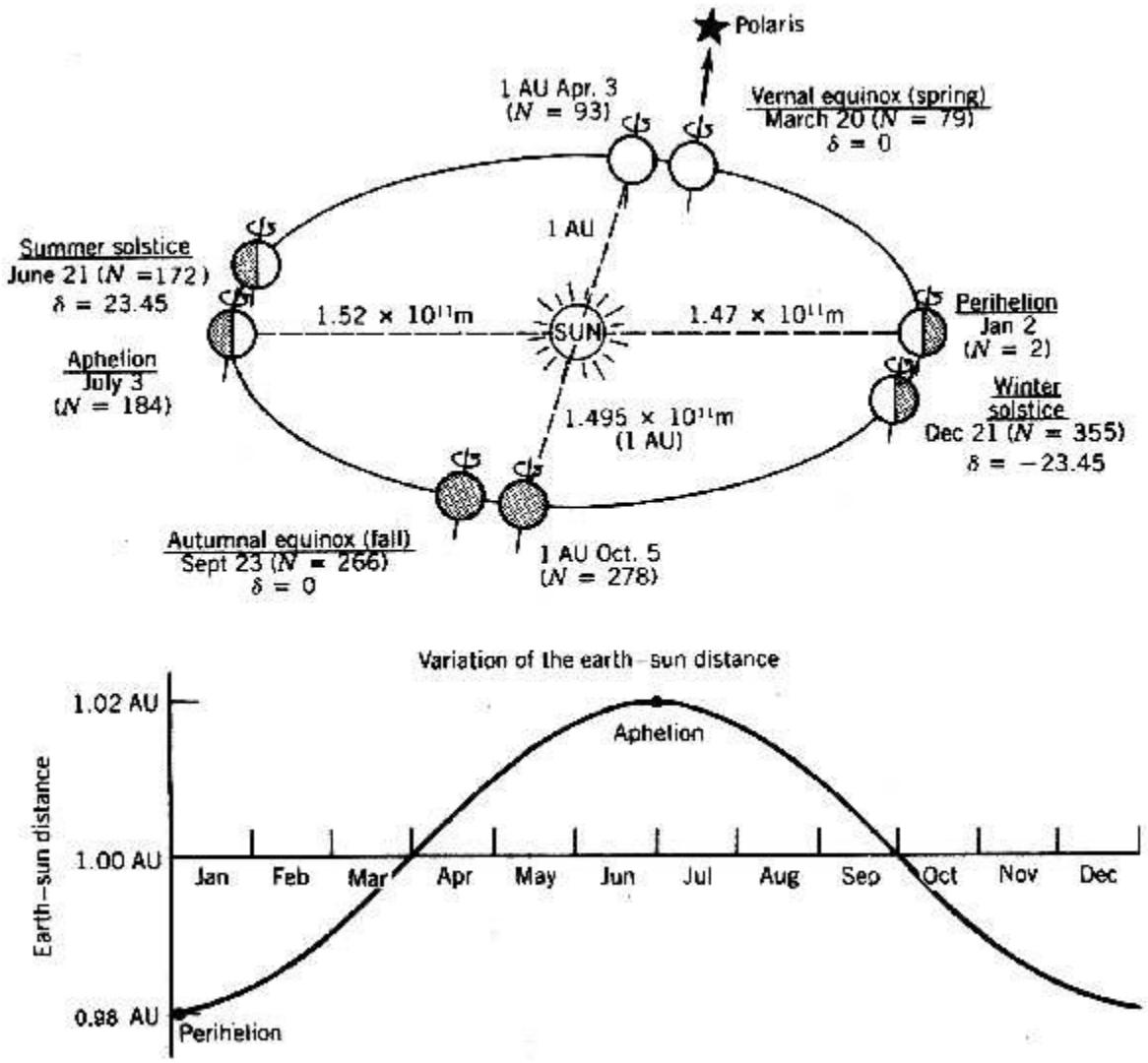

Figure 3.1 The ecliptic plane showing variations in the earth-sun distance and the equinoxes and solstices. The dates and day numbers shown are for 1981 and may vary by 1 or 2 days.

The earth rotates about its own polar axis, inclined to the ecliptic plane by 23.45 degrees, in approximately 24-hour cycles. The direction in which the polar axis points is fixed in space and is aligned with the North Star (Polaris) to within about 45 minutes of arc (13 mrad). The earth's rotation about its polar axis produces our days and nights; the tilt of this axis relative to the ecliptic plane produces our seasons as the earth revolves about the sun.

3.1.1 Time

We measure the passage of time by measuring the rotation of the earth about its axis. The base for time (and longitude) measurement is the meridian that passes through Greenwich, England and both poles. It is known as the *Prime Meridian.*

Today, the primary world time scale, *Universal Time* (previously called *Greenwich Mean Time*), is still measured at the Prime Meridian. This is a 24-hour time system, based on *mean time*, according to which the length of a day is 24 hours and midnight is 0 hours.

Mean time is based on the length of an average day. A mean second is l/86,400 of the average time between one complete transits of the sun, averaged over the entire year. In fact, the length of any one specific day, measured by the complete transit of the sun, can vary by up to 30 seconds during the year. The variable day length is due to four factors listed in order of decreasing importance (Jesperson and Fitz-Randolph, 1977):

- The earth's orbit around the sun is not a perfect circle but elliptical, so the earth travels faster when it is nearer the sun than when it is farther away.
- The earth's axis is tilted to the plane containing its orbit around the sun.
- The earth spins at an irregular rate around its axis of rotation.
- The earth `wobbles´ on its axis.

Standard Time Zones - Since it is conventional to have 12:00 noon be approximately in the middle of the day regardless of the longitude, a system of time zones has been developed. See (Blaise 2000) for an interesting story about how this unification developed. These are geographic regions, approximately 15 degrees of longitude wide, centered about a meridian along which local standard time equals mean solar time. Prior to about 1880, different cities (and even train stations) had their own time standards, most based on the sun being due south at 12:00 noon.

Time is now generally measured about *standard time zone meridians*. These meridians are located every 15 degrees from the Prime Meridian so that local time changes in 1-hour increments from one standard time zone meridian to the next. The standard time zone meridians east of Greenwich have times later than Greenwich time, and the meridians to the west have earlier times.

Ideally, the meridians 7 ½ degrees on either side of the standard time zone meridian should define the time zone. However, boundaries separating time zones are not meridians but politically determined borders following rivers, county, state or national boundaries, or just arbitrary paths. Countries such as Spain choose to be on `European Time (15° E) when their longitudes are well within the adjacent Standard Time Meridian (0°). Figure 3.2 shows these time zone boundaries within the United States and gives the standard time zone meridians (called *longitudes of solar time).*

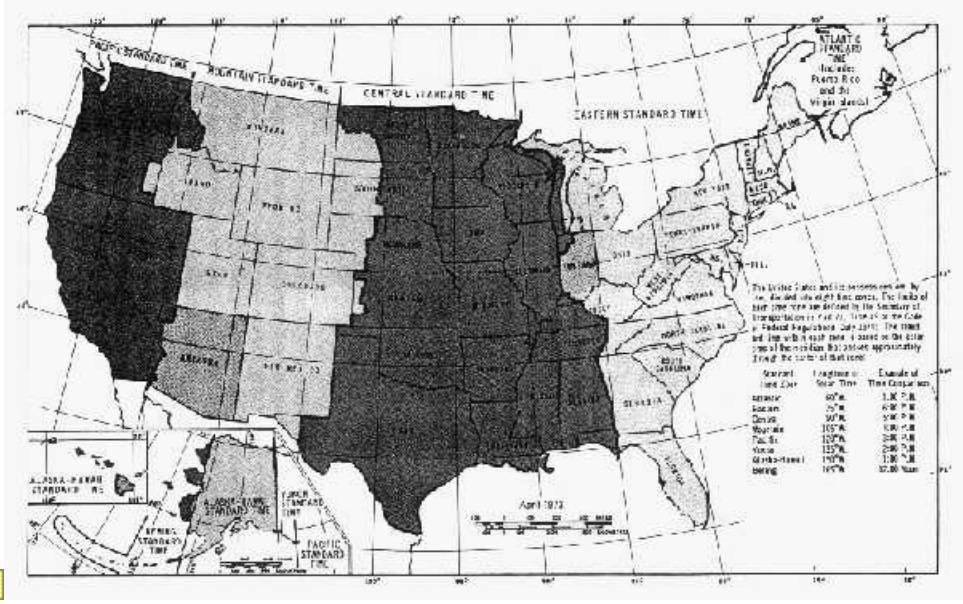

Figure 3.2 Time zone boundaries within the United States. From Jesperson and Fitz-Randolph 1977.

Daylight Savings Time -To complicate matters further in trying to correlate clock time with the movement of the sun, a concept known as *daylight savings time* was initiated in the United States in the spring of 1918 to "save fuel and promote other economies in a country at war" (Jesperson and Fitz-Randolph, 1977). According to this concept, the standard time is advanced by 1 hour, usually from 2:00 AM on the first Sunday in April until 2:00 AM on the last Sunday in October. Although various attempts have been made to apply this concept uniformly within the country, it is suggested that the designer check locally to ascertain the commitment to this concept at any specific solar site.

Sidereal Time - So far, and for the remainder of this text, all reference to time is to *mean time,* a time system based on the assumption that a day (86,400 seconds) is the average interval between two successive times when a given point on the earth faces the sun. In astronomy or orbital mechanics, however, the concept of *sidereal time* is often used. This time system is based on the sidereal day, which is the length of time for the earth to make one complete rotation about its axis.

The mean day is about 4 minutes longer than the sidereal day because the earth, during the time it is making one revolution about its axis, has moved some distance in its orbit around the sun. To be exact, the sidereal day contains 23 hours, 56 minutes, and 4.09053 seconds of mean time. Since, by definition, there are 86,400 sidereal seconds in a sidereal day, the sidereal second is slightly shorter than the mean solar second is. To be specific: *1 mean second = 1.002737909 sidereal seconds.* A detailed discussion of this and other time definitions is contained in another work (Anonymous, 1981, Section B).

3.1.2 The Hour Angle (ω)

To describe the earth's rotation about its polar axis, we use the concept of the *hour angle* (ω). As shown in Figure 3.3, the hour angle is the angular distance between the meridian of the observer and the meridian whose plane contains the sun. The hour angle is zero at *solar noon* (when the sun reaches its highest point in the sky). At this time the sun is said to be 'due south' (or 'due north', in the Southern Hemisphere) since the meridian plane of the observer contains the sun. The hour angle increases by 15 degrees every hour.

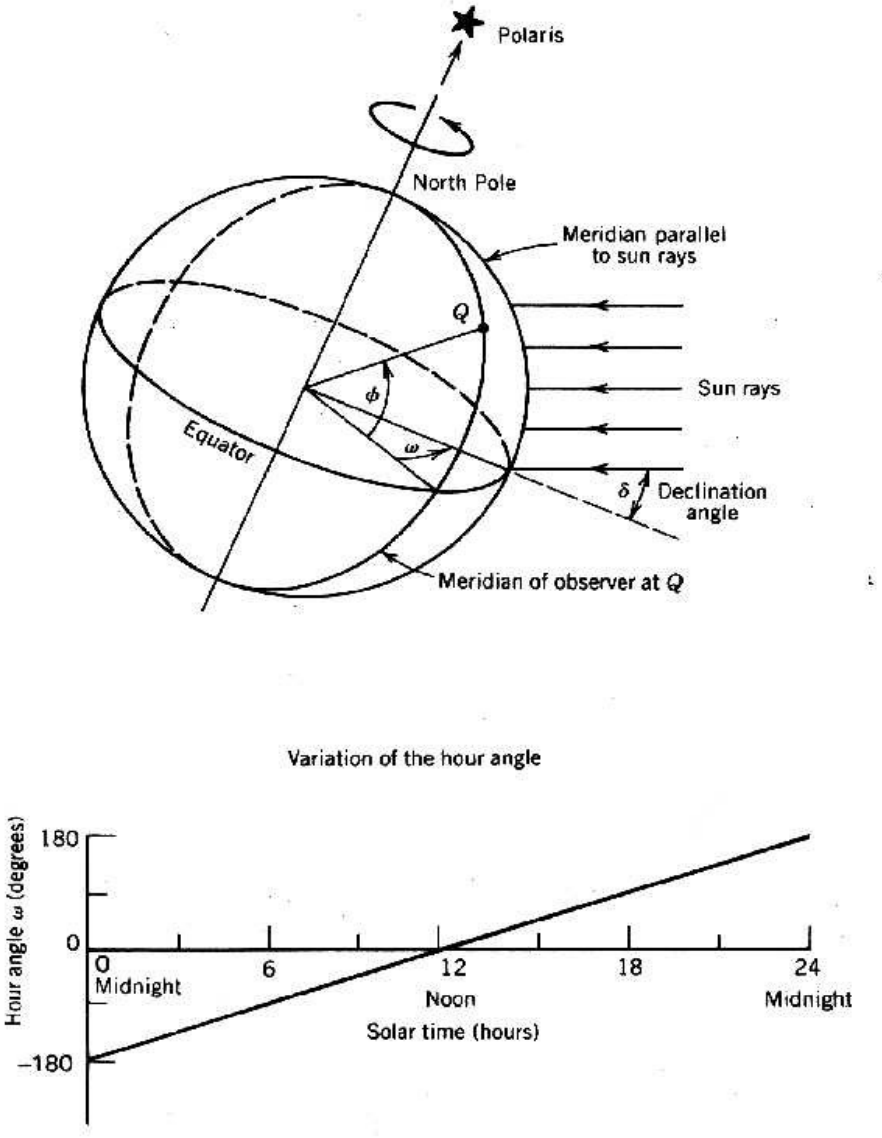

Figure 3.3 The hour angle (ω) This angle is defined as the angle between the meridian parallel to sun rays and the meridian containing the observer.

Solar Time - *Solar time* is based on the 24-hour clock, with 12:00 as the time that the sun is *exactly* due south. The concept of solar time is used in predicting the direction of sunrays relative to a point on the earth. Solar time is location (longitude) dependent and is generally different from local clock time, which is defined by politically defined time zones and other approximations.

Solar time is used extensively in this text to define the rotation of the earth relative to the sun. An expression to calculate the hour angle from solar time is

$$\omega = 15(t_s - 12) \qquad (\text{degrees}) \qquad (3.1)$$

where t_s is the solar time in hours.

EXAMPLE: When it is 3 hours after solar noon, solar time is 15:00 and the hour angle has a value of 45 degrees. When it is 2 hours and 20 minutes before solar noon, solar time is 9:40 and the hour angle is 325 degrees (or − 35 degrees).

The difference between solar time and local clock time can approach 2 hours at various locations and times in the United States, For most solar design purposes, clock time is of little concern, and it is appropriate to present data in terms of solar time. Some situations, however, such as energy demand correlations, system performance correlations, determination of true south, and tracking algorithms require an accurate knowledge of the difference between solar time and the local clock time.

Knowledge of solar time and Universal Time has traditionally been important to ship navigators. They would set their chronometers to an accurately adjusted tower clock visible as they left port. This was crucial for accurate navigation. At sea a ship's latitude could be easily ascertained by determining the maximum altitude angle of the sun or the altitude angle of Polaris at night. However, determining the ship's longitude was more difficult and required that an accurate clock be carried onboard. If the correct time at Greenwich, England (or any other known location) was known, then the longitude of the ship could be found by measuring the solar time onboard the ship (through sun sightings) and subtracting from it the time at Greenwich. Since the earth rotates through 360 degrees of longitude every 24 hours, the ship then has traveled 1 degree of longitude away from the Prime Meridian (which passes through Greenwich) for every 4 minutes of time difference. An interesting story about developing accurate longitude measurements may be found in Sobel, 1999.

Equation of Time - The difference between *mean solar time* and true solar time on a given date is shown in Figure 3.4. This difference is called the *equation of time* (EOT). Since solar time is based on the sun being due south at 12:00 noon on any specific day, the accumulated difference between mean solar time and true solar time can approach 17 minutes either ahead of or behind the mean, with an annual cycle.

The level of accuracy required in determining the equation of time will depend on whether the designer is doing system performance or developing tracking equations. An approximation for calculating the equation of time in minutes is given by Woolf (1968) and is accurate to within about 30 seconds during daylight hours.

$$EOT = 0.258\cos x - 7.416\sin x - 3.648\cos 2x - 9.228\sin 2x \qquad \text{(minutes)} \quad (3.2)$$

where the angle x is defined as a function of the day number N

$$x \equiv \frac{360(N-1)}{365.242} \qquad \text{(degrees)} \qquad (3.3)$$

with the day number, N being the number of days since January 1. Table 3.1 has been prepared as an aid in rapid determination of values of N from calendar dates.

Table 3.1 Date-to-Day Number Conversion

Month	**Day Number, N**	**Notes**
January	d	
February	d + 31	
March	d + 59	Add 1 if leap year
April	d + 90	Add 1 if leap year
May	d + 120	Add 1 if leap year
June	d + 151	Add 1 if leap year
July	d + 181	Add 1 if leap year
August	d + 212	Add 1 if leap year
September	d + 243	Add 1 if leap year
October	d + 273	Add 1 if leap year
November	d + 304	Add 1 if leap year
December	d + 334	Add 1 if leap year
Days of Special Solar Interest		
Solar Event	**Date**	**Day Number, N**
Vernal equinox	March 21	80
Summer solstice	June 21	172
Autumnal equinox	September 23	266
Winter solstice	December 21	355
NOTES:		

1. d is the day of the month
2. Leap years are 2000, 2004, 2008 etc.

3. Solstice and equinox dates may vary by a day or two. Also, add 1 to the solstice and equinox day number for leap years.

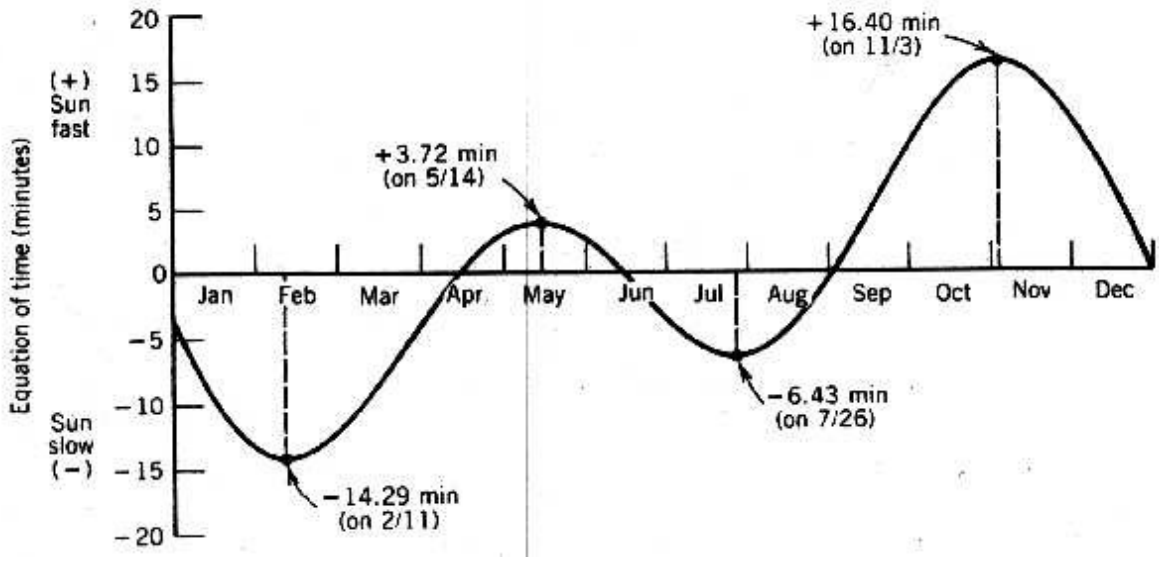

Figure 3.4 The equation of time (*EOT*). This is the difference between the local apparent solar time and the local mean solar time.

EXAMPLE: February 11 is the 42nd day of the year, therefore N = 42 and x is equal to 40.41 degrees, and the equation of time as calculated above is ≈ 14.35 minutes. This compares with a very accurately calculated value of -14.29 minutes reported elsewhere (Anonymous, 198l). This means that on this date, there is a difference between the mean time and the solar time of a little over 14 minutes or that the sun is "slow" relative to the clock by that amount.

To satisfy the control needs of concentrating collectors, a more accurate determination of the hour angle is often needed. An approximation of the equation of time claimed to have an average error of 0.63 seconds and a maximum absolute error of 2.0 seconds is presented below as Equation (3.4) taken from Lamm (1981). The resulting value is in minutes and is positive when the apparent solar time is ahead of mean solar time and negative when the apparent solar time is behind the mean solar time:

$$EOT = 60\sum_{k=0}^{5}\left[A_k \cos\left(\frac{360kn}{365.25}\right) + B_k \sin\left(\frac{360kn}{365.25}\right)\right] \qquad (\text{minutes})$$

(3.4)

Here n *is* the number of days into a leap year cycle with n = 1 being January 1 of each leap year, and n =1461 corresponding to December 31 of the 4th year of the leap year cycle. The coefficients A_k and B_k are given in Table 3.2 below. Arguments for the cosine and sine functions are in degrees.

Table 3.2 Coefficients for Equation (3.4)

k	A_k **(hr)**	B_k **(hr)**
0	2.0870×10^{-4}	0
1	9.2869×10^{-3}	-1.2229×10^{-1}
2	-5.2258×10^{-2}	-1.5698×10^{-1}
3	-1.3077×10^{-3}	-5.1602×10^{-3}
4	-2.1867×10^{-3}	-2.9823×10^{-3}
5	-1.5100×10^{-4}	-2.3463×10^{-4}

Time Conversion - The conversion between solar time and clock time requires knowledge of the location, the day of the year, and the local standards to which local clocks are set. Conversion between solar time, t_s and local clock time *(LCT)* (in 24-hour rather than AM/ PM format) takes the form

$$LCT = t_s - \frac{EOT}{60} + LC + D \qquad (\text{hours}) \qquad (3.5)$$

where EOT is the equation of time in minutes and LC is a longitude correction defined as follows:

$$LC = \frac{(local\ longitude) - \begin{pmatrix} longitude\ of\ standard \\ time\ zone\ meridian \end{pmatrix}}{15} \qquad (\text{hours}) \qquad (3.6)$$

and the parameter *D* in Equation (3.5) is equal to 1 (hour) if the location is in a region where daylight savings time is currently in effect, or zero otherwise.

EXAMPLE: Let us find the clock time for solar noon at a location in Los Angeles, having a longitude of 118.3 degrees on February 11. Since Los Angeles is on Pacific Standard Time and not on daylight savings time on this date, the local clock time will be:

$$LCT = 12.00 - \frac{-14.29}{60} + \frac{118.3 - 120}{15} = 12:07:29$$

3.1.3 The Declination Angle (δ)

The plane that includes the earth's equator is called the *equatorial plane.* If a line is drawn between the center of the earth and the sun, the angle between this line and the earth's equatorial plane is called the *declination angle* (δ), as depicted in Figure 3.5. At the time of year when the northern part of the earth's rotational axis is inclined toward the sun, the earth's equatorial plane is inclined 23.45 degrees to the earth-sun line. At this time (about June 21), we observe that the noontime sun is at its highest point in the sky and the declination angle δ = +23.45 degrees. We call this condition the *summer solstice,* and it marks the beginning of summer in the Northern Hemisphere.

As the earth continues its yearly orbit about the sun, a point is reached about 3 months later where a line from the earth to the sun lies on the equatorial plane. At this point an observer on the equator would observe that the sun was directly overhead at noontime. This condition is called an *equinox* since anywhere on the earth, the time during which the sun is visible (daytime) is exactly 12 hours and the time when it is not visible (nighttime) is 12 hours. There are two such conditions during a year; the *autumnal equinox* on about September 23, marking the start of the fall; and the *vernal equinox* on about March 22, marking the beginning of spring. At the equinoxes, the declination angle (δ) is zero.

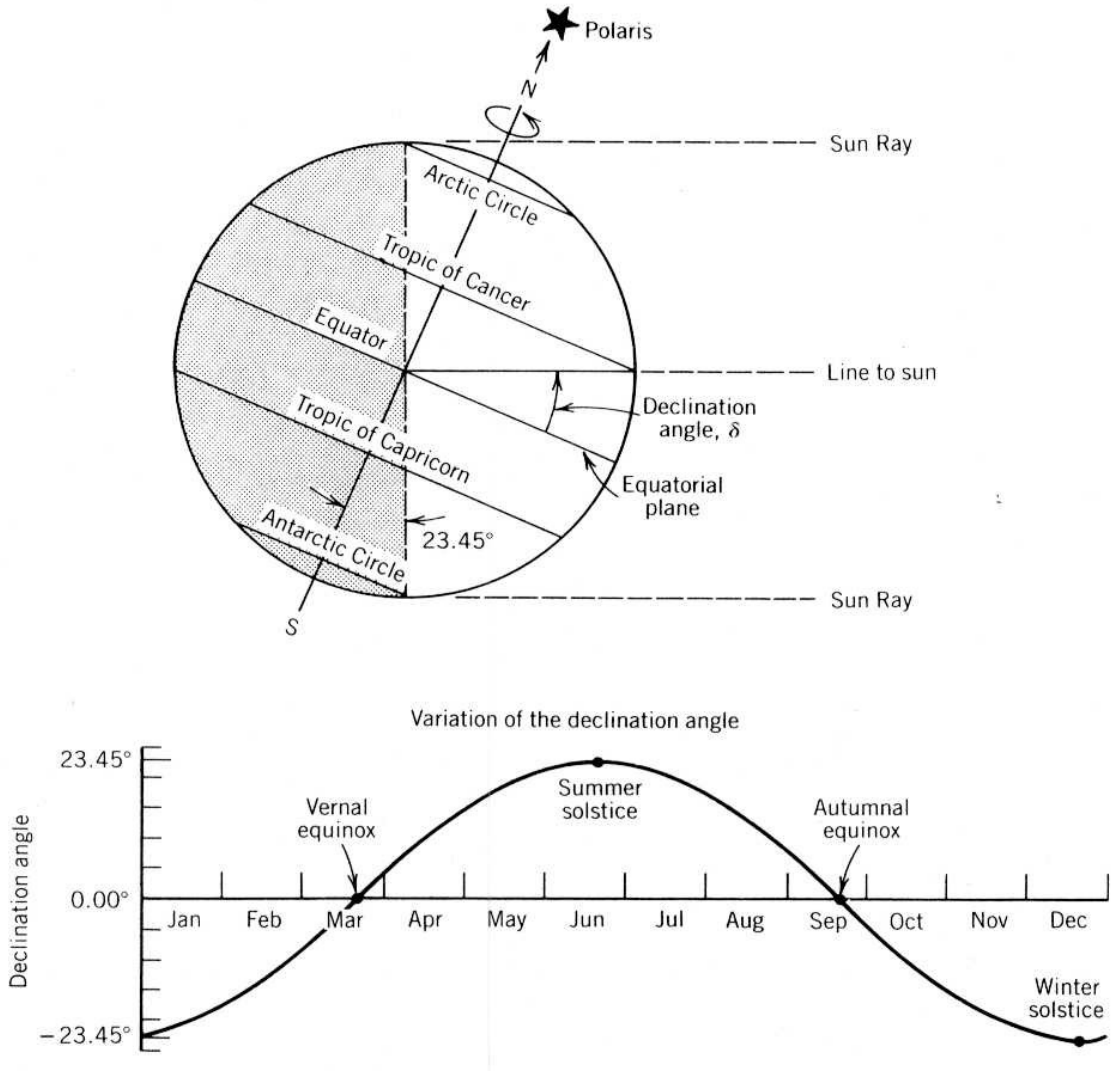

Figure 3.5 The declination angle (δ). The earth is shown in the summer solstice position when δ = +23.45 degrees. Note the definition of the tropics as the intersection of the earth-sun line with the surface of the earth at the solstices and the definition of the Arctic and Antarctic circles by extreme parallel sun rays.

The *winter solstice* occurs on about December 22 and marks the point where the equatorial plane is tilted relative to the earth-sun line such that the northern hemisphere is tilted away from the sun. We say that the noontime sun is at its "lowest point" in the sky, meaning that the declination angle is at its most negative value (i.e., δ = -23.45 degrees). By convention, winter declination angles are negative.

Accurate knowledge of the declination angle is important in navigation and astronomy. Very accurate values are published annually in tabulated form in an

ephemeris; an example being (Anonymous, 198l). For most solar design purposes, however, an approximation accurate to within about 1 degree is adequate. One such approximation for the declination angle is

$$\sin\delta = 0.39795\cos\left[0.98563\left(N-173\right)\right] \qquad (3.7)$$

where the argument of the cosine here is in degrees and N is the day number defined for Equation (3.3) The annual variation of the declination angle is shown in Figure 3.5.

3.1.4 Latitude Angle (ϕ)

The *latitude angle* (ϕ) is the angle between a line drawn from a point on the earth's surface to the center of the earth, and the earth's equatorial plane. The intersection of the equatorial plane with the surface of the earth forms the equator and is designated as 0 degrees latitude. The earth's axis of rotation intersects the earth's surface at 90 degrees latitude (North Pole) and -90 degrees latitude (South Pole). Any location on the surface of the earth then can be defined by the intersection of a longitude angle and a latitude angle.

Other latitude angles of interest are the Tropic of Cancer (+23.45 degrees latitude) and the Tropic of Capricorn (- 23.45 degrees latitude). These represent the maximum tilts of the north and south poles toward the sun. The other two latitudes of interest are the Arctic circle (66.55 degrees latitude) and Antarctic circle (-66.5 degrees latitude) representing the intersection of a perpendicular to the earth-sun line when the south and north poles are at their maximum tilts toward the sun. As will be seen below, the tropics represent the highest latitudes where the sun is directly overhead at solar noon, and the Arctic and Antarctic circles, the lowest latitudes where there are 24 hours of daylight or darkness. All of these events occur at either the summer or winter solstices.

3.2 Observer-Sun Angles

When we observe the sun from an arbitrary position on the earth, we are interested in defining the sun position relative to a coordinate system based at the point of observation, not at the center of the earth. The conventional earth-surface based coordinates are a vertical line (straight up) and a horizontal plane containing a north-south line and an east-west line. The position of the sun relative to these coordinates can be described by two angles; the *solar altitude angle* and the *solar zenith angle* defined below. Since the sun appears not as a point in the sky, but as a disc of finite size, all angles discussed in the following sections are measured to the center of that disc, that is, relative to the "central ray" from the sun.

3.2.1 Solar Altitude, Zenith, and Azimuth Angles

The solar altitude angle (α) is defined as the angle between the central ray from the sun, and a horizontal plane containing the observer, as shown in Figure 3.6. As an alternative, the sun's altitude may be described in terms of the *solar zenith* angle (θ_z) which is simply the complement of the solar altitude angle or

$$\theta_z = 90^\circ - \alpha \qquad (\text{degrees}) \qquad (3.8)$$

The other angle defining the position of the sun is the *solar azimuth angle* (A). It is the angle, measured clockwise on the horizontal plane, from the north-pointing coordinate axis to the projection of the sun's central ray.

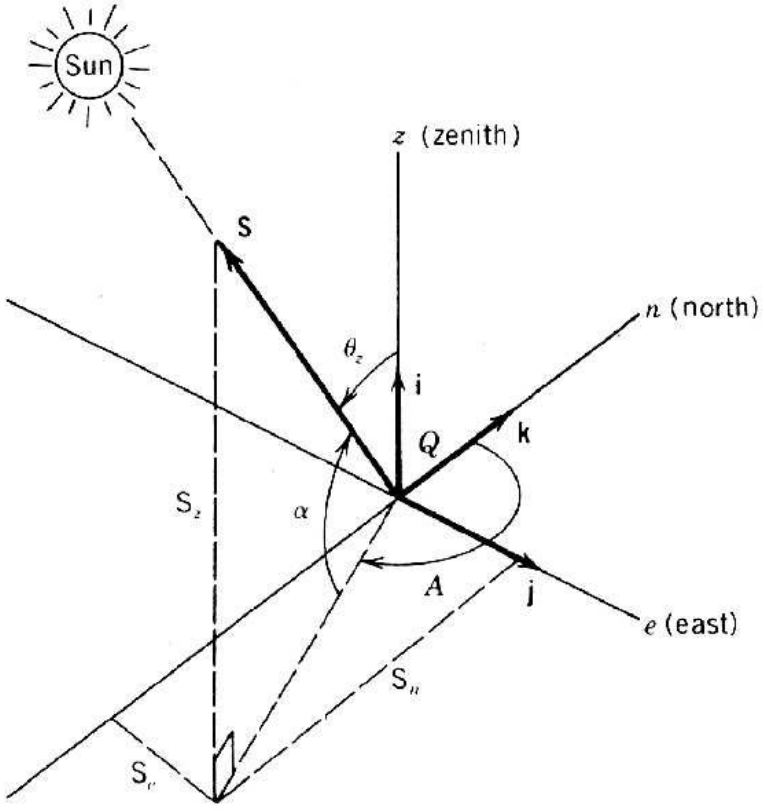

Figure 3.6 Earth surface coordinate system for observer at Q showing the solar azimuth angle A, the solar altitude angle (α) and the solar zenith angle (θ_z) for a central sun ray along direction vector $\boldsymbol{S}$. Also shown are unit vectors $\boldsymbol{i, j, k}$ along their respective axes.

The reader should be warned that there are other conventions for the solar azimuth angle in use in the solar literature. One of the more common

conventions is to measure the azimuth angle from the south-pointing coordinate rather than from the north-pointing coordinate. Another is to consider the counterclockwise direction positive rather than clockwise. The information in Table 3.3 at the end of this chapter will be an aid in recognizing these differences when necessary.

It is of the greatest importance in solar energy systems design, to be able to calculate the solar altitude and azimuth angles at any time for any location on the earth. This can be done using the three angles defined in Section 3.1 above; latitude (ϕ), hour angle (ω), and declination (δ). If the reader is not interested in the details of this derivation, they are invited to skip directly to the results; Equations (3.17), (3.18) and (3.19).

For this derivation, we will define a sun-pointing vector at the surface of the earth and then mathematically translate it to the center of the earth with a different coordinate system. Using Figure 3.6 as a guide, define a unit direction vector **S** pointing toward the sun from the observer location *Q:*

$$\mathbf{S} = S_z\mathbf{i} + S_e\mathbf{j} + S_n\mathbf{k} \qquad (3.9)$$

where **i**, **j,** and **k** are unit vectors along the *z, e,* and *n* axes respectively. The direction cosines of ***S*** relative to the *z, e,* and *n* axes are S_z, S_e and S_n, respectively. These may be written in terms of solar altitude and azimuth as

$$\begin{aligned} S_z &= \sin\alpha \\ S_e &= \cos\alpha \sin A \\ S_n &= \cos\alpha \cos A \end{aligned} \qquad (3.10)$$

Similarly, a direction vector pointing to the sun can be described at the center of the earth as shown in Figure 3.7. If the origin of a new set of coordinates is defined at the earth's center, the *m* axis can be a line from the origin intersecting the equator at the point where the meridian of the observer at *Q* crosses. The *e* axis is perpendicular to the *m* axis and is also in the equatorial plane. The third orthogonal axis *p* may then be aligned with the earth's axis of rotation. A new direction vector ***S´*** pointing to the sun may be described in terms of its direction cosines S'_m, S'_e and S'_p relative to the *m, e,* and *p* axes, respectively. Writing these in terms of the declination and hour angles, we have

$$\begin{aligned} S'_m &= \cos\delta \cos\omega \\ S'_e &= \cos\delta \sin\omega \\ S'_p &= \sin\delta \end{aligned} \qquad (3.11)$$

Note that S'_e is negative in the quadrant shown in Figure 3.7.

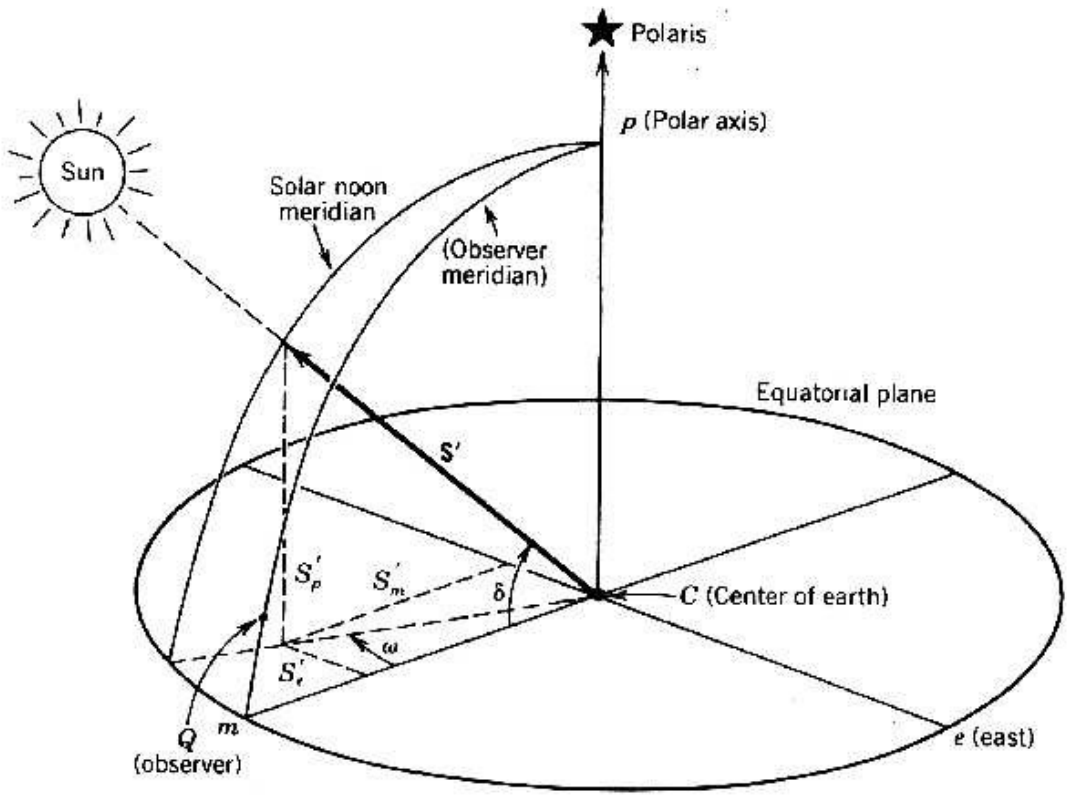

Figure 3.7 Earth center coordinate system for the sun ray direction vector **S** defined in terms of hour angle (ω) and the declination angle (δ).

These two sets of coordinates are interrelated by a rotation about the e axis through the *latitude angle* (ϕ) and translation along the earth radius QC. We will neglect the translation along the earth's radius since this is about 1 / 23,525 of the distance from the earth to the sun, and thus the difference between the direction vectors **S** and **S**′ is negligible. The rotation from the m, e, p coordinates to the z, e, n coordinates, about the e axis is depicted in Figure 3.8. Both sets of coordinates are summarized in Figure 3.9. Note that this rotation about the e axis is in the negative sense based on the right-hand rule. In matrix notation, this takes the form

$$\begin{vmatrix} S_z \\ S_e \\ S_n \end{vmatrix} = \begin{vmatrix} \cos\phi & 0 & \sin\phi \\ 0 & 1 & 0 \\ -\sin\phi & 0 & \cos\phi \end{vmatrix} \cdot \begin{vmatrix} S'_m \\ S'_e \\ S'_p \end{vmatrix} \qquad (3.12)$$

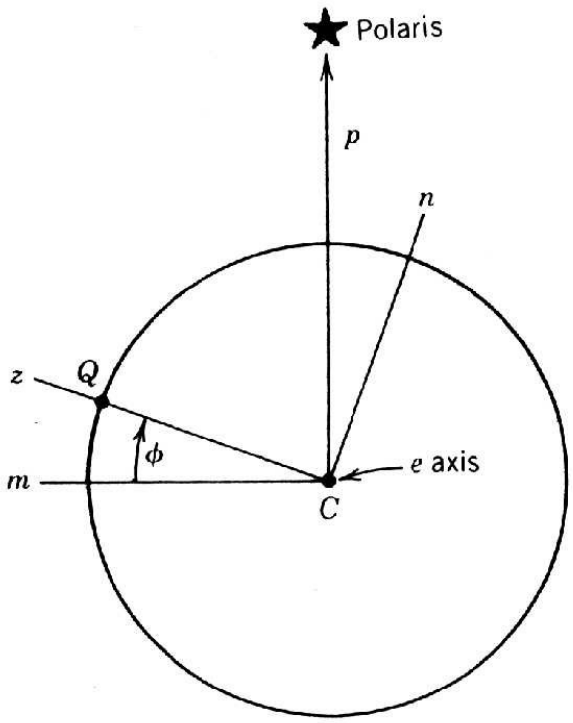

Figure 3.8 Earth surface coordinates after translation from the observer at *Q* to the earth center *C*.

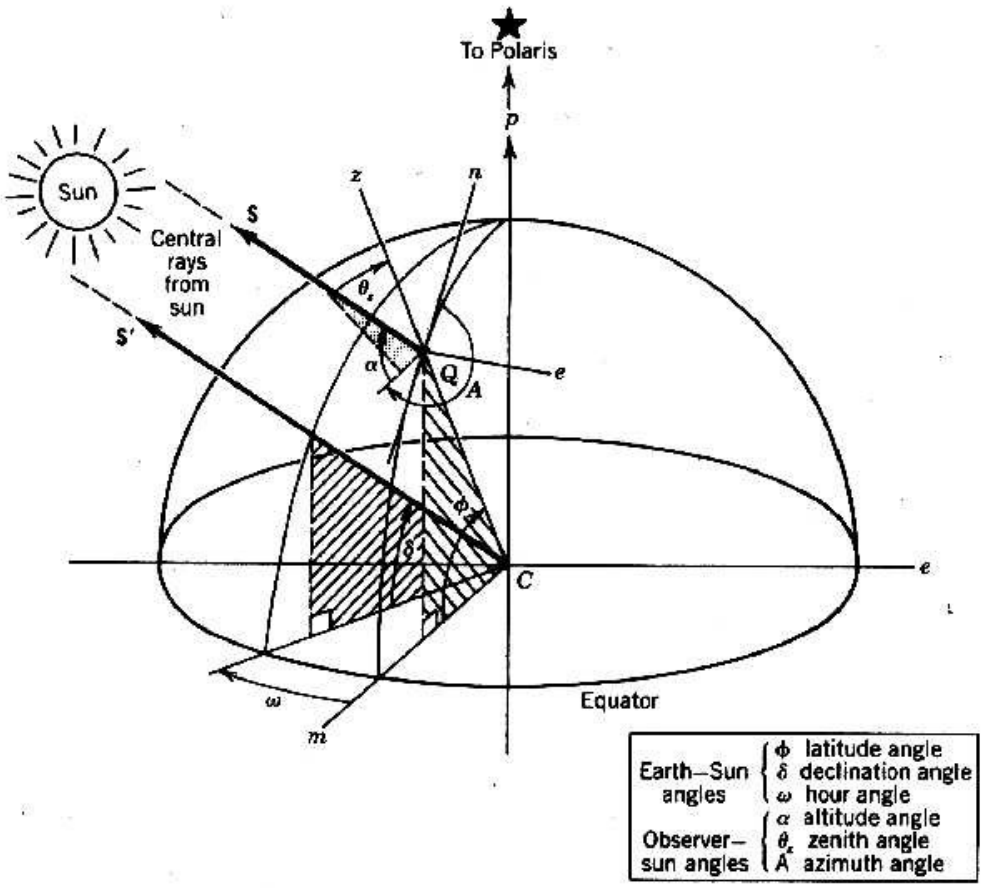

Figure 3.9 Composite view of Figures 3.6, 3.7 and 3.8 showing parallel sun ray vectors **S** and **S'** relative to the earth surface and the earth center coordinates.

Solving, we have

$$S_z = S'_m \cos\phi + S'_p \sin\phi$$

$$S_e = S'_e$$

$$S_n = S'_p \cos\phi - S'_m \sin\phi \qquad (3.13)$$

Substituting Equations (3.10) and (3.1)(3.11) for the direction cosine gives us our three important results

$$\sin\alpha = \sin\delta \sin\phi + \cos\delta \cos\omega \cos\phi \qquad (3.14)$$

$$\cos\alpha \sin A = -\cos\delta \sin\omega \qquad (3.15)$$

$$\cos\alpha \cos A = \sin\delta \cos\phi - \cos\delta \cos\omega \sin\phi \qquad (3.16)$$

Equation (3.14) is an expression for the solar altitude angle in terms of the observer's latitude (*location*), the hour angle (*time*), and the sun's declination (*date*). Solving for the solar altitude angle (α), we have

$$\alpha = \sin^{-1}\left(\sin\delta\sin\phi + \cos\delta\cos\omega\cos\phi\right) \qquad (\text{degrees}) \tag{3.17}$$

Two equivalent expressions result for the solar azimuth angle (A) from either Equation (3.15) or (3.16). To reduce the number of variables, we could substitute Equation (3.14) into either Equation (3.15) or (3.16); however, this substitution results in additional terms and is often omitted to enhance computational speed in computer codes.

The solar azimuth angle can be in any of the four trigonometric quadrants depending on location, time of day, and the season. Since the arc sine and arc cosine functions have two possible quadrants for their result, both Equations (3.15) and (3.16) require a test to ascertain the proper quadrant. No such test is required for the solar altitude angle, since this angle exists in only one quadrant.

The appropriate procedure for solving Equation (3.15) is to test the result to determine whether the time is before or after solar noon. For Equation (3.15), a test must be made to determine whether the solar azimuth is north or south of the east-west line.

Two methods for calculating the solar azimuth (A), including the appropriate tests, are given by the following equations. Again, these are written for the azimuth angle sign convention used in this text, that is, that the solar azimuth angle is measured from due north in a clockwise direction, as with compass directions. Solving Equation (3.15) the untested result, A' then becomes

$$A' = \sin^{-1}\left(\frac{-\cos\delta\sin\omega}{\cos\alpha}\right) \qquad (\text{degrees})$$

$$\text{where if:} \quad \cos\omega \geq \left(\frac{\tan\delta}{\tan\phi}\right), \quad \text{then} \quad A = 180^\circ - A'$$

$$\text{otherwise:} \quad \cos\omega < \left(\frac{\tan\delta}{\tan\phi}\right), \quad \text{and} \quad A = 360^\circ + A' \tag{3.18}$$

A graphical description of this test will follow in the next section.

Solving Equation (3.16), the untested result, A' becomes

$$A'' = \cos^{-1}\left(\frac{\sin\delta\cos\phi - \cos\delta\cos\omega\sin\phi}{\cos\alpha}\right) \qquad (\text{degrees})$$

where if: $\sin\omega > 0$ then $A = 360^\circ - A''$

otherwise $\sin\omega \le 0$ and $A = A''$ (3.19)

In summary, we now have equations for both the sun's altitude angle and azimuth angle written in terms of the latitude, declination and hour angles. This now permits us to calculate the sun's position in the sky, as a function of date, time and location (N, ω , ϕ).

EXAMPLE: For a site in Miami, Florida (25 degrees, 48 minutes north latitude/ 80 degrees, 16 minutes west longitude) at 10:00 AM solar time on August 1 (not a leap year), find the sun's altitude, zenith and azimuth angles.....For these conditions, the declination angle is calculated to be 17.90 degrees, the hour angle -30 degrees and the sun's altitude angle is then 61.13 degrees, the zenith angle 28.87 degrees and the azimuth angle 99.77 degrees.

3.2.2 A Geometric View of Sun's Path

The path of the sun across the sky can be viewed as being on a disc displaced from the observer. This "geometric" view of the sun's path can be helpful in visualizing sun movements and in deriving expressions for testing the sun angles as needed for Equation (3.18) to ascertain whether the sun is in the northern sky.

The sun may be viewed as traveling about a disc having a radius R at a constant rate of 15 degrees per hour. As shown in Figure 3.10, the center of this disc appears at different seasonal locations along the polar axis, which passes through the observer at Q and is inclined to the horizon by the latitude angle (ϕ) pointing toward the North Star (Polaris).

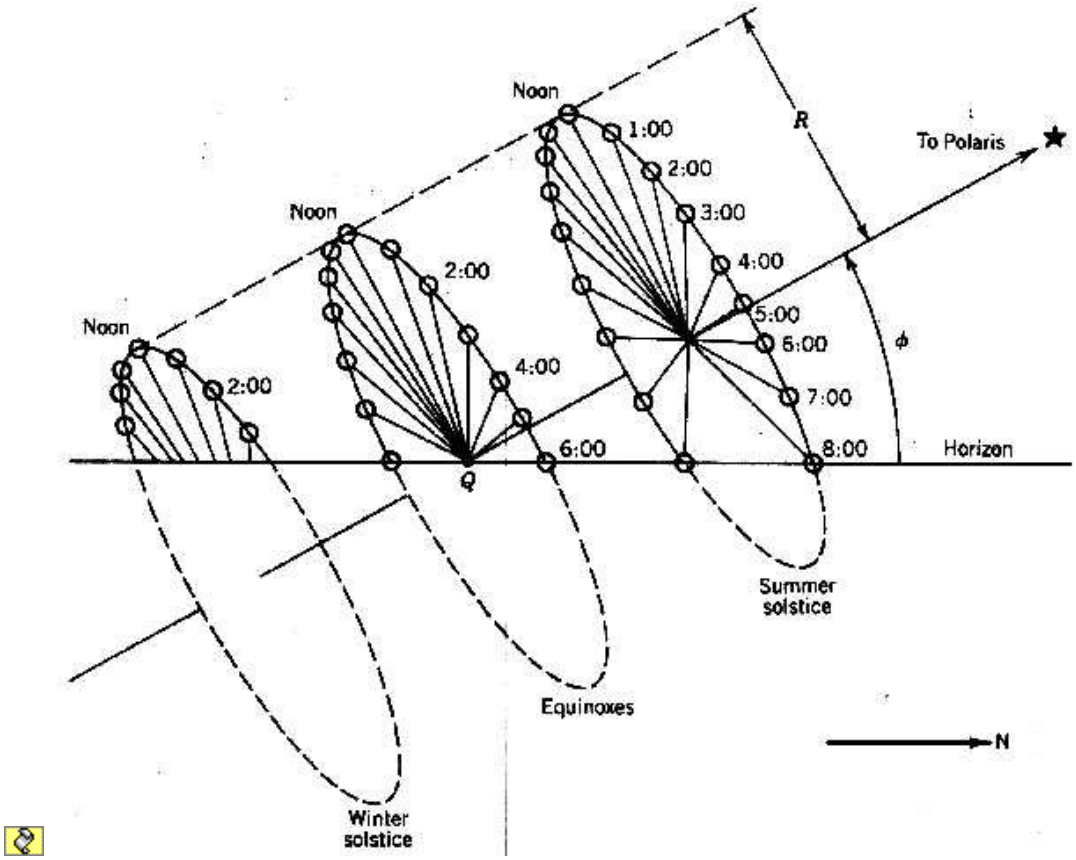

Figure 3.10 A geometric view of the sun's path as seen by an observer at Q. Each disc has radius R.

The center of the disc is coincident with the observer Q at the equinoxes and is displaced from the observer by a distance of $(R \tan \delta)$ at other times of the year. The extremes of this travel are at the solstices when the disc is displaced by ± 0.424 R along the polar axis. It can be seen that in the winter, much of the disc is "submerged" below the horizon, giving rise to fewer hours of daylight and low sun elevations as viewed from Q.

At the equinoxes, the sun rises exactly due east at exactly 6:00 AM (solar time) and appears to the observer to travel at a constant rate across the sky along a path inclined from the vertical by the local latitude angle. Exactly one-half of the disc is above the horizon, giving the day length as 12 hours. At noon, the observer notes that the solar zenith angle is the same as the local latitude. The sun sets at exactly 6:00 PM, at a solar azimuth angle of exactly 270 degrees or due west.

In the summer, the center of the disc is above the observer, giving rise to more hours of daylight and higher solar altitude angles, with the sun appearing in the northern part of the sky in the mornings and afternoons.

Since the inclination of the polar axis varies with latitude it can be visualized that there are some latitudes where the summer solstice disc is completely above the horizon surface. It can be shown that this occurs for latitudes greater than 66.55 degrees, that is, above the Arctic Circle. At the equator, the polar axis is horizontal and exactly half of any disc appears above the horizon surface, which means that the length of day and night is 12 hours throughout the year.

A test to determine whether the sun is in the northern part of the sky may be developed by use of this geometry. Figure 3.11 is a side view of the sun's disc looking from the east.

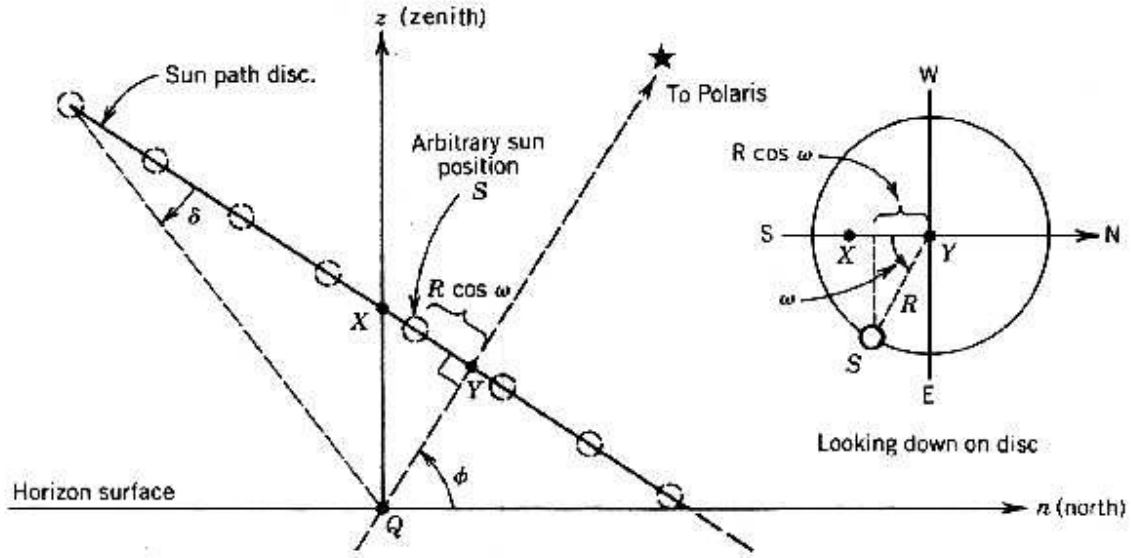

Figure 3.11 Side view of sun path disc during the summer when the disc center *Y* is above the observer at *Q*.

In the summer the sun path disc of radius R has its center Y displaced above the observer Q. Point X is defined by a perpendicular from Q. In the n - z plane, the projection of the position *S* onto the line containing X and Y will be $(R\cos\omega)$ where (ω) is the hour angle. The appropriate test for the sun being in the northern sky is then

$$R\cos\omega < \text{distance XY} \qquad (\text{m}) \qquad (3.20)$$

The distance XY can be found by geometry arguments. Substituting into Equation (3.20), we have

$$\cos\omega < \frac{\tan\delta}{\tan\phi}\cos\omega < \frac{\tan\delta}{\tan\phi} \qquad (3.21)$$

This is the test applied to Equation (3.18) to ensure that computed solar azimuth angles are in the proper quadrant.

3.2.3 Daily and Seasonal Events

Often the solar designer will want to predict the time and location of sunrise and sunset, the length of day, and the maximum solar altitude. Expressions for these are easily obtained by substitutions into expressions developed in Section 3.2. l.

The hour angle for sunset (and sunrise) may be obtained from Equation (3.17) by substituting the condition that the solar altitude at sunset equals the angle to the horizon. If the local horizon is flat, the solar altitude is zero at sunset and the hour angle at sunset ω_s becomes

$$\omega_s = \cos^{-1}\left(-\tan\delta\tan\phi\right) \qquad \left(\text{degrees}\right)$$

where if:

$\left(\tan\delta\tan\phi\right) \geq 1$, then no sunset that day

$\left(\tan\delta\tan\phi\right) \leq -1$, then no sunrise that day (3.22)

The above two tests relate only to latitudes beyond ± 66.55 degrees, i.e. above the Arctic Circle or below the Antarctic Circle.

If the hour angle at sunset is known, this may be substituted into Equation (3.18) or (3.19) to ascertain the solar azimuth at sunrise or sunset.

The hours of daylight, sometimes of interest to the solar designer, may be calculated as

$$\text{Hours of daylight} = \frac{2\omega_s}{15} \qquad \left(\text{hours}\right) \qquad (3.23)$$

where ω_s is in degrees. It is of interest to note here that although the hours of daylight vary from month to month except at the equator (where $\tan\phi = 0$), there are always 4,380 hours of daylight in a year (non leap year) at any location on the earth.

Another limit that may be obtained is the maximum and minimum noontime solar altitude angle. Substitution of a value of $\left(\omega = 0\right)$ into Equation (3.17) gives

$$\alpha_{max} = 90^{\circ} - |\phi - \delta| \quad \text{(degrees)}$$
$$\alpha_{min} = 90^{\circ} - |\phi + \delta| \quad \text{(degrees)} \qquad (3.24)$$

where $|\phi - \delta|$ denotes the absolute value of this difference. An interpretation of Equation (3.24) shows that at solar noon, the solar zenith angle (the complement of the solar altitude angle) is equal to the latitude angle at the equinoxes and varies by ±23.45 degrees from summer solstice to winter solstice.

EXAMPLE: At a latitude of 35 degrees on the summer solstice (June 21), find the solar time of sunrise and sunset, the hours of daylight, the maximum solar altitude and the compass direction of the sun at sunrise and sunset.....On the summer solstice, the declination angle is +23.45 degrees, giving an hour angle at sunset of 107.68 degrees. Therefore, the time of sunrise is 4:49:17 and of sunset, 19:10:43. There are 14.36 hours of daylight that day, and the sun reaches a maximum altitude angle of 78.45 degrees. The sun rises at an azimuth angle of 60.94 degrees (north of east) and sets at an azimuth angle of 299.06 degrees (north of west).

Other seasonal maxima and minima may be determined by substituting the extremes of the declination angle, that is, ±23.45 degrees into the previously developed expressions, to obtain their values at the solstices. Since the solar designer is often interested in the limits of the sun's movements, this tool can be very useful in developing estimates of system performance.

3.3 Shadows and Sundials

Now that we have developed the appropriate equations to define the direction of the sun on any day, any time and any location, let's look at two applications, which are interesting, and may be of value to the solar designer.

3.3.1 Simple Shadows

An important use of your understanding of the sun's position is in predicting the location of a shadow. Since sunlight travels in straight lines, the projection of an obscuring point onto the ground (or any other surface) can be described in terms of simple geometry.

Figure 3.12 shows a vertical pole on a horizontal surface. The problem here is to define the length and direction of the shadow cast by the pole. This will first be done in terms of radial coordinates and then in Cartesian coordinates.

In polar coordinates, for a pole height, OP and the shadow azimuth, θ_s defined in the same manner as the previous azimuth angles i.e. relative to true north with clockwise being positive, we have for the shadow length:

$$OS = \frac{OP}{\tan\alpha} \qquad (m) \qquad (3.25)$$

and for the shadow azimuth:

$$A_s = A - 180^o \qquad (\text{degrees}) \qquad (3.26)$$

In terms of Cartesian coordinates as shown on Figure 3.12, with the base of the pole as the origin, north as the positive y-direction and east the positive x-direction, the equations for the coordinates of the tip of the shadow from the vertical pole OP are:

$$x = OP\left[\frac{\sin\,(A-180^o)}{\tan\alpha}\right] \qquad (m) \qquad (3.27)$$

$$y = OP\left[\frac{\cos(A-180^o)}{\tan\alpha}\right] \qquad (m) \qquad (3.28)$$

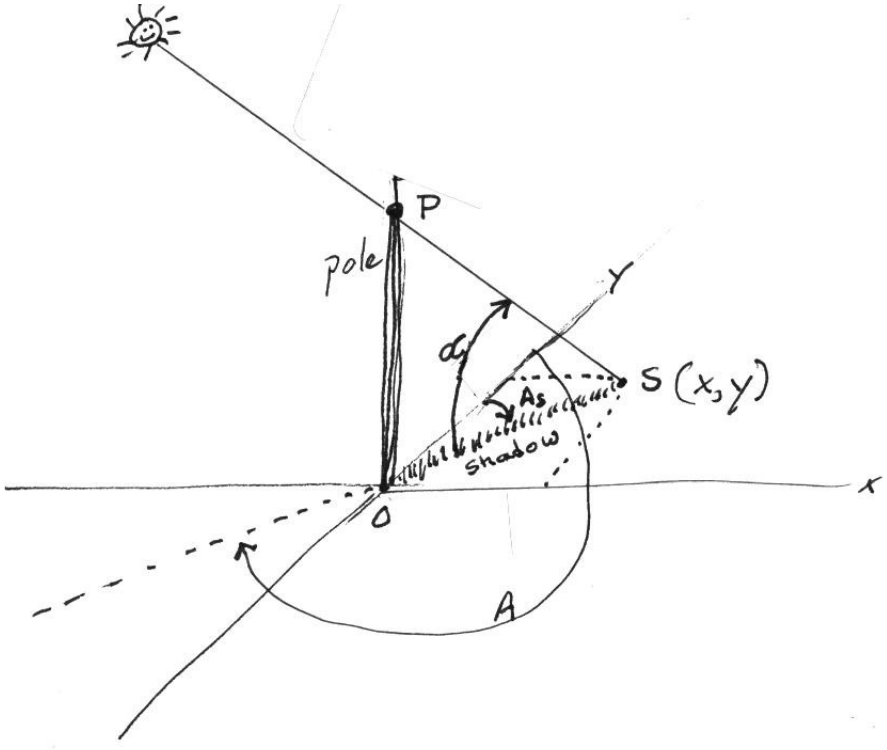

Figure 3.12 Shadow cast by pole OP showing x and y coordinates of shadow tip, and shadow azimuth (A_s).

Shadow coordinates are important for performing solar studies, especially related to the siting of solar energy systems. All that is needed is the latitude, hour angle and declination (i.e. the date) along with the location of the point causing the shadow. With a little bit of imagination, these equations can be used to predict shadowing of nearby terrain by trees or structures. All that is needed is to define a set of points on an object, and predict the shadow cast by that point

Example: At a latitude of 35.7 degrees north on August 24 (day number 236) at 14:00, the sun's altitude is 53.1 degrees and its azimuth 234.9 degrees. Then the shadow cast by a 10 cm high vertical pole is 7.51 cm long, and has a shadow azimuth (from north) of 54.9 degrees. The x- and y-coordinates of the tip of the shadow are: x = 6.14 cm and y = 4.32 cm.

3.3.1 Sundials

Throughout the history of mankind, the sun's shadow has been used to tell he time of day. Ingenious devices casting shadows on surfaces of all shapes and orientations have been devised. However, all of these can be understood with a simple manipulation of Equations (3.25) through (3.28) developed above.

The most common sundial consists of a flat, horizontal '*card'* with lines marked for each hour of daylight. These lines spread out from a point with the noon line pointing toward the North Pole. A '*gnomon'* or shadow-casting device, is mounted perpendicular to the card and along the noon line. The gnomon is tapered at the local latitude angle, (ϕ) with its height increasing toward the north. Figure 3.13 below shows a simple horizontal sundial with the important angles defined.

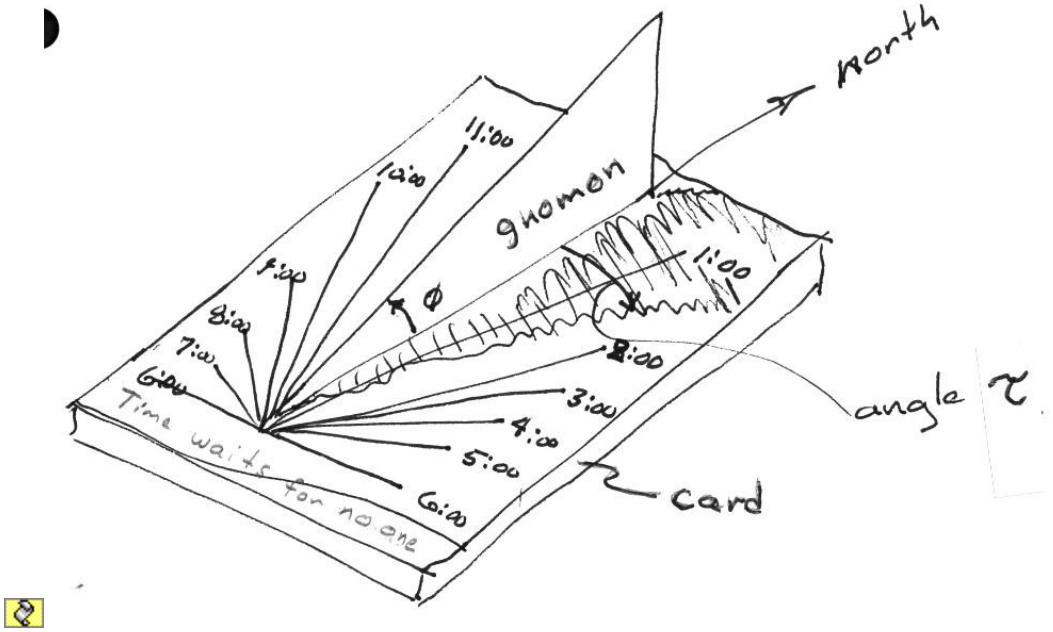

Figure 3.13 The simple horizontal sundial

In order to derive an equation for the directions of the time lines on the card, it must be assumed that the declination angle (δ) is zero (i.e. at the equinoxes). Using Equations (3.27) and (3.28) to define the coordinates of the shadow cast by the tip of the gnomon, and Equations (3.14), (3.15) and (3.16) to describe these in terms of the latitude angle (ϕ), and the hour angle (ω) with the declination angle being set to zero. An expression for the angle between the gnomon shadow and its base may be derived. Through simple geometric manipulations, the expression for this angle (τ) simplifies to

$$\tan\tau = \tan\omega\sin\phi \qquad (3.29)$$

In making a horizontal sundial, it is traditional to incorporate a wise saying about time or the sun, on the sundial card. An extensive range of sources of information about sundials, their history, design and construction is available on the internet.

3.4 Notes on the Transformation of Vector Coordinates

A procedure used often in defining the angular relationship between a surface and the sun rays is the transformation of coordinates. Defining the vector **V,** we obtain

$$\mathbf{V} = V_x\mathbf{i} + V_y\mathbf{j} + V_z\mathbf{k} \qquad (3.30)$$

where **i**, **j**, and **k** are unit vectors collinear with the *x, y,* and *z*-axes, respectively, and the scalar coefficients (V_x, V_y, V_z) are defined along these same axes. To describe **V** in terms of a new set of coordinate axes *x', y ', and z'* with their respective unit vectors **i', j'** and **k'** in the form

$$\mathbf{V} = V_x'\,\mathbf{i}' + V_y'\,\mathbf{j}' + V_z'\,\mathbf{k}' \qquad (3.31)$$

we must define new scalar coefficients V_x', V_y' and V_z'. Using matrix algebra will do this. A column matrix made of the original scalar coefficients representing the vector in the original coordinate system is multiplied by a matrix which defines the angle of rotation.

The result is a new column matrix representing the vector in the new coordinate system. In matrix form this operation is represented by

$$\begin{vmatrix} V'_x \\ V'_y \\ V'_z \end{vmatrix} = |A_{ij}| \cdot \begin{vmatrix} V_x \\ V_y \\ V_z \end{vmatrix} \qquad (3.32)$$

where A_{ij} is defined in Figure 3.14 for rotations about the x, y, or z axis.

Rotation about x axis

$$A_{ij} = \begin{vmatrix} 1 & 0 & 0 \\ 0 & \cos\theta & \sin\theta \\ 0 & -\sin\theta & \cos\theta \end{vmatrix}$$

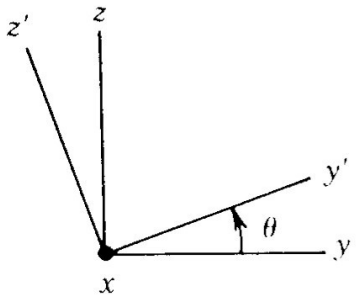

Rotation about y axis

$$A_{ij} = \begin{vmatrix} \cos\theta & 0 & -\sin\theta \\ 0 & 1 & 0 \\ \sin\theta & 0 & \cos\theta \end{vmatrix}$$

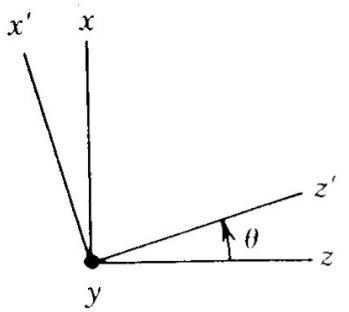

Rotation about z axis

$$A_{ij} = \begin{vmatrix} \cos\theta & \sin\theta & 0 \\ -\sin\theta & \cos\theta & 0 \\ 0 & 0 & 1 \end{vmatrix}$$

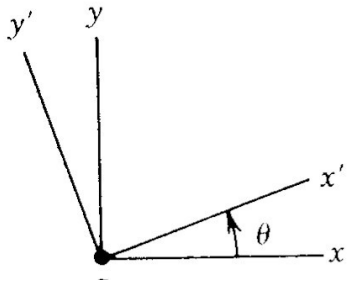

Figure 3.14 Axis rotation matrices A_{ij} for rotation about the three principal coordinate axes by the angle (θ).

It should be noted here that if the magnitude of **V** is unity, the scalar coefficients in Equations (3.30) and (3.31) are direction cosines. Note also that

the matrices given in Figure 3-22 are valid only for right-handed, orthogonal coordinate systems, and when positive values of the angle of rotation, (θ) are determined by the right-hand rule.

Summary

Table 3.3 summarizes the angles described in this chapter along with their zero value orientation, range and sign convention.

Table 3.3 Sign Convention for Important Angles

Title	Symbol	Zero	Positive Direction	Range	Equation No.	Figure No.
Earth-Sun Angles						
Latitude	ϕ	equator	northern hemisphere	+/- 90°	---	3.3
Declination	δ	equinox	summer	+/- 23.45°	(3.7)	3.5
Hour Angle	ω	noon	afternoon	+/- 180°	(3.1)	3.3
Observer-Sun Angles						
Sun Altitude	α	horizontal	upward	0 to 90°	(3.17)	3.6
Sun Zenith	θ_z	vertical	toward horizon	0 to 90°	(3.8)	3.6
Sun Azimuth	A	due north	clockwise*	0 to 360°	(3.18) or (3.19)	3.6
Shadow and Sundial Angles						
Shadow Azimuth	A_s	due north	clockwise	0 to 360°	(3.26)	3.12
Gnomon Shadow	τ	noon	afternoon	+/- 180°	(3.29)	3.13

* looking down + axis toward origin

References and Bibliography

Anonymous (1981), "The Astronomical Almanac for the Year 1981," issued by the Nautical Almanac Office of the United States Naval Observatory.

Blaise, C. (2000), Time Lord - Sir Sandford Fleming and the Creation of Standard Time, Pantheon Books, New York.

Jesperson, J., and J. Fitz-Randolph (1977), "From Sundials to Atomic Clocks," National Bureau of Standards Monograph 155, December.

Lamm, L. 0. (1981), "A New Analytic Expression for the Equation of Time," *Solar Energy* 26 (5), 465.

Sobel, D. (1995), Longitude - The True Story of a Lone Genius Who Solved the Greatest Scientific Problem of His Time ,Fourth Estate Ltd., London.

Woolf, H. M. (1968), "On the Computation of Solar Evaluation Angles and the Determination of Sunrise and Sunset Times, "National Aeronautics and Space Administration Report NASA TM-X -164, September.

Zimmerman, J. C. (1981), "Sun Pointing Programs and Their Accuracy," Sandia National Laboratories Report SAND81-0761, September.

4. Collecting Solar Energy

In Chapter 2, we developed an understanding of how to determine the rate and amount of energy coming from the sun. We introduced in that section the concept of the *cosine effect* or *cosine loss* representing the difference between the amount of energy falling on a surface pointing at the sun, and a surface parallel to the surface of the earth.

In order to collect solar energy here on the earth, it is important to know the angle between the sun's rays and a collector surface *(aperture*). When a collector is not pointing (or more exactly, when the collector *aperture normal* is not pointing) directly at the sun, some of the energy that could be collected is being lost.

In this chapter, we develop the equations to calculate the angle between a collector aperture normal and a central ray from the sun. This development is done first for fixed and then for tracking collectors. These equations are then used to provide insight into collector tracking and orientation design by predicting the integrated solar radiation energy that is incident on the collector aperture and could be collected. These concepts will be developed with the following outline:

- Aperture-sun angles: the angle of incidence (θ_i)
  - Fixed (non-tracking) apertures
  - Single-axis tracking apertures
    - *Horizontal tracking axis*
    - *Tilted tracking axis*
    - *Offset aperture*
    - *Vertical tracking axis*
    - *Vertical tracking axis with offset aperture*
    - *Tracking axis tilted at latitude angle*
  - Two-axis tracking apertures
    - *Azimuth / elevation tracking*
    - *Polar (equatorial) tracking*
- Collector aperture irradiance and solar radiation energy
  - Irradiance on a collector aperture
    - *Direct (beam) aperture irradiance*

4.1 Aperture-Sun Angles; The Angle of Incidence (θ_i)

In Chapter 3, we defined the sun's position angles relative to earth-center coordinates $(\phi,\ \delta \text{ and } \omega)$ and then to coordinates at an arbitrary location on the earth's surface (α) and (A) and a functional relationship between these angles, i.e., Equations (3.13), (3.14) and (3.15). In the design of solar energy systems, it is most important to be able to predict the angle between the sun's rays and a vector normal (perpendicular) to the aperture or surface of the collector. This angle is called the *angle of incidence* (θ_i). Knowing this angle is of critical importance to the solar designer, since the maximum amount of solar radiation energy that could reach a collector is reduced by the cosine of this angle.

The other angle of importance, discussed in this section is the *tracking angle,* (ρ). Most types of mid- and high-temperature collectors require a tracking drive system to align at least one axis and often two axes of a collector aperture normal to the sun's central ray. The tracking angle is the amount of rotation required to do this.

In this section we derive expressions for the angle of incidence for both fixed-axis and single-axis tracking apertures. We also derive equations for the tracking angle for both single-axis and two-axis (full) tracking apertures. Zimmerman (1981) has reviewed a number of sun pointing programs and evaluated their accuracy

4.1.1 Fixed (non-tracking) Apertures

The cosine of the angle of incidence for an arbitrarily oriented surface or aperture that does not track may be described in terms of the orientation of the collector and the solar altitude and azimuth angles. An expression for this is developed by taking the scalar or dot product of a unit vector **S** pointing from the collector aperture toward the sun and a unit vector **N** normal to the collector aperture. The unit vector **S** was defined in Chapter 3 by Equation (3.9) in terms of direction cosines given in Equation (3.10) which are functions of the solar altitude and azimuth angles.

To define **N** using the same axes, we will define an *aperture tilt angle* (β) and an *aperture azimuth angle* (γ) as pictured in Figure 4.1. The sign convention for (γ) is the same as for the solar azimuth (A); that is, north is zero and clockwise angles are positive. The direction cosines of **N** along the z, e, and n axes, respectively, are

$$N_z = \cos\beta$$
$$N_e = \sin\beta\sin\gamma$$
$$N_n = \sin\beta\cos\gamma \qquad (4.1)$$

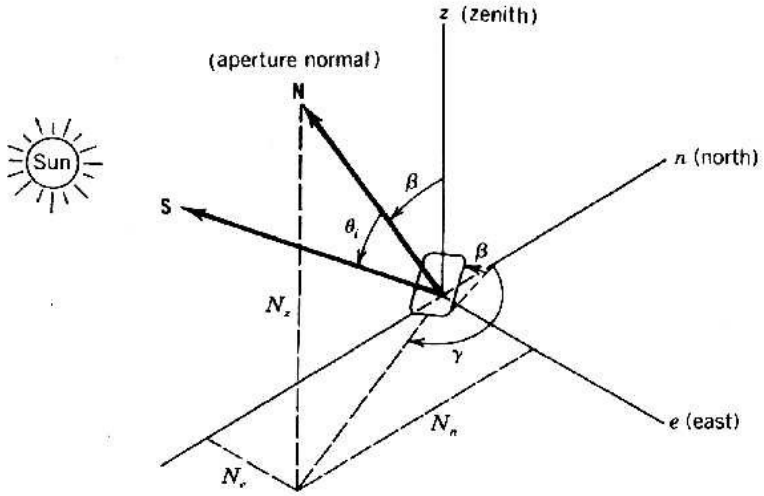

Figure 4.1 A fixed aperture with its orientation defined by the tilt angle (β) and the aperture azimuth angle (γ). The aperture normal $\mathbf{N}$ and sun position vector $\mathbf{S}$ are also shown.

The cosine of the angle between a sunray and the aperture normal is the dot product of these two unit vectors:

$$\cos\theta_i = \mathbf{S}\cdot\mathbf{N} \qquad (4.2)$$

Applying Equations (3.10) and (4.1), we have for the cosine of the angle of incidence for a fixed aperture:

$$\cos\theta_i = \sin\alpha\cos\beta + \cos\alpha\sin\beta\cos(\gamma - A) \qquad (4.3)$$

It is sometimes useful to write Equation (4.3) in terms of latitude, declination, and hour angle rather than solar altitude and azimuth. Using Equation (3.14), (3.15) and (3.16) does this, and the result is

$$\begin{aligned}\cos\theta_i = {} & \cos\beta(\sin\delta\sin\phi + \cos\delta\cos\phi\cos\omega) \\ & - \cos\delta\sin\omega\sin\beta\sin\gamma \\ & + \sin\beta\cos\gamma(\sin\delta\cos\phi - \cos\delta\cos\omega\sin\phi)\end{aligned} \qquad (4.4)$$

Special cases of Equation (4.3) are often of interest.

For horizontal apertures, the tilt angle (β) is zero and Equation (4.3) becomes

$$\cos\theta_i = \sin\alpha\cos\theta_i = \sin\alpha \qquad (4.5)$$

For vertical apertures, Equation (4.3) becomes

$$\cos\theta_i = \cos\alpha\cos(\gamma - A) \qquad (4.6)$$

and for a tilted aperture facing south, we have

$$\cos\theta_i = \sin\alpha\cos\beta - \cos\alpha\sin\beta\cos A \qquad (4.7)$$

4.1.2 Single-Axis Tracking Apertures

Certain types of concentrating collector are designed to operate with tracking rotation about only one axis. Here a tracking drive system rotates the collector

about an axis of rotation until the sun central ray and the aperture normal are coplanar. Figure 4.2 shows how rotation of a collector aperture about a tracking axis *r* brings the central ray unit vector **S** into the plane formed by the aperture normal and the tracking axis. The angle of incidence (θ_i) is also shown. *The tracking angle* (ρ) measures rotation about the tracking axis *r*, with $(\rho = 0)$ when **N** is vertical.

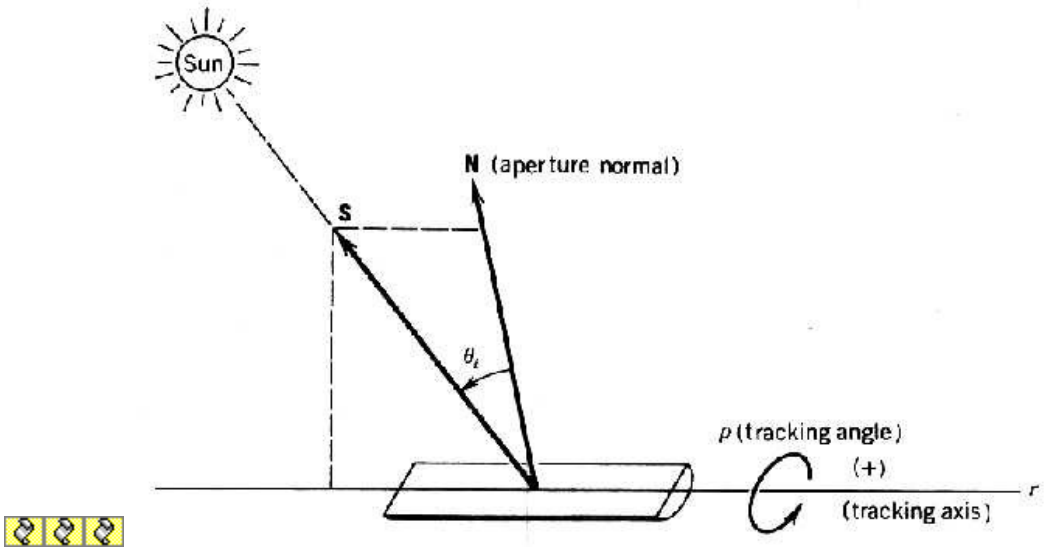

Figure 4.2 A single-axis tracking aperture where tracking rotation is about the r axis. The sun ray vector **S** is kept in the plane formed by the r axis and the aperture normal **N** by this rotation.

To write expressions for (θ_i) and (ρ) in terms of collector orientation and solar angles, we transform the coordinates of the central ray unit vector **S** from the z, e, and *n* coordinates used in Equation (3.10) to a new coordinate system that has the tracking axis as one of its three orthogonal axes. The other two axes are oriented such that one axis is parallel to the surface of the earth. This new coordinate system is shown in Figure 4.3, where *r* is the tracking axis, *b* is an axis that always remains parallel to the earth's surface, and *u* is the third orthogonal axis. Note that the coordinates remain fixed as the aperture normal **N** rotates in the *u*-*b* plane.

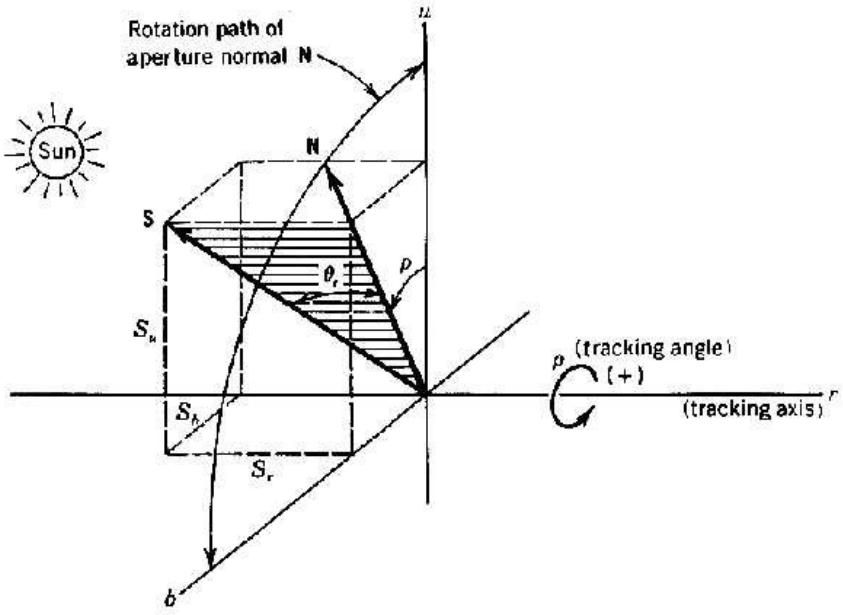

Figure 4.3 Single axis tracking system coordinates. The collector aperture rotates about the *r* axis, where **N** is a unit vector normal to the collector aperture.

Inspection of this figure reveals that both ρ and θ_i can be defined in terms of the direction cosines of the central ray unit vector **S** along the *u, b,* and *r* axes, denoted as S_u, S_b, and S_r respectively. The tracking angle is then

$$\tan \rho = \frac{S_b}{S_u} \qquad (4.8)$$

Remembering that **S** is a unit vector, the cosine of the angle of incidence is

$$\cos \theta_i = \begin{cases} \sqrt{S_b^2 + S_u^2} \\ \text{or} \\ \sqrt{1\text{-}S_r^2} \end{cases} \qquad (4.9)$$

In the sections that follow we develop equations for θ_i and ρ, first for cases where the tracking axis is arbitrarily oriented but still parallel to the surface of the earth, and then for cases where the tracking axis is inclined relative to the surface of the earth. Both cases require a coordinate transformation.

Horizontal Tracking Axis. To describe this category of tracking schemes, we must rotate the *u, b,* and *r* coordinates by an angle γ from the *z, e,* and *n*

coordinates that were used to describe the sun ray unit vector **S** in Equation (3.10). Since the tracking axis is to remain parallel to the surface of the earth, this rotation takes place about the z-axis as shown in Figure 4.4, with the u and z-axes coincident. Note that this rotation is in the negative direction based on the right-hand rule. The rotated direction cosines of **S** take the form

$$\begin{vmatrix} S_u \\ S_b \\ S_r \end{vmatrix} = \begin{vmatrix} 1 & 0 & 0 \\ 0 & \cos\gamma & -\sin\gamma \\ 0 & \sin\gamma & \cos\gamma \end{vmatrix} \cdot \begin{vmatrix} S_z \\ S_e \\ S_n \end{vmatrix} \qquad (4.10)$$

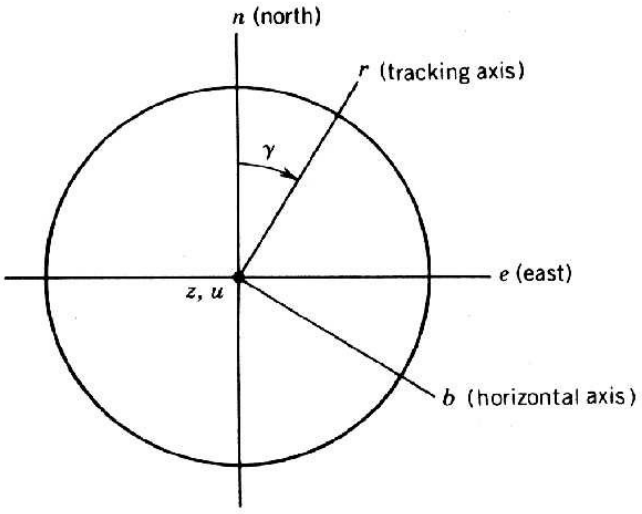

Figure 4.4 Rotation of the u, b, r coordinates from the z, e, n coordinates about the z-axis. Diagram shows view looking downward on the surface of the earth.

Solving and substituting into Equation (4.8), we have for the general case of a collector aperture tracking about a single, horizontal axis, the tracking angle

$$\tan\rho = \frac{\sin(A-\gamma)}{\tan\alpha} \qquad (4.11)$$

and from Equation (4.9), the angle of

$$\cos\theta_i = \sqrt{1-\cos^2(\alpha)\cos^2(A-\gamma)} \qquad (4.12)$$

A special case of this equation commonly found in practice is when the tracking axis is oriented in the north-south direction

$$\tan\rho = \frac{\sin A}{\tan\alpha} \qquad (4.13)$$

and

$$\cos\theta_i = \sqrt{1-\cos^2(\alpha)\cos^2(A)} \qquad (4.14)$$

When the tracking axis is oriented in the east-west direction, Equations (4.11) and (4.12) become

$$\tan\rho = \frac{-\cos A}{\tan\alpha} \qquad (4.15)$$

and

$$\cos\theta_i = \sqrt{1-\cos^2(\alpha)\sin^2(A)} \qquad (4.16)$$

Tilted Tracking Axis. Starting with the arbitrarily oriented horizontal tracking axis *r* from the previous section, we now tilt this axis from the horizon by an angle (β) as shown in Figure 4.5. Again, describing the direction cosines for the sunray unit vector in these new coordinates, we take a column matrix describing the solution to Equation (4.10) and rotate it in a positive direction through an angle (β). The direction cosines are found by solving

$$\begin{vmatrix} S_u \\ S_b \\ S_r \end{vmatrix} = \begin{vmatrix} \cos\beta & 0 & -\sin\beta \\ 0 & 1 & 0 \\ \sin\beta & 0 & \cos\beta \end{vmatrix} \cdot \begin{vmatrix} S_z \\ (S_e\cos\gamma - S_n\sin\gamma) \\ (S_e\sin\gamma + S_n\cos\gamma) \end{vmatrix} \qquad (4.17)$$

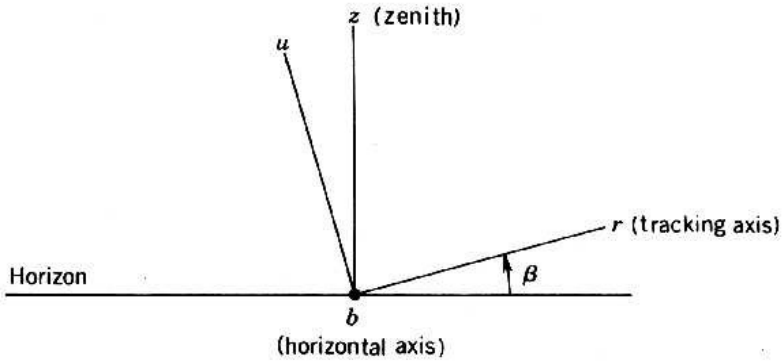

Figure 4.5 Rotation of the collector coordinates about the horizontal axis *b*.

Applying the solution of this to Equations (4.8) and (4.9), we have

$$\tan\rho = \frac{\cos\alpha\sin(A-\gamma)}{\sin(\alpha-\beta)+\sin\beta\cos\alpha[1-\cos A-\gamma]} \qquad (4.18)$$

and

$$\cos\theta_i = \sqrt{1-\left\{\cos(\alpha-\beta)-\cos\beta\cos\alpha\left[1-\cos(A-\gamma)\right]\right\}^2} \qquad (4.19)$$

If the tracking axis *r* is tilted toward the south as is often done, the equations above simplify on setting (γ) *to* 180 degrees.

Offset Aperture In some tracking designs, the collector aperture is offset relative to the tracking axis by an angle (μ) as shown in Figure 4.6. For this design, the tracking angle (ρ) is still as computed by Equation (4.18) since the aperture normal **N** remains in the plane formed by the tracking axis r and the sunray vector **S**. However, the angle of incidence (θ_i) is no longer that computed by Equation (4.19). The angle of incidence for this case is simply the sum of the angle of incidence found in Equation (4.19) and the *aperture offset* (μ). Appropriate signs must be used for each. The aperture offset (μ) is considered positive when offset counterclockwise (based on the right-hand rule) about the b axis. The sign for the angle found by Equation (4.19) would be the same as the sign of S_r found in Equation (4.17).

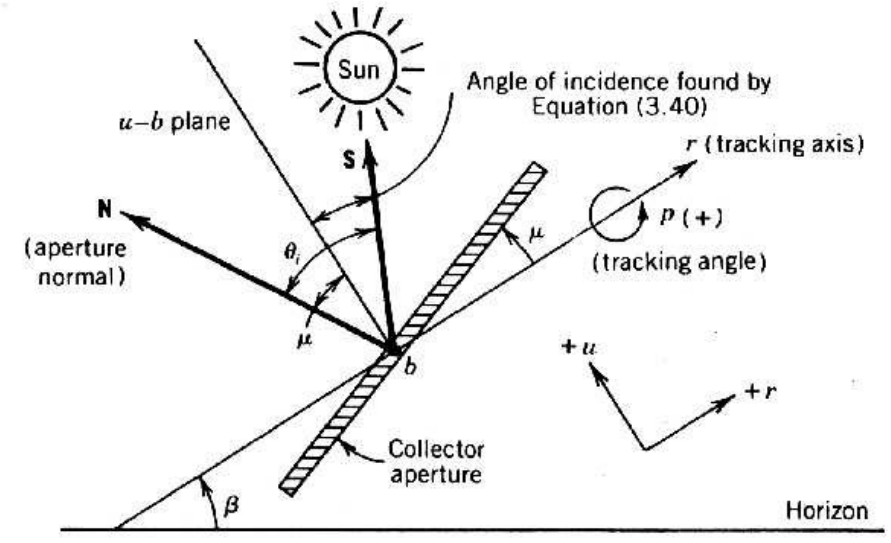

Figure 4.6 Tracking with the collector offset with respect to the tracking axis by an angle (μ). The sign of the aperture offset in this sketch is positive.

Two special cases of Equation (4.18) and (4.19) that occur in practice are the case of the vertical collector and the collector whose tracking axis is tilted toward the south at the local latitude angle ϕ.

Vertical Tracking Axis For the vertical tracking axis case, the tracking axis become collinear with the zenith axis and Equations (4.18) and (4.19) simplifies to

$$\rho = -A \quad and \quad \theta_i = \alpha \tag{4.20}$$

where by convention the tracking angle is counterclockwise about the zenith.

Vertical Tracking Axis With Offset Aperture In some designs the collector aperture is offset by an angle μ relative to the vertical tracking axis. In this case, the tracking angle and angle of incidence become

$$\rho = -A \quad and \quad \cos\theta_i = \cos(\alpha - \mu) \tag{4.21}$$

where $\mu = 0$ when the tracking axis is aligned with the plane of the aperture. Examples of this scheme are large concentrator arrays floating in a pond and arrays on circular railroad-like tracks.

Tracking Axis Tilted at Latitude Angle. When the tracking axis is tilted from the horizon by the latitude angle, toward the south, it is parallel to the earth's rotational pole and points toward the pole star, Polaris. Called either a *polar mounting* or an *equatorial mounting,* the solution of Equations (4.18) and (4.19) for this case reveals two important aspects of this class of mount. Substituting the latitude angle ϕ for the tilt angle β and then substituting Equations (3.17) and either (3.18) or (3.19) to replace the solar altitude and azimuth with latitude, declination, and hour angle does this.

An equivalent and analytically easier, procedure is to rotate the $z,\ e,\ n$ coordinates about the *e* axis by the latitude angle ϕ. This gives direction cosines of the central ray unit vector $\mathbf{S}$ in terms of our *u, b, r* coordinates.

$$\begin{vmatrix} S_u \\ S_b \\ S_r \end{vmatrix} = \begin{vmatrix} \cos\phi & 0 & -\sin\phi \\ 0 & 1 & 0 \\ \sin\phi & 0 & \cos\phi \end{vmatrix} \cdot \begin{vmatrix} S_z \\ S_e \\ S_n \end{vmatrix} \qquad (4.22)$$

Starting with Equation (3.10) and casting the direction cosines of **S** in terms of latitude, declination, and hour angles through application of Equation (3.14), (3.15) and (3.16), these are substituted into Equation (4.22) for S_z, S_e, and S_n. Taking the definition of ρ and θ_i from Equations (4.8) and (4.9) and after considerable simplification, we have for the tracking angle and angle of incidence for the polar mount:

$$\rho = \omega$$
$$and$$
$$\theta_i = \delta \qquad (4.23)$$

Since the hour angle ω changes at the exact rate of 15 degrees per hour, a simple constant speed "clock drive" can be used to turn the aperture about the tracking axis.

Furthermore, the angle of incidence, which is the declination angle, varies by only 23.45 degrees throughout the year, giving a minimum value to the cosine of the angle of incidence of 0.917. The result is a single-axis-tracking collector with a maximum cosine loss of 8.3% at the solstices.

Of more importance is the fact that the declination angle changes very slowly with a maximum rate of about 0.4 degree per day at the equinoxes. This gives rise to the possibility of periodic adjustments of the angle between the collector aperture and the tracking axis in order to maintain a small angle of incidence.

4.1.3 Two-axis Tracking, Apertures

With two-axis tracking, a collector aperture will always be normal to the sun. Therefore the cosine effect does not come into play and;

$$\cos\theta_i = 1.0 \qquad (4.24)$$

For aiming an aperture toward the sun at all times, rotation about two axes is always required. Two types of tracking mechanism are commonly in use for this purpose: *azimuth / elevation* tracking systems (also called *az-el systems)* and *polar* or *equatorial* tracking systems.

Azimuth / Elevation Tracking. With azimuth / elevation tracking, the collector aperture must be free to rotate about the zenith axis and an axis parallel to the surface of the earth. The tracking angle about the zenith axis is the solar azimuth angle (A), and the tracking angle (ρ) about the horizontal axis is the solar altitude angle (α), as defined in Equations, (3.18), (3.19) and (3.17) respectively.

Of primary interest to the designer of a two-axis tracking system is the rate at which these angles change called the *slew rate.* For the azimuth / elevation system, the rates of change of both the azimuth and elevation angles are not constant and depend on the location, time of day, and season. An expression for the slew rate about the horizontal axis may be found by taking the derivative of Equation (3.17) with respect to time. If we neglect the very slow variation in declination angle, the result is

$$\frac{d\alpha}{dt} = \frac{-\cos\phi \sin\delta \sin\omega}{\cos\alpha}\left(\frac{d\omega}{dt}\right) \qquad (4.25)$$

The slew rate about the vertical axis is found similarly from Equation (3.18) and is

$$\frac{dA}{dt} = \frac{\cos\delta}{\cos A \cos^2\alpha}\left(\cos\delta \sin^2\omega \tan\alpha \cos\phi - \cos\alpha \cos\omega\right)\frac{d\omega}{dt} \qquad (4.26)$$

Figure 4.7 shows the variation of these slew rates at a specific location. Note the very high azimuth slew rates required near the summer solstice at noon. This must be considered in the design of tracking drive mechanisms and tracking controls.

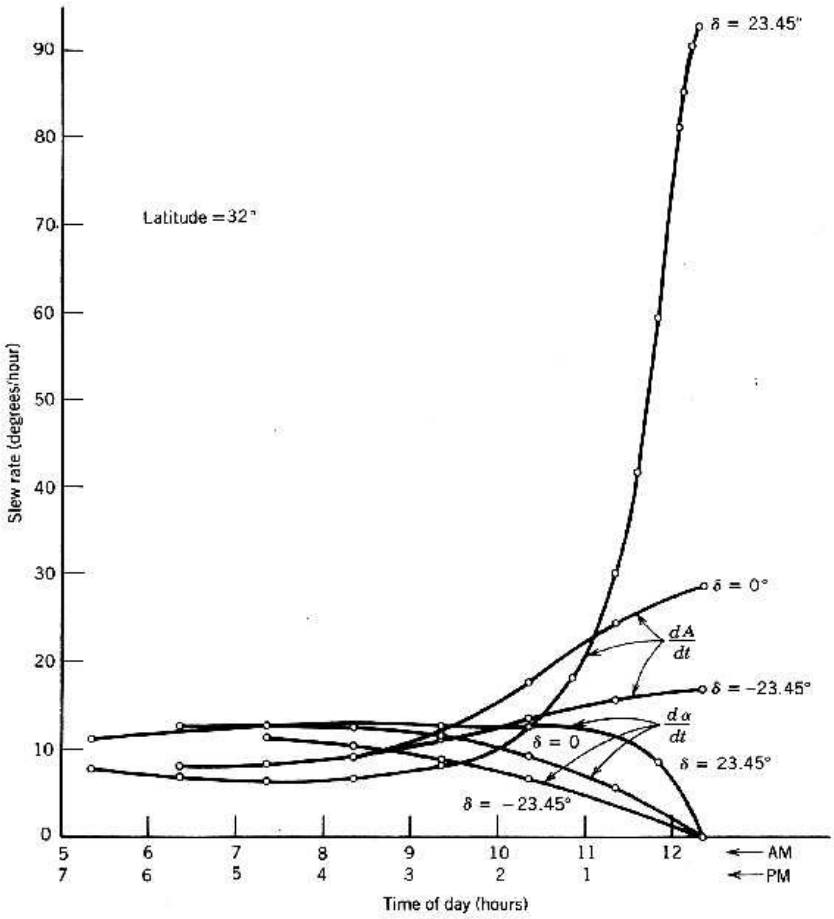

Figure 4.7 Variation in the rate at which the solar azimuth and altitude angles change for three representative days. The latitude is 32 degrees for this example.

Polar (Equatorial) Tracking. For polar or equatorial tracking systems, one axis of rotation is aligned parallel to the earth's rotational pole, that is, aimed toward the star Polaris. This gives it a tilt from the horizon equal to the local latitude angle. As described in the previous section, the tracking angle about the polar axis is equal to the sun's hour angle (ω). The other axis of rotation is perpendicular to this polar axis. The tracking angle about this axis (called the *declination axis)* is the declination angle (δ).

The slew rate about the polar axis is constant at 15 degrees per hour. The slew rate about the declination axis is very slow, giving rise to the possibility of incremental adjustment. The rate is dependent on the time of year and can be found by taking the derivative of Equation (3.7) with respect to time. The result is

$$\frac{d\delta}{dt} = \frac{0.01634}{\cos\delta}\sin\left[0.98563\left(N-173\right)\right] \qquad \left(\text{deg / hour}\right) \tag{4.27}$$

which give a maximum tracking rate of 0.0163 degrees per hour (0.28 mrad/h) at the equinoxes. With many types of concentrating collector optics, incremental adjustment rather than a continuous tracking motion may do this slow rate of tracking.

4.2 Collector Aperture Irradiance and Solar Radiation Energy

The *aperture area* of a solar collector is the area of the opening into which insolation passes. This is the area one would obtain by direct measurement and does not include any area reduction due to angle of incidence effects or shadowing. After passing through the aperture, that insolation may be concentrated or absorbed as is the case for the flat-plate collector.

4.2.1 Irradiance on a Collector Aperture

The rate at which solar energy enters a collector aperture, divided by the aperture area is called the *aperture irradiance.* This is usually made up of beam aperture irradiance and diffuse aperture irradiance. The angle of incidence between the aperture normal and a central ray of the sun depends on the time of day, the day of the year, the location and orientation of the aperture, and whether it is stationary or tracks the sun's movement about one or two axes as described above.

For concentrating solar collectors, the solar designer is only interested in the direct (beam) irradiance on the aperture since most concentrating collectors only concentrate the direct irradiance. For flat-plate solar collectors, the global (total) aperture irradiance is of interest since flat-plate collectors are able to absorb both direct and diffuse irradiance.

Direct (Beam) Aperture Irradiance - In Chapter 2, Section 2.1 we discussed the rate of energy falling on a horizontal surface outside the earth's atmosphere and found that it was reduced by the cosine of the angle between the sun and a line normal to the surface. This was called the *cosine effect* or sometimes the *cosine loss* and is described by Equation (2.2) for the extraterrestrial horizontal surface.

The collector aperture irradiance, the rate at which solar energy is incident on the aperture per unit aperture area, may be found from the irradiance measurements discussed to this point. If only the beam component of insolation is of interest (as with most concentrating collectors), the aperture irradiance for beam insolation may be calculated as:

$$I_{b,a} = I_{b,n} \cos\theta_i \qquad \left(W/m^2\right) \qquad (4.28)$$

where $I_{b,n}$ is the beam normal irradiance and (θ_i) is the angle of incidence. Here, the reader can see here the importance of being able to calculate the angle of incidence

Global (Total) Aperture Irradiance - The global aperture irradiance is the sum of the beam plus diffuse and reflected irradiance. The beam irradiance is the same as given in Equation *(4.28)*. The diffuse (sky) and the reflected (ground) irradiance are apportioned by the fraction of the hemispherical view by the aperture above or below the horizon.

$$I_{t,a} = I_{b,n}\cos\theta_i + \left[I_{d,h}\left(\frac{1+\cos\beta}{2}\right) + \rho I_{t,h}\left(\frac{1-\cos\beta}{2}\right)\right] \qquad \left(W/m^2\right) \tag{4.29}$$

where $I_{d,h}$ is the diffuse (scattered) irradiance, $I_{t,h}$ the global (total) irradiance falling on a horizontal surface, the angle β is the tilt angle of the aperture relative to the horizontal and ρ the reflectance of the surrounding surface.

Note here that if the aperture is horizontal, the angle $\beta = 0^\circ$, and only the diffuse (sky) irradiance contributes to the global irradiance. If the aperture is vertical, $\beta = 90^\circ$ and both the diffuse (sky) irradiance and the irradiance reflected from the ground contribute equally.

Data for both direct normal irradiance and global horizontal irradiance are generally available in the TMY2 and other databases (see Chapter 2). The diffuse irradiance can be calculated using Equation (2.9). A table of various ground surface reflectance values is provided in the Appendix.

Using the appropriate equation for angle of incidence derived in Section 4.1 above, the solar designer can now calculate how much global (direct) solar energy is coming to a collector aperture at any time, date and location, and with any orientation or tracking design.

4.2.2 Solar Radiation Energy on a Collector Aperture

The aperture solar radiation energy is the irradiance on the aperture summed (integrated) over a period of time, usually a full day. In some texts and figures in this book, solar radiation energy is also called *irradiation*.

As in Equation (2.3), the daily beam (direct) aperture solar radiation energy is found by integrating the beam aperture irradiance given in Equation (4.28), from sunrise to sunset

$$H_{b,a} = \int_{sunrise}^{sunset} I_{b,a}\,dt \qquad \left(J/m^2\right) \tag{4.30}$$

Likewise, the daily global (total) aperture solar radiation energy is found by integrating the global aperture irradiance given in Equation (4.29), from sunrise to sunset

$$H_{t,a} = \int_{sunrise}^{sunset} I_{t,a}\,dt \qquad \left(J/m^2\right) \tag{4.31}$$

Also of interest are the monthly and annual solar radiation available to a collector. These are obtained by summing values of daily aperture solar radiation energy over the appropriate period.

4.2.3 Examples for Clear Days

The expressions developed so far may be used, along with TMY insolation data to predict the solar resource available to collectors using different tracking methods and orientations. Figure 4.8 and 4.9 show the results of such a study made for Albuquerque, NM. Figure 4.8 represents a typical clear summer day and Figure 4.9 represents a clear winter day. Below we describe some insights that may be observed from inspection of these data.

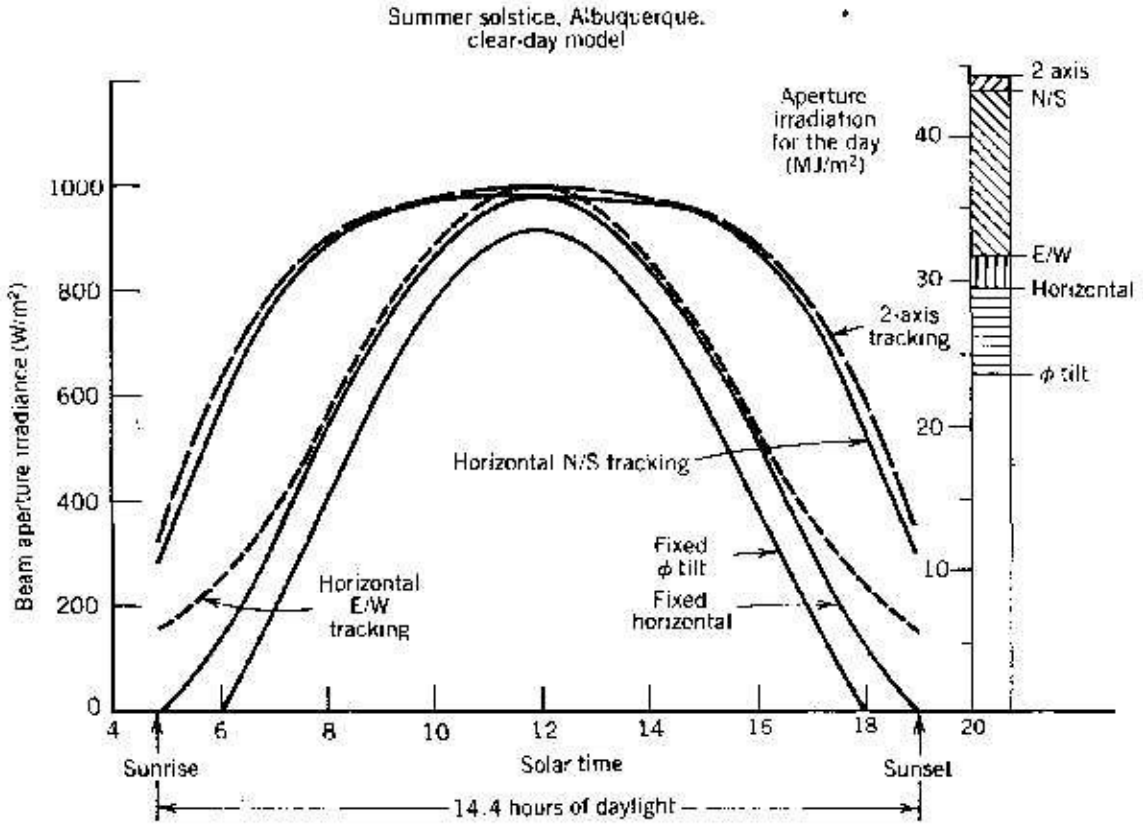

Figure 4.8 Clear-day aperture irradiance for different fixed and tracking aperture configurations for Albuquerque, NM on June 22.

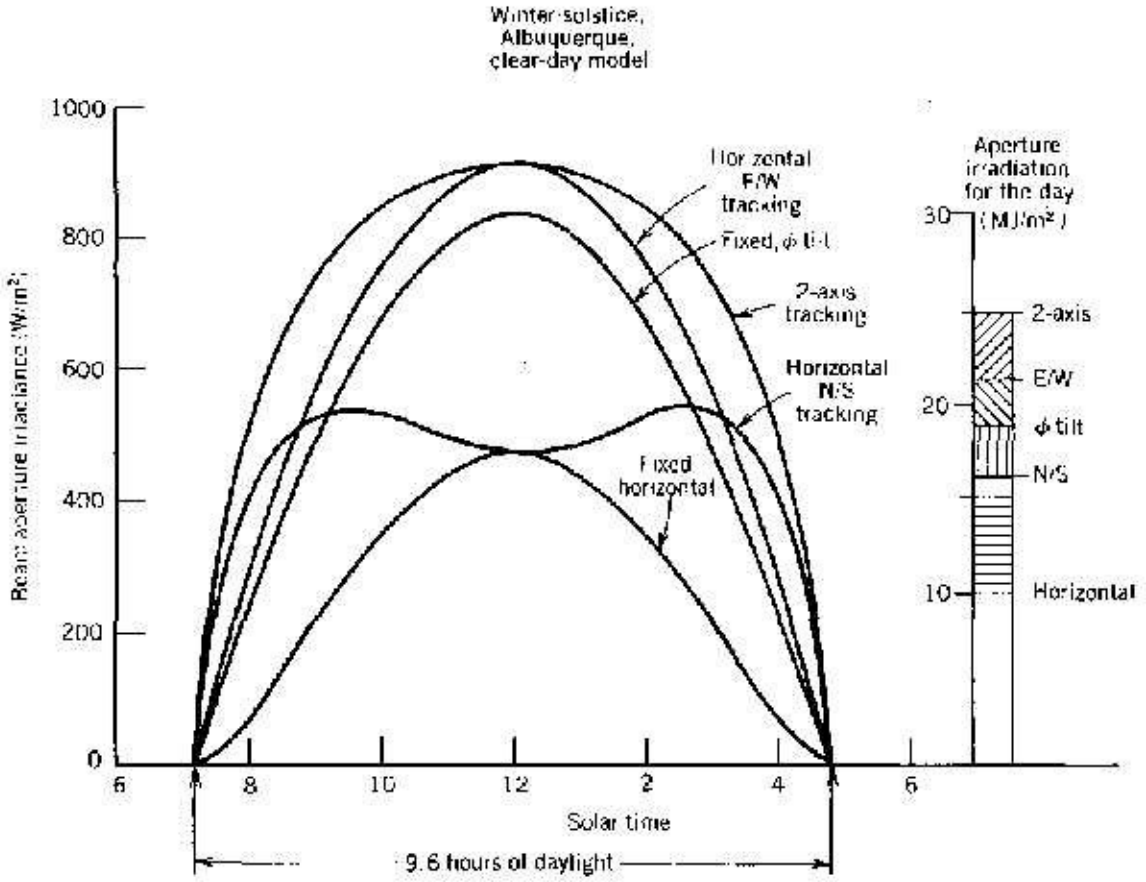

Figure 4.9 Clear-day aperture irradiance for different fixed and tracking aperture configurations for Albuquerque, NM on December 22.

Two-Axis Tracking Apertures - The maximum amount of insolation is collected when a collector aperture points directly toward the sun, and hence the angle of incidence is zero. If a collector aperture can be tracked about two independent axes, the angle of incidence can be maintained at zero throughout the day.

We show in Figures 4.8 arid 4.9 the beam aperture irradiance for a two-axis tracking aperture on the summer solstice and the winter solstice in Albuquerque, using insolation values calculated by the Hottel clear-day model. Also shown on the right-hand side of these figures is the daily aperture solar radiation energy. No method of concentration or tracking can increase these values since there is no cosine effect for a two-axis tracking aperture.

Single-Axis Tracking Apertures - If an aperture tracks the sun by rotation about a single axis, the beam aperture irradiance is reduced by the cosine of the angle between the tracking axis and the sun. This single tracking axis is often about a

horizontal axis that can be oriented in any direction. The equation for the angle of incidence for these apertures was developed as Equation (4.12).

Figure 4.8 shows that in Albuquerque (35º latitude) in the summer, if the single axis is oriented in the north-south (N/S) direction, the reduction in beam aperture irradiance from the two-axis tracking case is minimal. As can be seen on the right-hand side, the difference between the day's solar radiation energy on a N/S-oriented single-axis-tracking aperture and on a two-axis tracking aperture is only about 2 percent.

If the single tracking axis is oriented in the east-west (E/W) direction, the situation is different. For the E/W case, the only time the aperture points toward the sun is at noon. As the sun rises and sets, the cosine effect significantly reduces the rate of energy incident upon the aperture. Over the entire day, the amount of beam solar energy entering the aperture of the E/W single-axis tracker is only 73 percent of the energy that could have been collected if the cosine effect had been zero all day.

In the winter, as shown in Figure 4.9, the reverse is true. The performance of the E/W oriented single axis tracked aperture approaches that of the two-axis tracked aperture even in the morning and afternoon. In fact, the E/W tracking aperture receives 86 percent of the maximum amount of energy, whereas the N/S-oriented single -axis tracking aperture receives only 64 percent of the maximum solar energy for that day.

Taken over the entire year, the N/S-oriented single-axis-tracking aperture receives slightly more energy than does the E/W axis aperture. However, the variation of the daily irradiance over the year is much greater for the N/S axis orientation than for the E/W orientation.

If the demand for energy in a specific solar energy system design is higher in the summer than in the winter (i.e., for crop irrigation or cooling demands), this characteristic of the cosine effect on N/S tracking aperture as may be an advantage. If a somewhat constant demand is envisioned, however, the E/W orientation is usually chosen.

It is interesting that at noontime, the irradiance on the N/S-oriented single axis tracking aperture equals that on a horizontal fixed surface whereas the E/W-oriented single-axis tracking aperture irradiance equals that for a two-axis tracking aperture (i.e., the maximum possible). This is because at noon, the N/S single-axis tracker is pointing straight up and the E/W single-axis tracker is pointing directly at the sun. An examination of Equations (3.35) and (3.37) will convince the reader of this phenomenon.

Fixed Apertures The beam aperture irradiance for fixed-aperture collectors is also shown on Figures 4.8 and 4.9 for summer and winter in Albuquerque. The

equation for the angle of incidence on fixed surfaces was developed as Equation (3.24). One of the surfaces shown here is horizontal and the other tilted up toward the south horizon by an angle equal to the local latitude. This orientation is often selected for flat-plate collector installations since it averages the noontime insolation peaks over the year.

A few points are interesting to note here also. First, a fixed horizontal surface receives more aperture solar radiation energy over the day (28 percent more in Albuquerque) than does a latitude-tilted, south-facing surface in the summer. In the winter, however, the horizontal fixed surface in Albuquerque receives only 49 percent of the daily energy that a latitude- tilted surface does.

4.2.4 Examples Using the TMY Database

Although a clear-day analysis of the cosine effect on apertures with different orientations and tracking capabilities is instructive, the most important solar radiation energy information to a system designer is the impact of tracking and collector orientation over a typical year with its varied insolation patterns. For example, in the winter, N/S-oriented single-axis tracking apertures receive much of their daily solar radiation energy in the early morning and late afternoon. If there were considerable morning and afternoon cloud cover in a particular climate, the performance of this tracking scheme would be even worse than predicted by our clear-day analysis.

Taking TMY beam insolation and applying the cosine of the appropriate angle of incidence to these data, we can develop a plot showing the variation of the monthly average aperture radiation energy over the year. Such a plot is shown in Figure 4.10 for Albuquerque, NM for the same apertures used in Figures 4.8 and 4.9. Even though typical weather data were used to produce these plots, trends similar to those noted before are shown to occur. Note the wide variation in the N/S single-axis tracking aperture solar radiation energy and the relatively constant solar radiation energy on the E/W single-axis-tracking aperture.

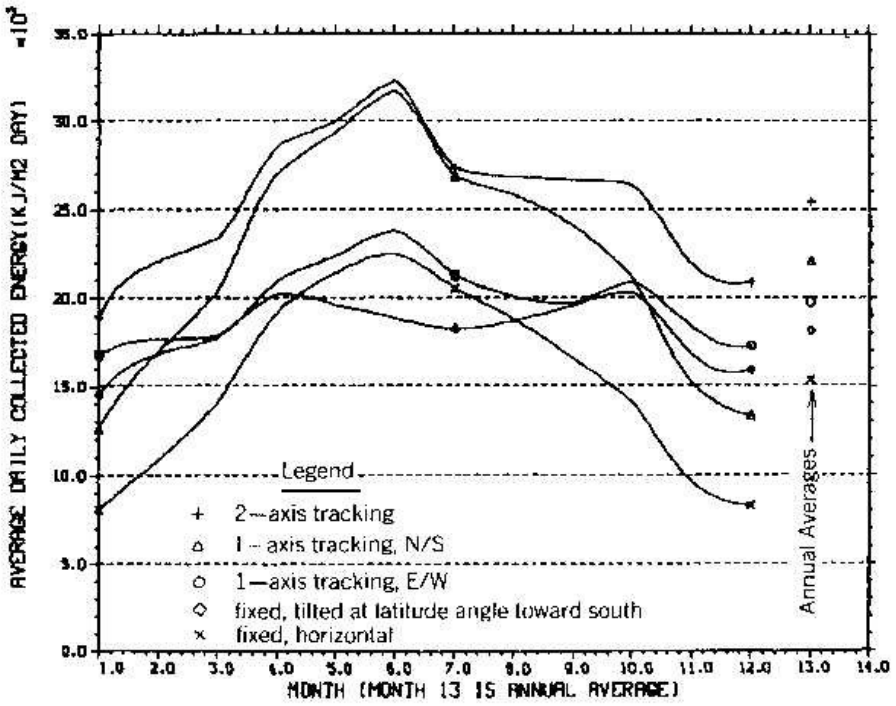

Figure 4.10 Monthly average and annual direct (beam) solar radiation energy incident on different fixed and tracking apertures using TMY data for Albuquerque, NM.

The yearly average daily solar radiation energy on each aperture is shown on the right-hand side, indicating about a 9 percent difference between the E/ W and the N/S single-tracking axis orientation over the year. Note that the increase in aperture solar radiation energy over the year for providing a second tracking axis is about 17 percent for a N/S single-axis-tracking aperture. However, the penalty (relative to the N/S system output) for not tracking an aperture on even one axis is about 31 percent. It is obvious that the system designer must make some important choices as to the type of tracking and orientation of the solar collectors to be used in a system design.

4.3 Algorithm for Aperture Irradiance

We are now at a point where a computer code can be developed to predict aperture irradiance and solar radiation energy. Using the insolation models or databases discussed in Chapter 2 and applying the appropriate sun angle calculations developed here, we can make hour-by-hour computations of the solar energy entering the aperture of a collector. With appropriate summing, the daily aperture solar radiation energy may also be calculated.

In this section we describe the computer code APIRAD, which was written as an example of the use of the equations developed in Chapter 2, Chapter 3 and this

chapter. In actual system design, a code similar to APIRAD would form a portion of the larger system design code package and provide the energy input to the collector model.

A flow diagram for a computer code for calculation of aperture irradiance and solar radiation energy is shown in Figure 4.11. Program APIRAD follows this diagram and calculates the beam irradiance and daily solar radiation energy on a collector aperture. This code is listed in the Appendix**.** The input data required are the day, the location, and the orientation of the collector and whether the collector is fixed or tracks the sun about one or two axes.

Since it doesn't change rapidly, the declination angle may be calculated only once a day. Hourly calculations are then made of the hour angle and the sun's altitude and azimuth. These values are used in the appropriate equation for the cosine of the angle of incidence.

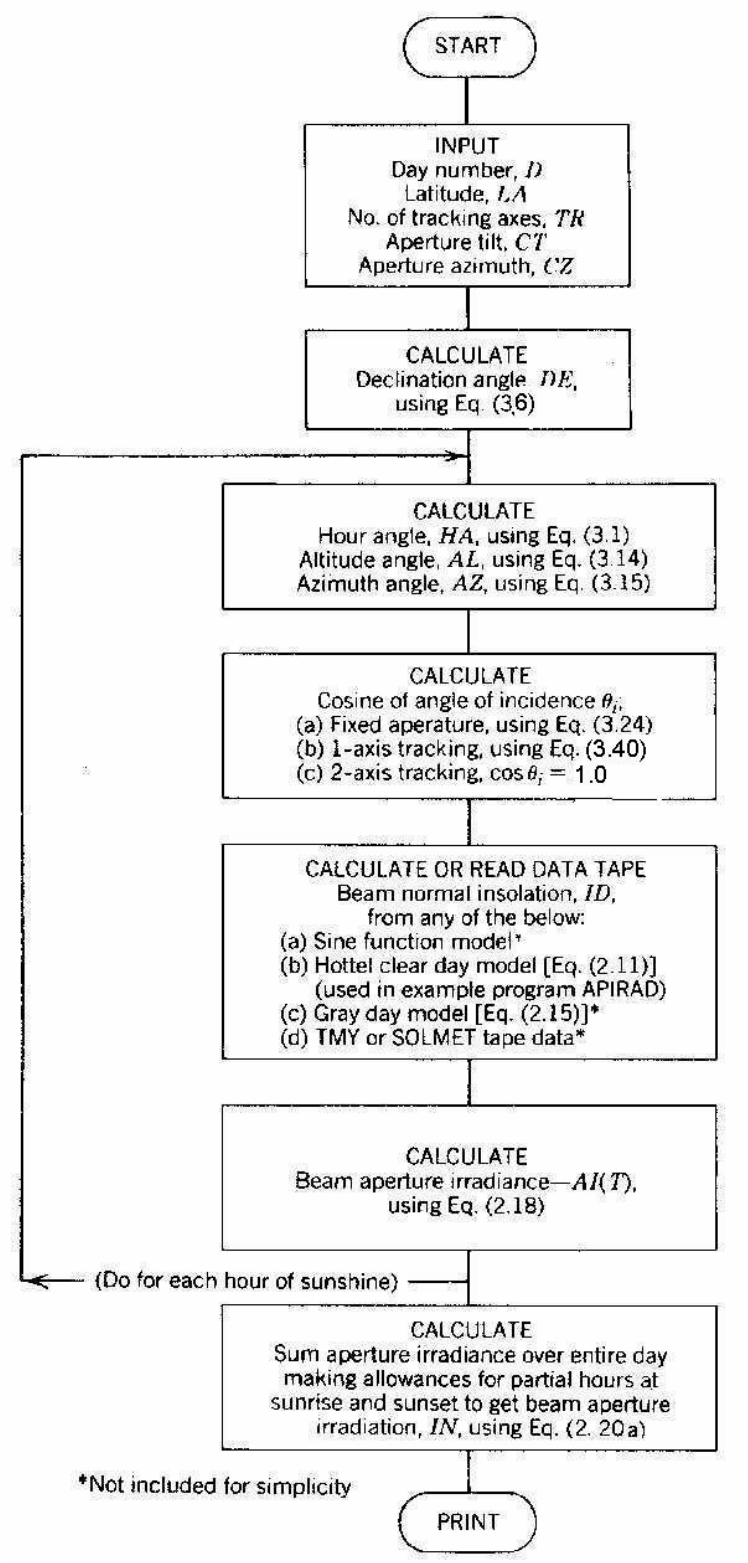

Figure 4.11 Flow diagram for a general program that calculates beam aperture irradiance and solar radiation energy. Program APIRAD in Appendix H follows this sequence.

Aperture irradiance is calculated once per hour and stored in an array *AI* (*T*), where the symmetry about solar noon is used to reduce the number of these computations. If real weather data were used, symmetry would not exist and full -day computations would be required. A test is made at sunrise to determine the daylight portion of that hour. The irradiance is then summed over the day through application of linear averaging between hours to give the daily aperture solar radiation energy.

The program uses the Hottel clear-day model to give the beam insolation component. Using Equation (2.15), we could include diffuse insolation and the global aperture irradiance would then be determined by applying Equation (4.29). The program is not restricted to the use of the Hottel clear-day model. As noted in Figure 4.11, a different insolation model or an insolation database such as the TMY2 tapes could also be used.

4.4 SHADOW - A Simple Model for Collector Field Shadowing

Typically, a solar thermal collector is not an isolated unit but, part of a large assemblage of collectors deployed on a field of finite dimensions. As a result, one collector may block (i.e., shadow) the sun, which would normally be incident on the aperture of another collector. Usually, enough land is provided so that the solar collectors can be spaced far enough apart to minimize shadowing. However, shadowing does occur, and the designer must be able to determine the appropriate field size on which to deploy the solar collectors.

Most computer programs used to analyze shadowing within a field of solar collectors are quite complex and require large computers for execution. However, a reasonable approximation of the impact of shadowing on collector performance can be obtained using a simple geometric model named *SHADOW.*

4.4.1 Parabolic Trough and Flat-Plate Collector Fields

The SHADOW model approximates the non-shadowed collector aperture area. The basic idea is that the total aperture area projected along a line pointing to the sun can never be greater than the field area projected along the same line. For a horizontal collector field, this can be expressed mathematically as

$$A_a \cos\theta_i \le A_f \sin\alpha \qquad \left(m^2\right) \tag{4.32}$$

where:

A_a = total collector aperture area (m^2)

A_f = collector field land area (m^2)

θ_i = angle of incidence between the sun's rays and collector aperture

α = solar altitude angle

If the collector field land is not horizontal, the sine of the altitude angle must be replaced by the cosine of the angle between the sun's rays and a normal to the field surface. To compute collector shadowing in a system performance model, we must incorporate the logic flow outlined in Figure 4.12.

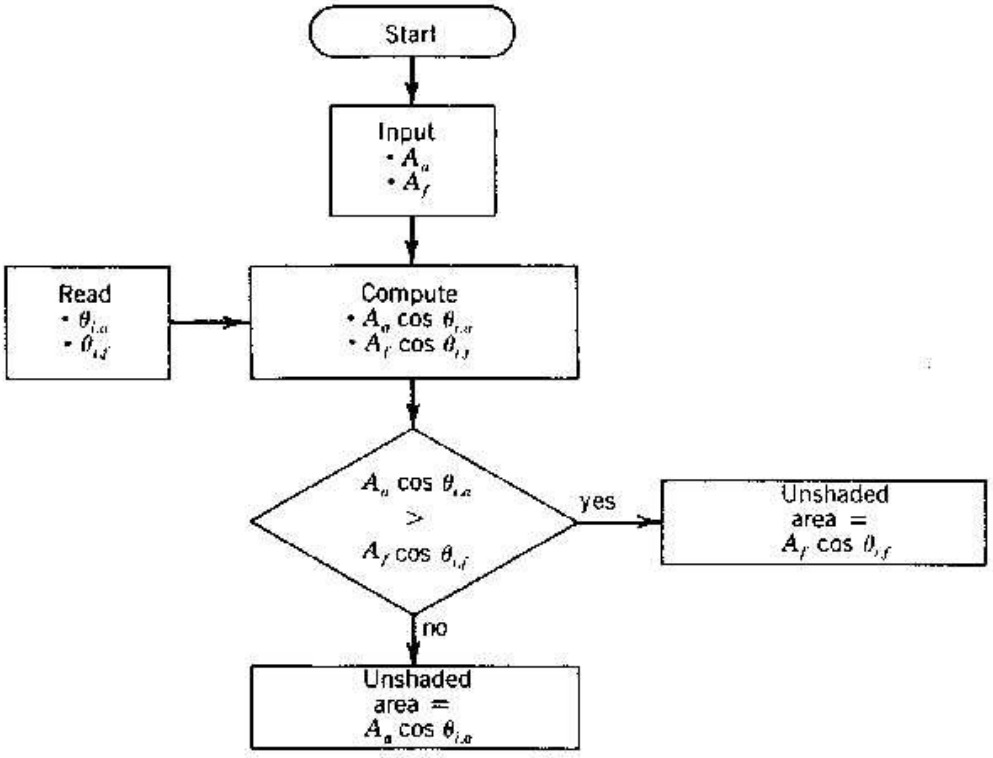

Figure 4.12 Logic flow for the collector shadowing program SHADOW. In actual code, all computations are usually done as ratios of A_a/A_f to provide a "per unit area" basis.

As an example of the impact of shadowing on the amount of direct (beam) solar radiation energy incident on a collector's aperture, Figure 4.13 was prepared for parabolic troughs having two different orientations. The use of the adjective non-first-row refers to the fact that in any collector field; one row of collectors will be non-shaded since there are no collectors between it and the line to the sun. Thus, for example, in an E/W parabolic trough collector field, the north row, is non-shaded when the sun is north of the east-west line whereas the south row is non-shaded when the sun is south of the east-west line.

Likewise, the east row in a N/S-oriented field of parabolic troughs is non-shaded before solar noon whereas the west row is non-shaded after noon. In order to use Figure 4.13, one must remember to also account for the front, non-shaded

row. Similar plots could be generated for flat plates and dishes (if the field layout pattern is known) by using SHADOW as the basic computational tool.

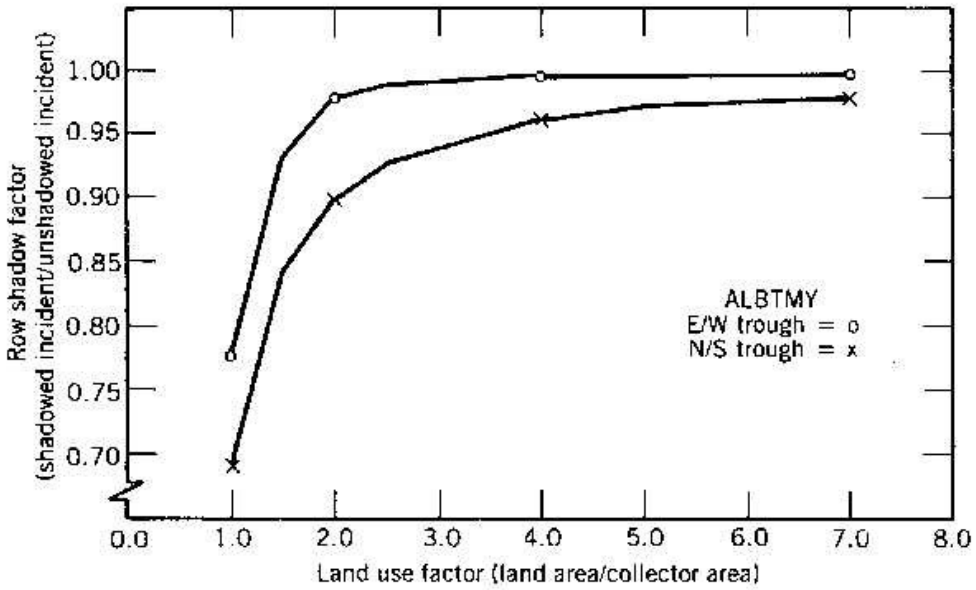

Figure 4.13 Non-first-row shading of annual direct (beam) solar radiation energy incident on parabolic trough collectors.

EXAMPLE: Consider a N/S collector field containing two rows with a land use factor of 2.0. The annual direct (beam) solar radiation energy incident on the non-first-row collector is reduced to 0.895 (i.e., row shadow factor = 0.895 from Figure 4.13) of the non-shaded solar input. However, the annual direct (beam) solar radiation energy incident on the total field is reduced only (1.0 + 0.895)/2 or 0.948 that of the non-shaded field.

4.4.2 Parabolic Dish Fields

For parabolic dishes, the relationship in Equation (4.32) must be modified slightly to account for the fact that circular dishes cannot be packed perfectly into a rectangular field, (this entire analysis assumes land is available in rectangular shapes suited for the deployment of solar collectors.)

As shown in Figure 4.14 for dishes assembled in a diamond pattern, some space remains between the dishes even when they are packed together as closely as

possible. In the layout represented in Figure 4.14, only 90.6 percent of the land area can be covered with dish aperture. Thus, for this case, Equation (4.32) must be modified to

$$A_a \cos\theta_i \le 0.906 \; A_f \sin\alpha \qquad (m) \qquad (4.33)$$

The factor of 0.906 will vary according to the dish layout chosen. Dishes deployed in a square pattern, for example, would have a factor of 0.785. Linn and Zimmerman (1979) discuss dish shadowing in some detail and provide a computer program to compute detailed shadowing within a dish field.

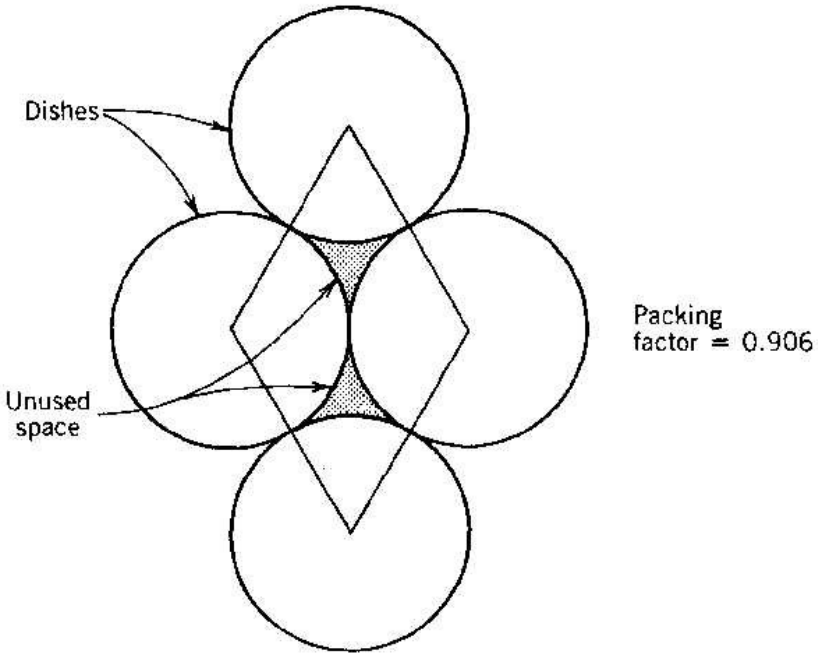

Figure 4.14 Land use for parabolic dishes deployed in a diamond pattern

Summary

Table 4.1 summarizes the angles developed so far, along with their zero value orientation, range and sign convention.

Table 4.1 Sign Convention for Important Angles

Title	Symbol	Zero	Positive Direction	Range	Equation No.	Figure No.
Earth-Sun Angles						
Latitude	ϕ	Equator	northern hemisphere	+/- 90°	---	3.3

Declination	δ	Equinox	summer	+/- 23.45°	(3.7)	3.5
Hour Angle	ω	Noon	afternoon	+/- 180°	(3.1)	3.3
Observer-Sun Angles						
Sun Altitude	α	Horizontal	upward	0 to 90°	(3.17)	3.6
Sun Zenith	θ_z	Vertical	toward horizon	0 to 90°	(3.8)	3.6
Sun Azimuth	A	Due north	clockwise*	0 to 360°	(3.18) or (3.19)	3.6
Aperture-Sun Angles						
Angle of Incidence	θ_i	Perpendicular to aperture	toward aperture	0 to 90°	(4.2)	4.1
Aperture or Axis Tilt	β	horizontal	toward equator	0 to 180°	---	4.1
Aperture or Axis Zenith	γ	due north	clockwise*	0 to 360°	---	4.1
Tracking Angle	ρ	aperture normal vertical	counter-clockwise*	0 to 360°	(4.8)	4.2
Aperture Offset on Axis	μ	parallel to tracking axis	counter-clockwise*	+/- 90°	---	4.6

* looking down + axis toward origin

References

Linn, J.K. and J.C. Zimmerman (1979), *A Method for Calculating Shadows Cast by Two-axis Tracking Solar Collector*s, Report SAND79-0190, Sandia National Laboratories, Albuquerque NM, November.

Zimmerman, J. C. (1981), *"Sun Pointing Programs and Their Accuracy"* Sandia National Laboratories Report SAND81-0761, September.

5.

Solar Collectors

Solar collectors capture incident solar radiation energy and either convert it to heat (thermal energy) or directly to electricity (photovoltaic cells). In Chapter 4 we developed the equations necessary to predict the amount of solar irradiance or energy falling on a solar collector. We looked at different cases of tilting and tracking the collectors to optimize the solar input. In this chapter, we study how a solar collector absorbs and converts solar energy into thermal energy or electricity as in the case of photovoltaic panels. The topics covered in this chapter are:

We will first look at solar thermal collectors and then at photovoltaic modules. Here we derive the energy balance for thermal collectors, without regards to the specific type; that will be dealt with in the following chapters. We will also understand the energy balance for a photovoltaic module, without going into the details of the electro-physics of the processes happening within the cells.

Prior to an examination of specific collector concepts, this chapter shows the development of a widely used yet simple model for prediction of the thermal energy output (i.e., performance) of various solar collectors. The model is applicable to all (including the central receiver with some extension) collector concepts and hence is discussed separately from any one collector concept to avoid the misunderstanding that the model is useful only for that one concept.

Although the presentation of a model for computation of collector performance before discussion of the individual collector design concepts may seem strange, system design can proceed if certain thermodynamic characteristics are known, without detailed knowledge of what the collector looks like. Usually, collector performance is determined from experimental data of prototype hardware. A particularly important feature of the performance models discussed in this chapter is that it exploits such data and extends it to different operating conditions. If experimental data are not available, the designer must resort to an analytical description of the collector's performance, which is always risky.

In a similar manner, a simple model of photovoltaic panel performance is presented. Like the thermal collector performance model, it is based on experimental data that is modified for operating parameters different from a 'standard' condition.

5.1 Thermal Collector Capture and Loss Mechanisms

To perform an energy balance on a solar thermal collector, one usually isolates the surface that absorbs the incoming radiation, and balances energy inflow and outflow to and from it. In a flat-plate collector, this is called the 'absorber plate' and for a concentrating collector, it is often called the 'receiver'. In subsequent chapters we will describe many details of construction, surfaces for each type of collector, but for now, this is not important. The energy balance on a solar collector absorber or receiver can be written as;

$$\dot{Q}_{useful} = \dot{E}_{opt} - \dot{Q}_{loss} \qquad (W) \qquad (5.1)$$

where:

$\dot{Q}_{useful}$ - rate of 'useful' energy leaving the absorber (W)

$\dot{E}_{opt}$ - rate of optical (short wavelength) radiation incident on absorber (W)

$\dot{Q}_{loss}$ - rate of thermal energy loss from the absorber (W)

The 'useful' energy for a solar thermal collector is the rate of thermal energy leaving the collector, usually described in terms of the rate of energy being added to a heat transfer fluid passing through the receiver or absorber, i.e.:

$$\dot{Q}_{useful} = \dot{m} c_p \left(T_{out} - T_{in} \right) \qquad (W) \qquad (5.2)$$

where:

$\dot{m}$ - mass flow rate of heat transfer fluid (kg/s)

c_p - specific heat of heat transfer fluid (J/kg·K)

T_{out} - temperature of heat transfer fluid leaving the absorber (K)

T_{in} - temperature of heat transfer fluid entering the absorber (K)

These losses are shown schematically in Figure 5.1.

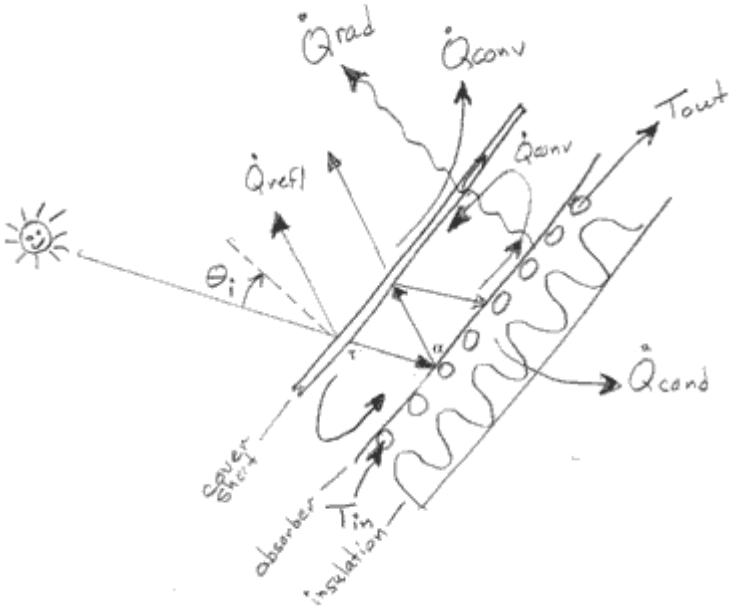

Figure 5.1 Energy balance on a solar collector absorber / receiver.

5.1.1 Optical Energy Capture

The rate of optical (short wavelength) radiation incident on absorber/receiver will be the solar irradiance resource for that type of collector and its tracking (global (total) solar irradiance for a flat-plate collector and direct (beam) solar irradiance for a concentrating collector). Since the capture area of the collector may not be aimed directly at the sun, this resource must be reduced to account for the angle of incidence as described previously in Section 4.1. The area of the collector on which the solar irradiance falls is called the *aperture* (opening) area of the collector. The incident solar resource then is:

$$\dot{E}_{inc} = I_a A_a \qquad (W) \qquad (5.3)$$

where:

I_a - solar irradiance entering the collector aperture (global (total) or direct (beam))(W/m^2)

A_a - aperture area of the collector (m^2)

This solar resource is reduced by a number of losses as it passes from the aperture of the collector to the absorber. These processes depend on the type and design of the specific collector, but here we include the important optical loss mechanisms, and will drop the unimportant terms in future chapters as we discuss specific types of collectors. The rate of optical (short wavelength) energy reaching the absorber or receiver is the product of the incoming solar resource multiplied by a number of factors, all less than 1.0 describing this reduction:

$$\dot{E}_{opt} = \Gamma \rho \tau \alpha I_a A_a \qquad (W) \qquad (5.4)$$

where:

Γ - capture fraction (fraction of reflected energy entering or impinging on receiver)

ρ - reflectance of any intermediate reflecting surfaces

τ - transmittance of any glass or plastic cover sheets or windows

α - absorptance of absorber or receiver surface

The first two terms above apply only to concentrating collectors. The *capture fraction* Γ is a measure of both the quality of the shape of the reflecting surface, and the size of the receiver. Often this is described in terms of '*spillage'*

i.e. the fraction of reflected energy not impinging on or entering the receiver. A poorly shaped concentrator, or a receiver too small will make this number considerably less than 1.0. An analytical method for calculating this term is presented in Chapter 8, Concentrator Optics.

Reflectance is a property of any reflecting surface associated with the collector. The importance of this property will also will be discussed in more detail in Chapter 8 (Concentrator Optics). Properly designed concentrators will have capture fractions of 0.95 or higher, and silver/glass mirrors can have a reflectance of 0.94 and new aluminum reflecting surfaces have a reflectance of about 0.86.

The *transmittance* is the fraction of solar radiation passing through all transparent cover material that sunlight passes through on its way to the absorber. Cover sheets of glass or plastic are used on flat-plate collectors, above the absorber to reduce convective heat loss.

For parabolic trough collectors a glass tube surrounds the absorber tube for the same reason. High-temperature cavity receivers may incorporate a quartz glass cover to keep the gas in the receiver separate from outside air or to permit pressurization of the gas within the cavity. In all cases, the use of a cover sheet reduces the solar radiation passing to the receiver/absorber. Their benefit for reducing heat losses from the absorber must at least balance this reduction.

The transmittance in Equation (5.4) is the average overall transmittance and represents the total reduction in transmitted energy in the solar spectrum by all covers. For example, flat-plate collectors may have two or more cover sheets, sometimes of different materials, with the transmittance, τ being the product of each individual cover transmittance.

Transmittance of the cover also depends on the wavelength of light passing through it. Glass for example transmits most radiation in the visible spectrum, but does not transmit much in the infrared region. Therefore, an absorber covered with glass will receive most of the incoming, short wavelength radiation, but will not transmit much of the long wavelength radiation loss coming from the absorber. This characteristic of glass is the reason that glass greenhouses loose very little energy at nighttime. Carbon dioxide buildup gives our atmosphere a similar property and therefore the name ‘greenhouse effect’.

On the other hand, plastic covers have high transmittance values at very long wavelengths. Solar collectors using plastic covers can be used for nighttime cooling since radiation loss to the nighttime sky can be significant. This is also why greenhouses in warm climates use plastic rather than glass as a cover. Without nighttime long-wavelength radiation loss, the average temperatures would be too high for optimal plant growth.

The *absorption* term α represents the fraction of solar energy incident upon the surface, that is absorbed (the remainder being reflected). A good black surface can have an absorption of greater than 0.98, however, as surfaces degrade, this value can decrease. It is important to point out that this property is for radiation in the solar or 'visible' spectrum. For most real surfaces, the absorption varies as a function of the wavelength of the incident energy. We will discuss below that there is a class of surfaces used in solar collectors, called '*selective surfaces'* that have a higher absorptance in the visible spectrum than at longer wavelengths, thereby reducing thermal radiation loss.

In summary then, when performing an energy balance on the absorber plate or receiver of a solar collector, there are four important mechanisms that reduce the amount of solar energy that is incident on the collector aperture; imperfect reflection, imperfect geometry, imperfect transmission and imperfect absorption. This is a general statement, and different collector types will either include or not include these losses depending on the design.

5.1.2 Heat Loss Mechanisms

Once the solar energy resource (short wavelength radiation) has made its way down to the surface of the absorber or receiver of a collector, it raises the temperature of the absorber above ambient temperature. This in turn starts a process of heat loss from the absorber as with any surface heated above the temperature of the surroundings. These loss mechanisms are convection, radiation and conduction, and all are dependent on, among other things, the difference in temperature between the absorber and the surroundings.

$$\dot{Q}_{loss} = \dot{Q}_{loss,convection} + \dot{Q}_{loss,radiation} + \dot{Q}_{loss,conduction} \qquad (W) \qquad (5.5)$$

Because a solar thermal collector is designed to heat a fluid, there is a balance between the rate of heat being removed by the heat transfer fluid and the heat loss by radiation, convection and conduction as defined by Equation (4.1). Since heat loss increases with temperature, this balance between heat removal and heat loss defines the operating temperature of the collector.

If the heat transfer fluid removes too much heat, the temperature of the absorber decreases, reducing heat loss. If not enough heat is removed from the absorber, the absorber temperature increases, increasing the rate of heat loss. This can pose a major problem for concentrating collectors, because when not enough heat is being removed (as can happen if the flow of heat transfer fluid is interrupted), the temperature of the absorber can increase to its melting temperature.

Convection Loss - Convective heat loss of a solar collector receiver is proportional to the surface area of the absorber or receiver, and the difference in temperature between the absorber surface and the surrounding air. It can be written in general terms as:

$$\dot{Q}_{loss,convection} = \bar{h}_c A_r \left(T_r - T_a\right) \qquad (W) \qquad (5.6)$$

where:

$\bar{h}_c$ - average overall convective heat transfer coefficient ($W/m^2 K$)

A_r - surface area of receiver or absorber (m^2)

T_r - average temperature of receiver (K)

T_a - ambient air temperature (K)

As with the other heat loss equations below, this is a simplified, instructive model. Usually there are a number of convective processes that cause an absorber or receiver to loose heat to the surroundings. For example, a flat-plate collector often has a glass cover sheet between the absorber plate and outside ambient air. There is one convection process between the hot absorber and the cover sheet, and a second between the cover sheet and outside air. Also, wind increases the heat transfer coefficient on the cover sheet and must be included in any serious analysis of convective heat loss.

For parabolic dish concentrators, the absorbing surface is typically placed inside of a cavity. This protects it from wind, and naturally driven air currents. Little is known about convective heat loss from an open cavity, but it is clear that the position of the cavity and its internal temperature, along with wind speed and direction all affect the rate of heat loss from a cavity (Stine & McDonald, 1989, Paitoonsurikarn et. al., 2003).

Finally, the average temperature of the absorber / receiver, T_r $T_r T_r$ is not a fixed or measurable quantity. The temperature of the absorber / receiver near the heat transfer fluid inlet will be lower than near the outlet, and both will be less than intermediate surfaces not in contact with the heat transfer fluid. Further, since convection is a surface phenomenon, also is driven by the surface temperature, this temperature may be that of a paint or coating rather than the metal below.

Even with all of these imperfections, it is instructive to consider the convective heat loss as being proportional to surface area and the difference between some average temperature, and ambient temperature.

Since convective heat loss is the major heat loss term for most solar collectors, inventors and designers have incorporated many features to collector design to reduce this term. Examples that will be discussed under the different collector designs are; multiple transparent cover sheets for flat-plate collectors, glass tubes surrounding linear absorbers with a vacuum drawn in the intervening space, concentration of solar energy so that the absorber area is small relative to the capture area, absorbers within cavities incorporating glass windows, just to name a few.

Radiation Loss - Radiation heat loss is important for collectors operating at temperatures only slightly above ambient, and becomes dominant for collectors operating at higher temperatures. Figure 5.2 illustrates this transition for a black vertical surface in still air. The rate of radiation heat loss is proportional to the emittance of the surface and the difference in temperature to the fourth power. Described in equation form, we have:

$$\dot{Q}_{loss,radiation} = \varepsilon \sigma A_r \left(T_r^4 - T_{sky}^4 \right) \qquad (W) \qquad (5.7)$$

where:

ε - emittance of the absorber surface (or cavity in the case of a cavity receiver)

σ - the Stefan-Boltzmann constant (5.670×10^{-8} W/m^2 K^4)

T_{sky} - the equivalent black body temperature of the sky (K)

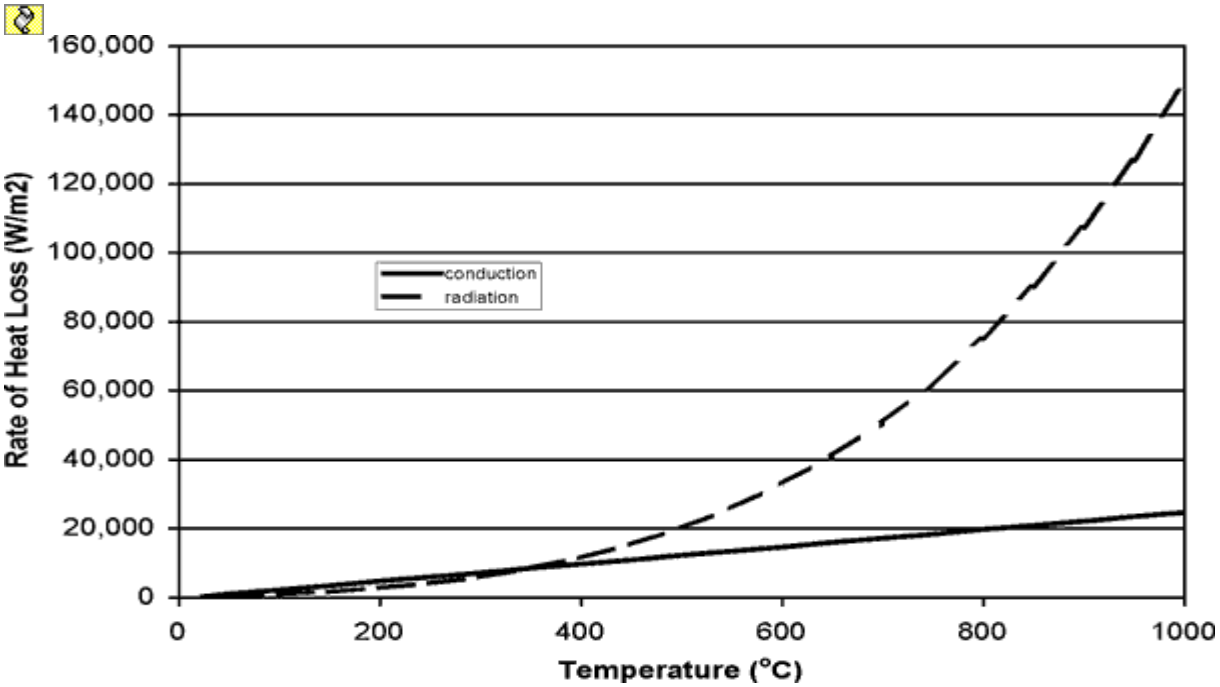

Figure 5.2 Comparison of radiation and convection heat loss for a black, vertical surface in free air at 25◦C.

Terms in this equation over which the collector designer has some control, are the surface emittance and receiver. Surfaces that have a low emittance often have a low absorptance as well, reducing the absorbed solar energy as described in Equation (4.4). However there is a class of surface coatings called '*selective coatings*, that have low values of emittance when the surface is at relatively low temperatures, but high values of absorptance for solar energy. These surfaces are discussed in Section 4.1.4 below.

The other term, which may be minimized, is the receiver surface area. As with convection loss, concentration of solar energy is the main design tool for reducing radiation heat loss by reducing receiver surface area. In addition, cavity receivers can be used since they have small openings through which concentrated solar energy passes, onto larger absorbing surfaces.

Since solar collectors operate out of doors, and generally face the open sky, they exchange radiation with the sky. The equivalent radiation temperature of the sky depends on the air density and its moisture content. When the relative humidity is high and at sea level, the sky temperature can be assumed to be the same as ambient air temperature. However, for low relative humidity or at high altitudes, the sky radiation temperature can be 6 to 8◦C less than ambient temperature. Of course if there is no atmosphere as with space applications, the equivalent sky temperature approaches 0K.

Conduction Loss - The final mode of heat loss to consider in collector design is heat conduction. This is generally described in terms of a material constant, the thickness of the material and its cross-section area:

$$\dot{Q}_{loss,conduction} = \bar{k}\,\Delta\bar{x} A_r \left(T_r - T_a\right) \qquad (W) \qquad (5.8)$$

where:

$\bar{k}$ - equivalent average conductance (W/m·K)

$\Delta\bar{x}$ - the average thickness of insulating material

Conduction loss is usually small compared to convection and radiation losses and therefore is combined with the convection loss term in most analyses. However, it is displayed here for completeness, and to emphasize the importance of ensuring that this mode of heat loss is minimum in any collector design.

In flat-plate collectors, the sides and back surface of the absorber plate should incorporate good insulation (low k) and the insulation should be thick enough to render this heat loss insignificant.

Another important mode of conduction loss is the way the high-temperature absorber is attached to the frame and support structure. Use of low conductance materials such as stainless steel can reduce conduction loss into the frame or support casing. However, since most design issues around conduction can be handled without reducing the solar input, the term is generally combined with the convective heat loss term.

5.1.3 Thermal Energy Balance

In order to provide a single expression for the useful energy produced from a solar collector based on an energy balance of the receiver or absorber, we can combine Equations (4.1) through (4.8) into a single equation. This equation will be repeated in the next few chapters as we develop an understanding of how and why specific types of collectors are designed the way they are.

$$\dot{Q}_{useful} = \dot{m} c_p \left(T_{out} - T_{in}\right) = \Gamma\rho\tau\alpha I_a A_a - A_r\left[h'\left(T_r - T_a\right) + \varepsilon\sigma\left(T_r^4 - T_{sky}^4\right)\right] \qquad (W)$$

(5.9)

where:

h' - combined convection and conduction coefficient (W/m²K)

This equation states that the rate of useful energy produced by a solar collector equals the optical (short wavelength) energy absorbed on the absorber surface, minus the rate of heat loss from the absorber. We have combined the convection heat loss term with the convection term for simplicity.

5.1.4 Selective Surfaces

At this point in developing an understanding of solar energy capture and loss mechanisms, we have introduced two important properties in solar collector design, absorptance, α and emittance, ε. A category of surfaces called '*selective surfaces'* has been developed to optimize these parameters for the collection of solar energy and it is important to understand their physical principles.

Looking at Equation (4.9), one can see that, to maximize the useful heat collected by a solar collector, the absorber or receiver of a solar collector should have a high absorptance and a low emittance. However, we remember from radiation heat transfer theory that, at least for black body and gray surfaces, the absorptance α equals the emittance ε. However for all surfaces, Kirchoff's Law states that they are equal only for radiation at a specific wavelength, not as an average property integrated over a spectrum. Kirchoff's law states that:

$$\alpha_\lambda = \varepsilon_\lambda \qquad (5.10)$$

where the subscript indicates that these are 'spectral' properties and must be integrated over all wavelengths to represent the properties used in Equations (4.4) and (4.7). If the spectrums are different, the integrated properties can be different.

In solar collectors, the spectrum of the energy being absorbed is from a 6,050K black body emitter with peak intensity at a wavelength of 0.48 microns (see Table 2.3). The spectrum of the energy being emitted by the absorber / receiver is defined by the temperature of the absorber surface, T_r which is considerably less. For example if the receiver surface temperature is 80°C, the peak intensity is at a wavelength of 8.21 microns.

Selective surfaces have a high absorptance (and emittance) for short wavelength (visible) light and have low average absorptance and emittance for long wavelength radiation (thermal or infra-red radiation). They do not violate Kirchoff's law, however, we say that they have 'high absorption and low emittance' meaning high absorption for short wavelength radiation, and low emittance for long wavelength radiation. The end result is a surface that absorbs solar energy well, but does not radiate thermal energy very well.

The concept of a selective surface is illustrated in Figure 5.3. Consider a hypothetical surface with 0.95 absorptance at wavelengths shorter than 5

microns and 0.25 for longer wavelengths. Since 99.5% of solar energy occurs at wavelengths below 5 microns as discussed in Chapter 2, Section 2.1.2, the effective absorptance of such a surface is 0.945. The integrated emittance for this hypothetical surface depends on its temperature. If this surface is 80◦C as is typical for hot water system collectors, 99.1% of its radiant energy is at wavelengths above microns and the integrated emittance for this surface is 24.8%.

On the other hand, the effect of using a selective surface is less dramatic on higher temperature absorbers. If the absorber surface is at a temperature of 700◦C as is typical for receivers in parabolic dish concentrating collectors, only 43.6 % of its radiated energy is at wavelengths above 5 microns and the integrated emittance is 64.5%.

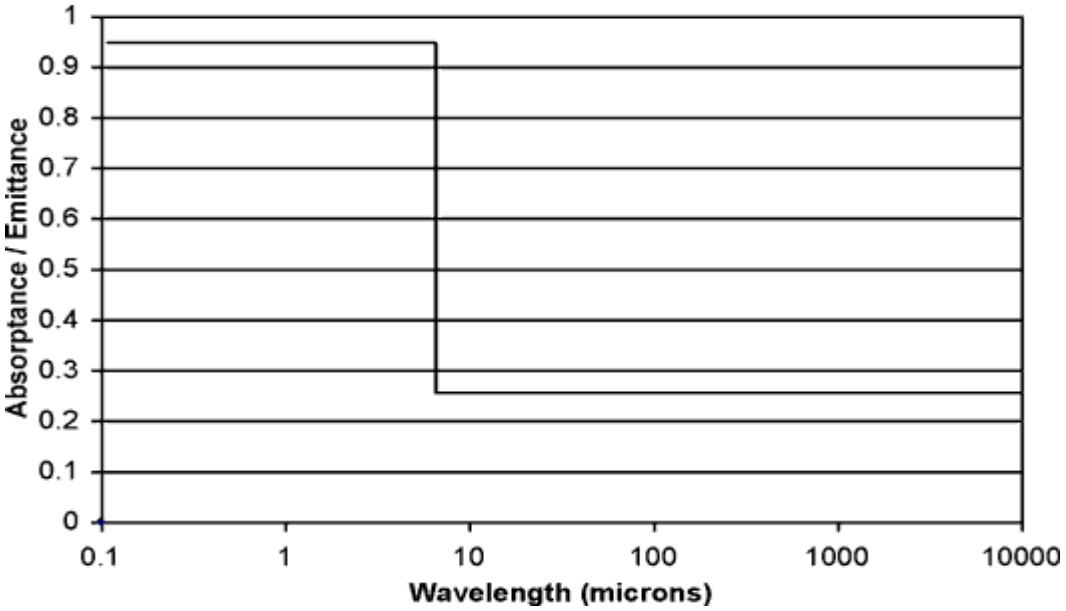

Figure 5.3 Radiation properties of a hypothetical selective surface.

Selective absorbers have been developed that employ composite coating to produce absorbers with the combined properties of high absorptance in the solar spectrum and low emittance in the IR part of the spectrum.

Several coatings have been examined for potential application as selective absorbers. Perhaps the most widely used selective surface in thermal collectors is *black chrome.* Typically, a thin (2-3 μm thick) black chrome coating is electro-deposited on a mild steel receiver tube that has been electroplated with 25 μm of bright nickel.

The coating is deposited, as microscopic particles of chromium metal that, because of their geometry, effectively trap the incident light, making the coating look black. Although the black chrome coating is highly absorbing in the visible

spectrum, it is transparent in the IR region. Thus the receiver takes on the lower emittance of the bright nickel substrate. The resultant composite bright nickel-black chrome coating thus has high absorptance (approximately equal to 0.95) for the incident solar radiation and low emittance (less than 0.25) in the infrared region.

5.1.5 Parabolic Trough End-loss

One final loss mechanism to consider, which is particular to parabolic troughs, is called *end-loss.* This is the fraction of energy being reflected from the trough that falls beyond the receiver. This loss is proportional to the angle of incidence. End-loss will be illustrated in Chapter 9 of this text.

5.2 Photovoltaic Panel Capture and Loss Mechanisms

An energy balance on a photovoltaic panel provides less useful information to the solar energy system designer. However since the photovoltaic cell efficiency decreases with increases in panel temperature, it is important for the rate of heat loss from the panel to be high rather than low! In other words, while the solar thermal panel must be hot to provide useful energy, photovoltaic panels should remain cool to maximize their output of useful energy (electricity in this case).

An energy balance of a photovoltaic cell incorporated within a panel can be written as:

$$P_{elect} = i \cdot v = \dot{E}_{opt} - \dot{Q}_{loss} \qquad (W) \qquad (5.11)$$

where:

i - electrical current through the cell (amps)

v - voltage across the cell (volts)

and the rate of optical radiation incident on the cell and the rate of thermal energy loss from the cell have the same meaning as in Equation (5.1).

There is a physical limit to the fraction of useful energy that can be produced from the incident optical radiation. Depending on the type and design of the cell this can be from 1 percent to 30 percent. This requires that the rest of the remaining 70% to 99% of the incident energy, be lost through heat loss mechanisms.

5.2.1 Optical Energy Capture

Just as Equation (4.4) was instructive in understanding the potential loss mechanisms for a thermal collector, it likewise describes the potential loss mechanisms for a photovoltaic cell. In a concentrating photovoltaic panel, energy incident on the cell is reduced by the reflectance, ρ of the intermediate reflecting surfaces, and the fraction of reflected energy that falls on the cell, Γ. The transmittance, τ of the cover sheet used to physically protect the cell surface and to keep moisture and oxygen away from the electrical contacts, further reduces the optical energy incident on the cell.

5.2.2 Heat Loss

Heat loss from the panel follows the same three paths, convection, radiation and conduction. Optimizing those factors that *increase* heat loss without increasing cell temperature are important for well designed photovoltaic panels. Maximizing heat loss for concentrating PV collectors is more difficult due to the reduced cell surface area resulting from concentration.

5.2.3 Energy Balance

The detailed energy balance for a photovoltaic cell in a panel can be written in a manner similar to Equation (4.9), replacing the receiver/absorber temperature term with the temperature of the cell:

$$P_{elect} = i \cdot v = \Gamma \rho \tau \alpha I_a A_a - A_r \left[h' \left(T_c - T_a \right) + \varepsilon \sigma \left(T_c^4 - T_{sky}^4 \right) \right] \qquad (W)$$

(5.12)

where:

T_c- temperature of the cell (K)

A_c - area of the cell surface (m^2)

5.2.4 Photovoltaic Panel Performance

Performance of a photovoltaic panel or concentrating photovoltaic collector can be described in terms of its voltage and current output. The electrical power output from the panel is the product of these two variables. Voltage and current vary with the intensity of the solar irradiance and the temperature of the cell, all of which are described in the following figures. These figures were derived from real data taken on a commercial photovoltaic panel of approximately 0.65 m^2. However, only the trends are important here and the solar designer should obtain similar information from the manufacturer of the specific panel or concentrator to be used in their design.

The I-V Curve - The fundamental performance of a photovoltaic panel is represented by Figure 5.4, called an *I-V curve*. It is a plot of the voltage across the panel for different values of current. Since the voltage is a product of the current and the load resistance, lines of constant load resistance are shown to complete the description.

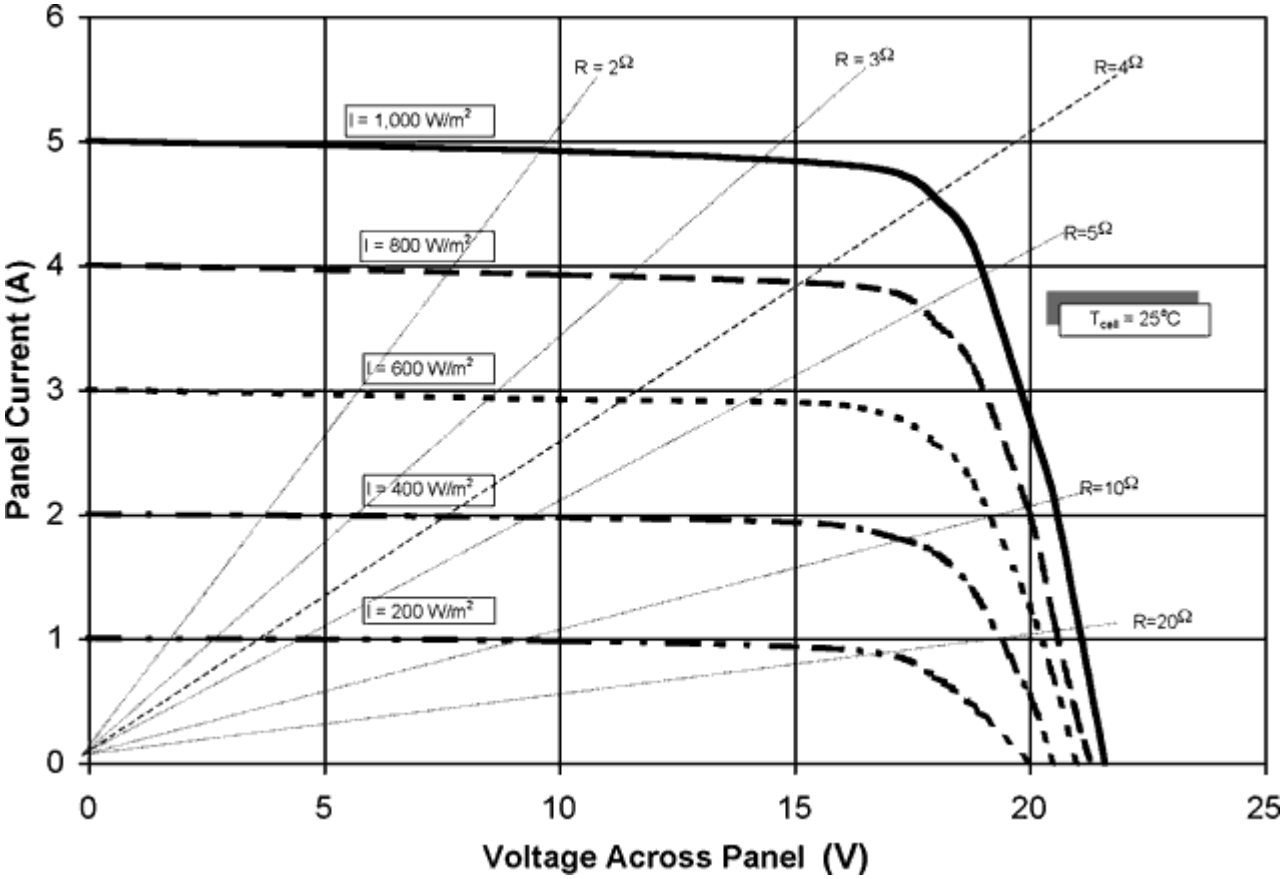

Figure 5.4 Photovoltaic panel output current as a function of the voltage across the panel. These I-V curves are shown for different levels of insolation. Also superimposed on graph are lines of constant load resistance. Data are for a cell temperature of 25°C and an air mass of 1.5.

At low values of load resistance, the current is a maximum and the voltage across the cell approaches zero. This condition is equivalent to a short-circuit across the cell, and the current output at zero voltage is called the *short-circuit current* or I_{sc}. This current is a function of the size of the photovoltaic cell, and the number of cells connected in parallel.

It can also be seen that the short-circuit current is also directly proportional to the level of solar irradiance. This characteristic is why photovoltaic cells can be used as a transducer to measure solar irradiance as discussed in Chapter 2.

As the load resistance increases, the current decreases slightly until a point is reached where the cell can no longer maintain a high current level, and it falls to zero. The point at which the panel current falls to zero represents an infinite resistance or an open circuit. The voltage across the panel at zero current is called the open-circuit voltage, V_{oc}, and represents the output of the unloaded panel. Note that the open-circuit voltage varies only a small amount as a function of solar irradiance (except at very low levels).

A single silicon photovoltaic cell produces an open-circuit voltage of slightly over 0.55 volts. The voltage produced by a photovoltaic panel is a function of how many cells are connected in series. In the case of the panel described below, there must be about 36 photovoltaic cells connected in series in order to produce over 20 volts.

Peak Power Point The basic performance parameter required for a photovoltaic panel is neither voltage nor current but electrical power. Since electrical power is the product of current times voltage, one notes that there is no power produced at either extreme of the I-V curve. However, as the load resistance increases from the short-circuit current condition, the voltage rises until the I-V curve starts falling to the open circuit point. There is a point along the curve where the maximum power is generated which occurs just as the I-V curve 'breaks'. This point is called the *peak power point* (PPP). Figure 5.5 shows the electrical power output of the photovoltaic panel in Figure 5.4.

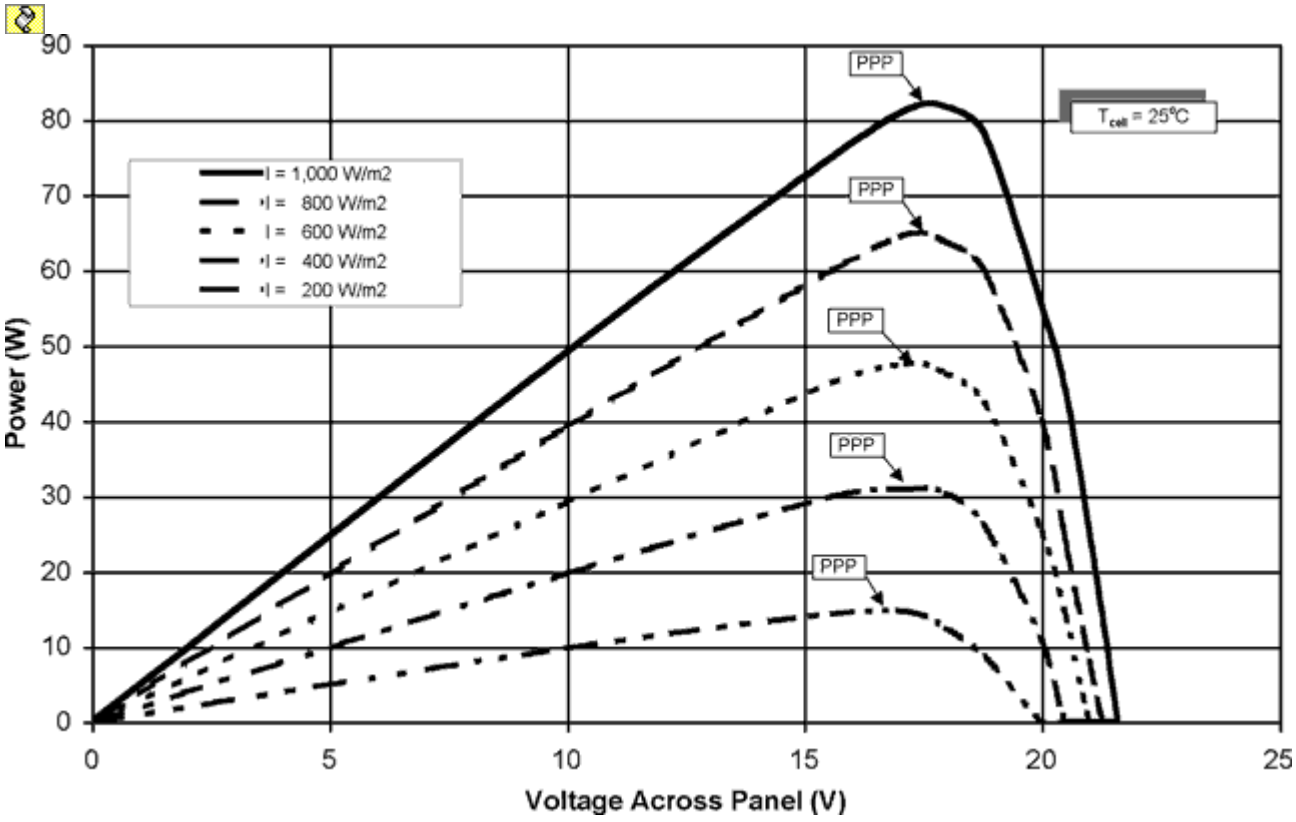

Figure 5.5 Power output of a photovoltaic panel at different levels of solar irradiance. The notation PPP defines the peak power point. Data are for a cell temperature of 25°C and an air mass of 1.5.

Note that the peak power output occurs at a panel voltage of about 80% of the maximum open-circuit voltage, for a wide range of solar irradiance levels. In order to maintain maximum electrical power output from a photovoltaic panel, the load resistance should match this point. As can be seen on Figure 5.4, the load resistance must increase as solar irradiance decreases in order to maintain maximum power output from the panel.

Since the resistance of most electrical loads are fixed (except for electrical motors and batteries), special consideration must be taken in the system design to ensure that the maximum potential of the solar panel is utilized. There are electronic devices, called *peak power trackers* that ensure that the panels are operating close to their peak power point.

Cell Temperature Loss - An important characteristic of the photovoltaic cell is the reduction of output voltage as cell temperature increases. Figure 5.6 shows this characteristic for the photovoltaic panel described in Figures 5.4and 5.5. Although not obvious on this curve, the short circuit current increases slightly with temperature. Typical values for these changes are — 4% V_{oc} and +0.5% I_{sc} for a 10°C change in cell temperature.

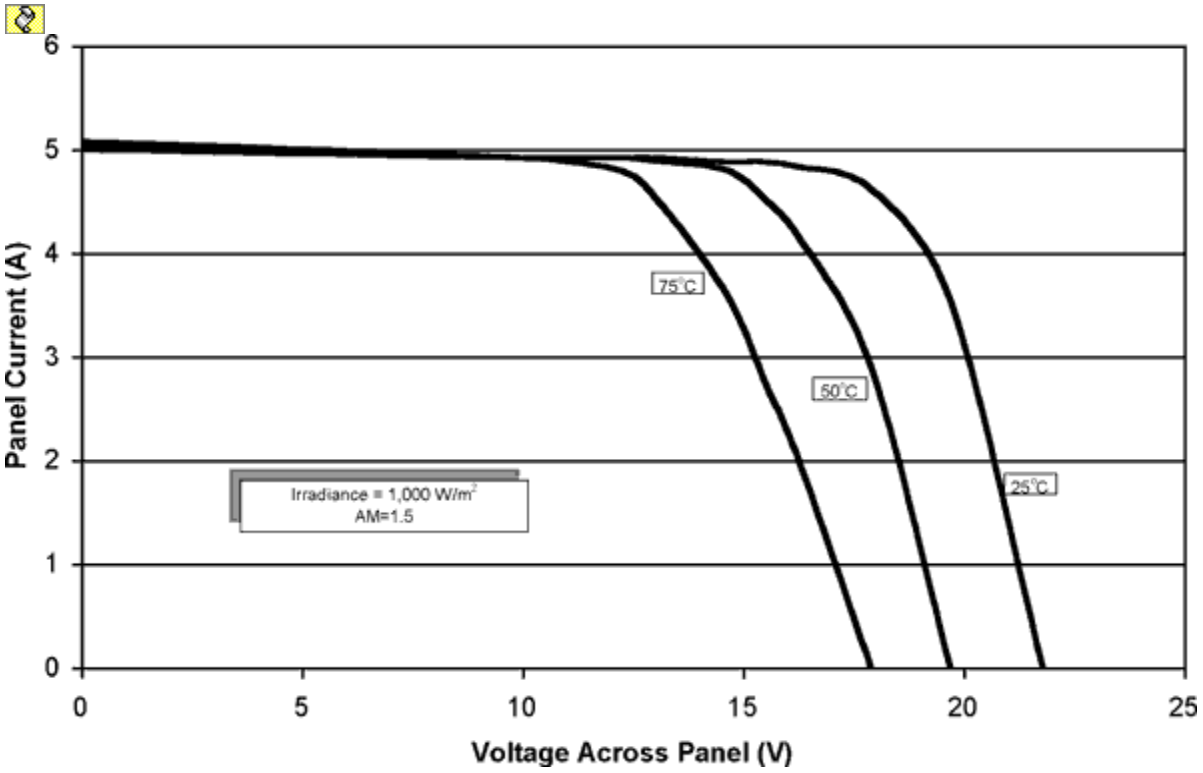

Figure 5.6 Effect of cell temperature on photovoltaic panel output. Data shown are for an irradiance of 1,000 W/m² and an air mass of 1.5.

All of the data presented so far have been for photovoltaic cells at a temperature of 25°C. In a real system design, this is seldom the case. Photovoltaic cells are usually encapsulated in a panel to provide rigidity and physical protection of the front surface. Since panels must reject 80% to 90% of the solar energy incident upon them, and usually this transfer is to the ambient air, both the air temperature and the wind speed and direction have great effects on this.

The concept of a *normal operating cell temperature* (NOCT) has been defined in order to provide some sense of the ability of a specific panel to reject heat and provides a design guideline for system performance analysis. Normal operating cell temperature is the cell temperature under 'standard operating conditions', ambient air temperature of 20°C, solar irradiance of 800 W/m^2 and wind speed of 1 m/s. NOCT values are specific to a particular panel or collector, but generally are about 50°C for flat-plate panels.

All data presented above are for an air mass of 1.5 (AM=1.5). The concept of air mass was introduced in Chapter 2, Section 2.2.2. The *air mass* is an indication of the path length that solar irradiance travels through the atmosphere. An air mass of 1.0 means the sun is directly overhead and the radiation travels through one atmosphere (thickness). The air mass is approximately equal to the reciprocal of the cosine of the zenith angle and an air mass of 1.5 would represent a zenith angle of 48.2 degrees or an altitude angle of 41.8 degrees.

5.3 Collector Efficiency

At this point in our discussion of how solar energy is collected, we will define the basic performance parameter, *collector efficiency*. We will then describe how this is measured and then how these measurements can be combined into an analytical model to predict collector output. This is done in general terms, applicable to flat-plate and concentrating collectors for either thermal or photovoltaic applications.

The solar energy collection efficiency, η_{col} $\eta_{col}\eta_{col}$ of both thermal collectors and photovoltaic collectors is defined as the ratio of the rate of useful thermal energy leaving the collector, to the useable solar irradiance falling on the aperture area. Simply stated, collector efficiency is:

$$\eta_{col} = \frac{\dot{Q}_{useful}}{A_a I_a} \qquad (5.13)$$

where:

$\dot{Q}_{useful}$ = rate of (useful) energy output (W)

A_a = aperture area of the collector (m^2)

I_a = solar irradiance falling on collector aperture (W/m^2)

This general definition of collector efficiency differs depending on the type of collector. The rate of useful energy output from thermal collectors is the heat addition to a heat transfer fluid as defined by Equation (5.2) whereas the useful energy output of a photovoltaic collector is electrical power defined in Equation (5.11). The incoming solar irradiance falling on the collector aperture, I_a, multiplied by the collector aperture area represents the maximum amount of solar energy that could be captured by that collector.

5.3.1 Optical Efficiency

In some of the development that follows, we will use the concept of *optical efficiency*. The optical efficiency of a solar collector is defined as the rate of optical (short wavelength) energy reaching the absorber or receiver, divided by the appropriate solar resource. Dividing Equation (4.3) by Equation (4.4), we have for optical efficiency;

$$\eta_{opt} = \Gamma\rho\tau\alpha \qquad (5.14)$$

This term is often used in separating out the non-thermal performance of a solar collector. It also forms the maximum limit for collection efficiency as will be seen in our discussions below.

5.3.2 Flat-plate Collectors

Since flat-plate collectors (both thermal and photovoltaic) are capable of absorbing both direct (beam) and diffuse solar irradiance, the appropriate aperture irradiance is the global (total) irradiance falling on the collector aperture.

$$I_a = I_{t,a} \qquad \left(W/m^2\right) \qquad (5.15)$$

where $I_{t,a}$ is the global irradiance on a collector aperture.

Equations for calculating global (total) irradiance on an aperture were the subject of Chapter 4, Section 4.2.1 and for the general case we may use Equation (4.29). Various schemes of orientation and tracking were discussed in Section 4.1 and may be applicable to determining the angle of incidence. Equation (4.29) includes both direct (beam) and scattered and reflected energy.

Adding the appropriate useful energy term to Equation (5.13) we have for thermal and photovoltaic flat-plate collectors, the following definitions of collector efficiency

Flat-plate thermal collectors: $$\eta_{col} = \frac{\dot{m} c_p \left(T_{out} - T_{in}\right)}{I_{t,a} A_a} \qquad (5.16)$$

Flat-plate photovoltaic collectors: $$\eta_{col} = \frac{i \cdot v}{I_{t,a} A_a} \qquad (5.17)$$

5.3.3 Concentrating Collectors

Concentrating collectors on the other hand can only concentrate direct (beam) solar irradiance and therefore the appropriate irradiance term is direct (beam) normal solar irradiance, reduced by the cosine of the angle of incidence. For two-axis tracking collectors, the angle of incidence is zero.

$$I_a = I_{b,a} \qquad \left(W / m^2\right) \qquad (5.18)$$

where $I_{b,a}$ is the direct (beam) irradiance on a collector aperture.

Equations for calculating direct (beam) irradiance on an aperture were the subject of Chapter 4, Section 4.2.1 and for the general case we may use Equation (4.28). Various schemes of orientation and tracking were discussed in Section 4.1 and may be applicable in determining the angle of incidence. Equation (4.28) includes both direct (beam) and scattered and reflected energy.

Adding the appropriate useful energy term to Equation (5.13) we have for thermal and photovoltaic concentrating collectors, the following definitions of collector efficiency:

Concentrating thermal collectors: $$\eta_{col} = \frac{\dot{m} c_p \left(T_{out} - T_{in}\right)}{I_{b,n} \cos\theta_i A_a} \qquad (5.19)$$

and

Concentrating photovoltaic collectors: $$\eta_{col} = \frac{i \cdot v}{I_{b,n} \cos\theta_i A_a} \qquad (5.20)$$

5.3.4 Non-imaging Concentrators

One further caveat must be mentioned for non-imaging concentrators such as vee-troughs, conical concentrators and compound parabolic concentrators (CPC). Since these accept some diffuse solar irradiance, the appropriate I_a would be the direct (beam) normal, reduced by the cosine of the angle of incidence plus the circumsolar diffuse solar irradiance falling within the acceptance angle of that specific concentrator.

$$I_a = A_a \left[I_{b,n} \cos\theta_i + I_{d,aa} + I_{r,aa} \right] \qquad \left(W / m^2 \right) \qquad (5.21)$$

where the terms $I_{d,aa}$ and $I_{r,aa}$ are the sky diffuse and reflected diffuse energy that are available within the acceptance angle of the non-imaging concentrator. The definition of these terms is beyond the scope of this book. However, this solar irradiance may be easily measured by reducing the tube length of a pyrheliometer and attaching this to the aperture of the non-imaging concentrator.

5.4 Models of Collector Performance

Models of collector performance that will predict collector output under varying solar irradiance, operating temperature and weather conditions, are important to the system designer. This type of model can be used in system performance prediction programs such as SIMPLES, to predict the output of the collector field.

The most prevalent solar collector performance model is called the 'delta-T over I curve' and permits prediction of useful energy out under varying solar irradiance, ambient temperature and system operating temperature. Although its required simplifications work well for low- temperature flat-plate collector systems, it has been modified for use with higher temperature systems as described below. This model has no applicability to photovoltaic collectors.

Figure 5.7 summarizes the performance of a typical flat-plate collector. Plots a) and b) show that, the rate of useful energy produced decreases as the temperature of the fluid entering the collector increases. As expected the higher the solar irradiance level, the higher the rate of useful energy produced. Curve b) shows the same data plotted in inverse order. Plots c) and d) show collector efficiency rather than useful energy produced. Curve c) shows that efficiency is independent of solar irradiance when fluid inlet temperature equals ambient temperature. This point defines the optical efficiency. Curves c) and d) can be combined into a single curve e) defining the relationship between collector efficiency, solar irradiance and fluid inlet temperature as described below.

5.4.1 Flat-plate Collectors, The $\Delta T / I$ Curve

Starting with Equation (4.9), the following simplifications can be made for a flat-plate collector operating at low temperatures (below approximately 90°C):

There is no reflection of incoming solar irradiance and therefore Γ and ρ are eliminated.

The aperture area is the same as the absorber area ($A_a = A_r$)

Radiation heat loss can be combined with convection and conduction into a single overall heat loss coefficient, U_L (W/m²K). This coefficient is a constant for the particular collector being modeled. (Temperature dependence of this term due to natural convection and radiation causes non-linear affects to occur and will be discussed below).

The average receiver panel temperature, $\overline{T}_r$ can be replaced by the temperature of the fluid entering the collector, T_{in} , if the useful energy is divided by a 'heat removal factor', F_R, defined as the ratio of useful energy if $(T_{in} - T_a)$ is used rather than $(\overline{T}_r - T_a)$. Note that the heat removal factor is a function of the rate of flow of heat transfer fluid.

The appropriate solar irradiance resource for a flat-plate collector, I_a is the global (total) solar irradiance on a tilted surface, $I_{t,\beta}$

With these simplifications, Equation (4.9), for normal incident solar irradiance becomes:

$$\eta_{col,n} \equiv \frac{\dot{Q}_{useful}}{I_{t,a} A_a} = F_R \tau\alpha - F_R U_L \left[\frac{(T_{in} - T_a)}{I_{t,a}} \right] \qquad (5.22)$$

If it is further assumed that F_R, τ, α, U_L are constants for a given collector and flow rate, then the efficiency is a linear function of the three parameters defining the operating condition; solar irradiance, fluid inlet temperature and ambient air temperature. This is the single line shown on curve e) in Figure 5.7.

The slope of this line represents the rate of heat loss from the collector. For example, collectors with cover sheets will have less of a slope than those without cover sheets. The intercept of the line on the efficiency axis is sometimes called the optical efficiency. Most low-temperature solar collector performance data are presented in terms Equation (4.21). It

should be remembered that both of these terms are multiplied by the heat removal factor, F_R making them a function of flow rate. Therefore the flow rate for any $\Delta T / I$ $\Delta T / I \Delta T / I$ curve should be specified.

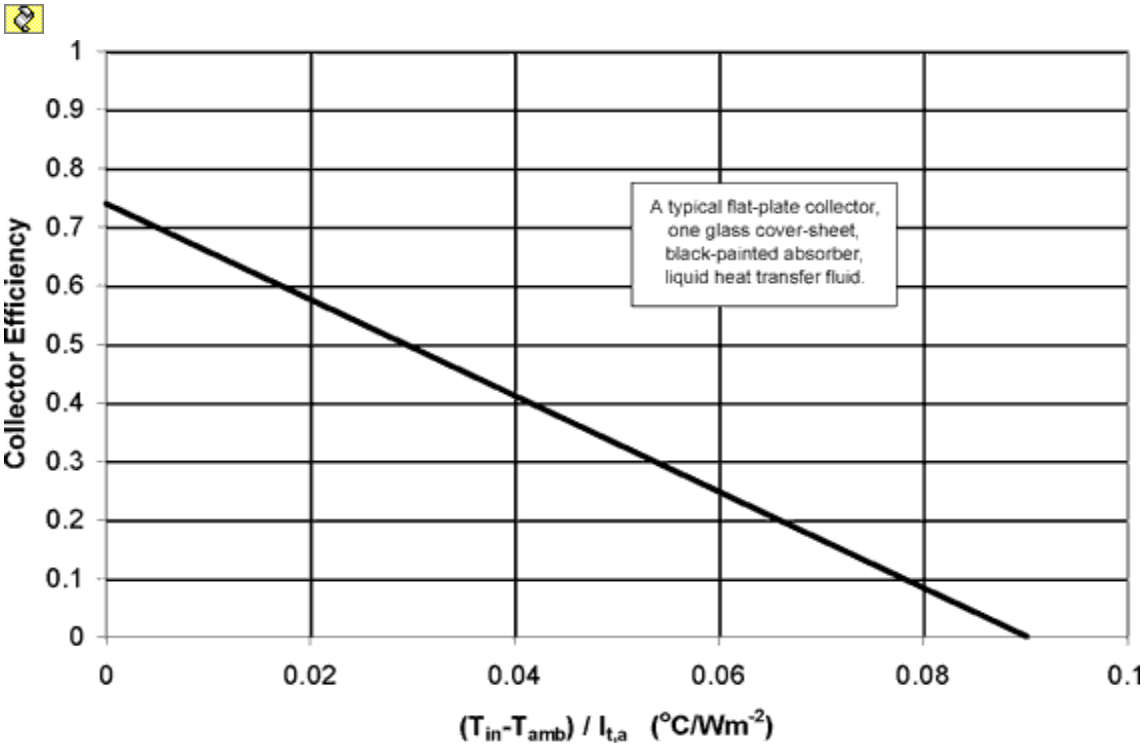

Curve a)

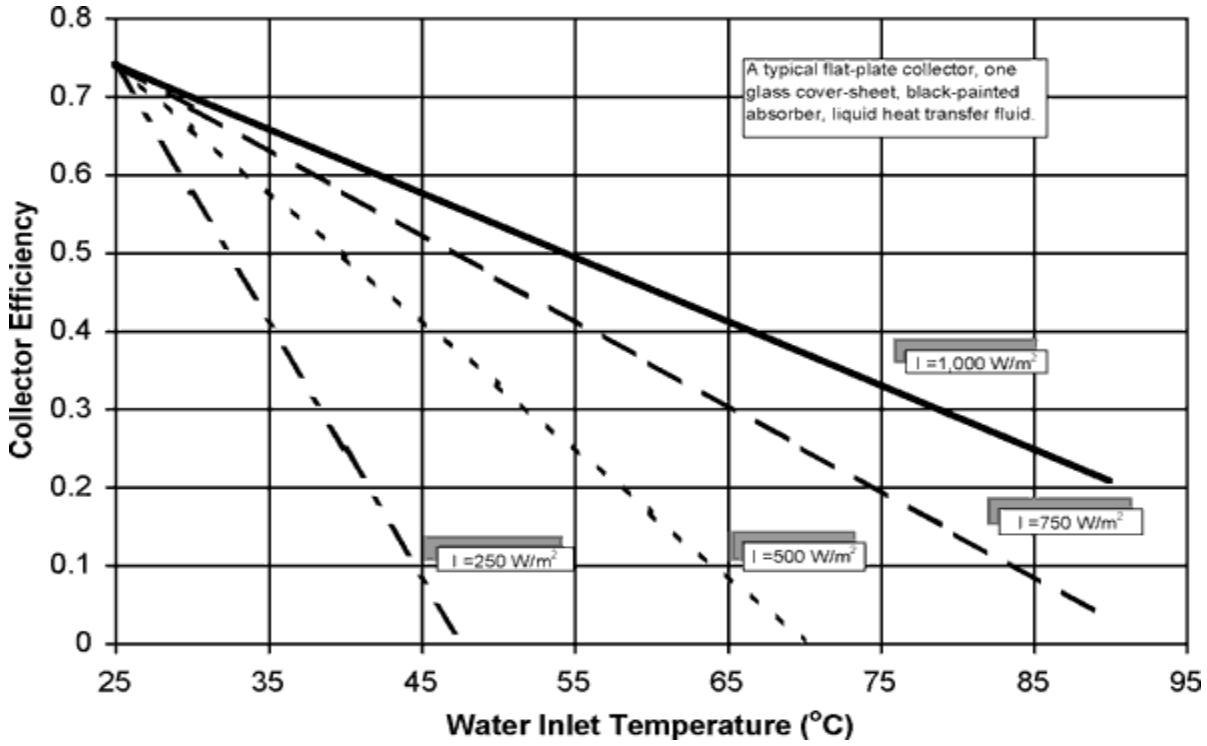

Curve b)

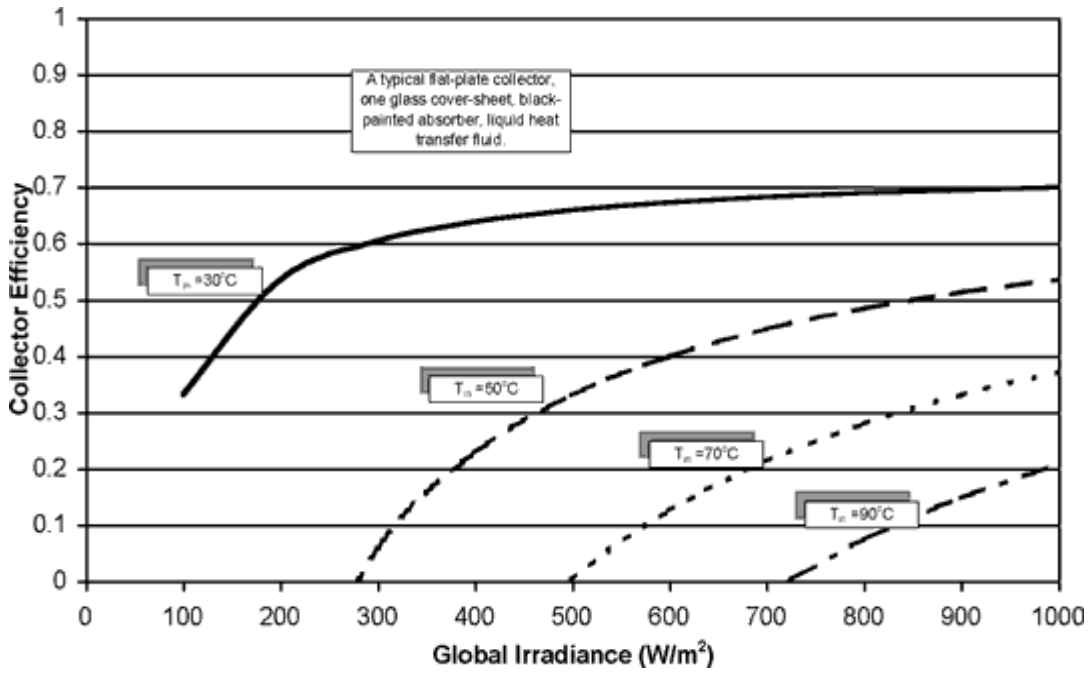

Curve c)

Figure 5.7 Performance of a typical flat-plate thermal collector (one glass cover, black-painted absorber, water transfer fluid and ambient temperature 25◦C). Curve a) shows the performance as a function of the $\Delta T / I$ variable described above. Curve b) and c) for the same collector,

show how the output varies with fluid temperature and irradiance. Curves b) and c) are derived from curve a).

There are two interesting operating points on Figure 5.7, curve a). The first is the maximum collection efficiency, called the optical efficiency. This occurs when the fluid inlet temperature equals ambient temperature. For this condition, the $\Delta T / I$ value is zero. This is the test point described above as part of a collector performance measurement procedures.

The other point of interest on Figure 5.7, curve a) is the intercept with the $\Delta T / I$ axis. This point of operation can be reached when useful energy is no longer removed from the collector, a condition that can happen if fluid flow through the collector stops (power failure). In this case, the optical energy coming in must equal the heat loss, requiring that the temperature of the absorber increase until this balance occurs. This maximum temperature difference or '*stagnation temperature'* is defined by this point. For well-insulated collectors or concentrating collectors the stagnation temperature can reach very high levels causing fluid boiling and, in the case of concentrating collectors, the absorber surface can melt.

Curves b) and c) of Figure 5.7 are derived from curve a); the $\Delta T / I$ curve. Curve b) shows the dependence of collector output (efficiency) as a function of the water inlet temperature for different levels of irradiance. Note that more energy is derived from a collector when the water temperature entering the collector is low. It is important in solar energy system design to only heat the water or heat transfer fluid to the lowest temperature consistent with system output requirements.

Curve c) of Figure 5.7 shows the relationship of system output to the irradiance level. It shows that systems operating at low temperature levels (such as swimming pool heating systems) can derive heat from the sun at very low levels of irradiance. Higher temperature operating systems such as domestic hot water systems only derive energy from the sun when the irradiance level is high. Further study of curves b) and c) will reveal most of the important aspects of the thermal design of solar energy systems.

5.4.2 Parabolic Troughs, The Non-Linear $\Delta T / I$ Curve

For parabolic trough collectors operating at higher temperatures, the above assumptions must be modified. In order to better approximate the temperature at which heat loss takes place, an average receiver temperature, is calculated as the average between the inlet and outlet fluid temperatures:

$$T_r = \frac{T_{in} + T_{out}}{2} \equiv \overline{T}_f \qquad (K) \qquad (5.23)$$

where:

T_{in} - incoming heat transfer fluid temperature (K)

T_{out} - outgoing heat transfer fluid temperature (K)

The $\Delta T / I$ curves produced during testing have significant non-linearity. Thus the $\Delta T / I$ curve must be fit analytically. Typically this is done using an expansion of Equation (4.21) of the form

$$\eta_{col} \equiv \frac{\dot{Q}_{useful}}{I_{b,n} \cos\theta_i A_a} = K_i \eta_{opt} - a \frac{\left(\overline{T}_f - T_a\right)}{I_{b,n} \cos\theta_i} - b \frac{\left(\overline{T}_f - T_a\right)^2}{I_{b,n} \cos\theta_i} \qquad (5.24)$$

where the coefficients *a* and *b* are determined by a curve fit to test data.

The addition of the $\Delta T^2 / I_a$ term to Equation (5.22) is a simplified attempt to account for the fact that U_L is, in fact, not independent of temperature. In fact, the temperature dependence of U_L is quite complex. The attempt here is to utilize available test data by using a curve fitting technique. Figure 5.8 shows typical values and trends for these two concentrators.

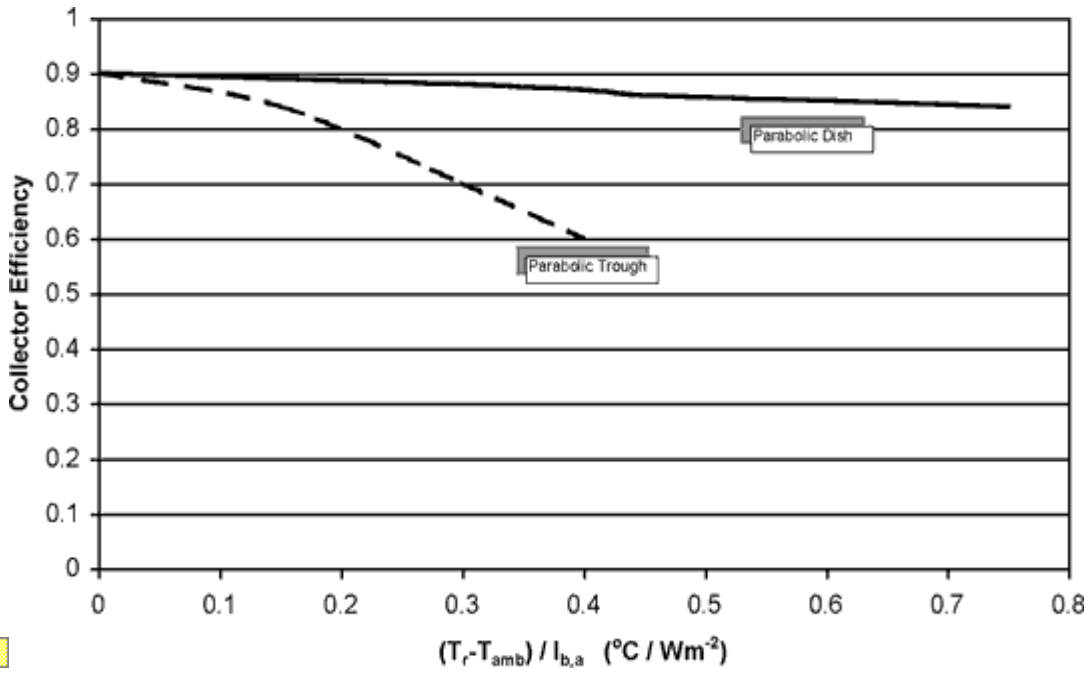

Figure 5.8 Collector efficiency for a typical parabolic trough and a typical parabolic dish collector.

The largest source of error arises from the fact that, in using a simple $\Delta T / I$ model, one is usually extrapolating along the $\Delta T / I$ curve, not interpolating.

As discussed earlier, the test data from which a $\Delta T / I$ curve is generated is obtained at a constant value of I_a (usually near 1,000 W/m^2). This is about as large as I_a becomes. Thus, as I_a decreases in the course of an analysis due to either poor solar irradiance or at large incidence angles, the quantity $\Delta T / I$ increases, usually to an extent much larger than the range of test data.

Now if the $\Delta T / I$ curve is indeed close to a straight line, extrapolation may not introduce much error. If there is significant curvature, however, extrapolation can lead to large errors and simple models should be used with caution. Experience has indicated that, if the $\Delta T / I$ curve is reasonably straight, the computed collector performance agrees fairly well with all-day test results, which include significant incidence angle effects. In addition, long-term (year-long) performance projections agree well with the results obtained from the very complex thermo-optical design codes in use at Sandia National Laboratories for parabolic troughs (Harrigan, 198l).

It is noteworthy that in some of the literature, non-linearity on the $\Delta T / I$ test data is fit with a polynomial curve having a $\Delta T / I^2$ term. Although this expression may indeed produce a reasonable fit to the data, there is really no physical reason to introduce an I^2 functional dependence. This point is discussed in some detail by Tabor (1980).

5.4.3 Parabolic Dish and Central Receivers - Constant-T Models

When a collector operates at a fixed temperature, and it is designed for operation at that temperature, there is little need to determine its performance under varying temperature operating conditions. Parabolic dish collectors that are part of dish/engine systems, and central receiver systems are usually in this category.

If operated at a constant temperature, and that temperature is significantly higher than ambient temperature, the rate of heat loss term in Equation (5.9) is a constant, and the useful energy out is optical energy collected minus this constant. The result is a thermal output linearly proportional to solar irradiance once a minimum 'threshold' solar irradiance level has been reached. This simple behavior is pictured in Figure 4.8 d).

$$\eta_{col} \equiv \frac{\dot{Q}_{useful}}{I_{b,n} A_a} = \eta_{opt} - \frac{const.}{I_{b,n}} \qquad (5.25)$$

The only variable unaccounted for here, is the variation in the overall heat loss coefficient, U_L caused by variations in wind velocity and direction. For parabolic dishes using cavity receivers, U_L will also change with the tilt angle of the cavity relative to the earth. This angle changes as the dish tracks the sun

across the sky. Data on both of these effects can be found in Stine & McDonald (1989).

Usually for these combined concentrator/engine systems, the combined collector/engine system performance is modeled. The output curve is similar to Figure (4.8d) but with the offset including both collector thermal losses, and engine losses. These will be discussed in Chapter 11.

5.4.4 Photovoltaic Collectors

The performance of a photovoltaic panel or concentrating photovoltaic collector is defined in terms of its efficiency as a function of load resistance and cell temperature. Equations defining the appropriate efficiency are given as Equation (5.17) for flat-plate photovoltaic panels and (5.20) for concentrating photovoltaic collectors. Normally, the efficiency of a photovoltaic panel or collector is determined based on experimental data.

A curve of efficiency as a function of voltage across the panel at different levels of irradiance is shown in Figure 5.9. This curve is derived from the basic I-V data shown in Figure 5.4 and is for a cell temperature of 25◦C, air mass = 1.5.

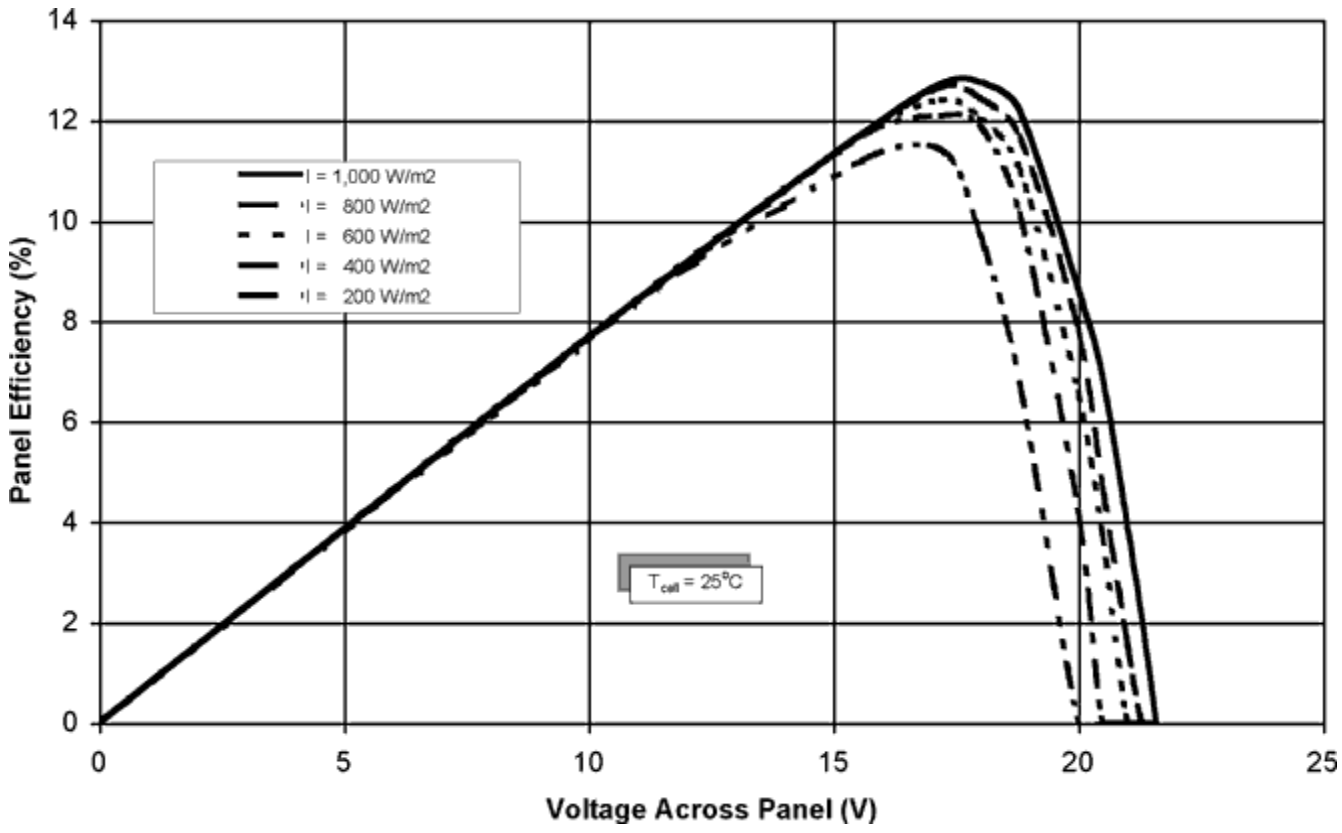

Figure 5.9 Photovoltaic panel efficiency at different levels of solar irradiance. Data shown are for a cell temperature of 25 ◦C and an air mass of 1.5.

The peak power points described in Section 5.2.4 above are obvious in this plot, however we are now looking at efficiency variation rather than power variation as in Figure 5.5. It is important to note that the panel efficiency remains almost the same at all levels of insolation Although Figure 5.5 shows a marked decrease in power as solar irradiance decreases, the efficiency decreases only slightly with irradiance level.

The effect of elevated cell temperatures on panel efficiency is shown in Figure 5.10. Here we see a significant reduction in panel efficiency as cell temperature increases. The typical temperature coefficient of efficiency is between value here is -0.5 to -0.6%/°C

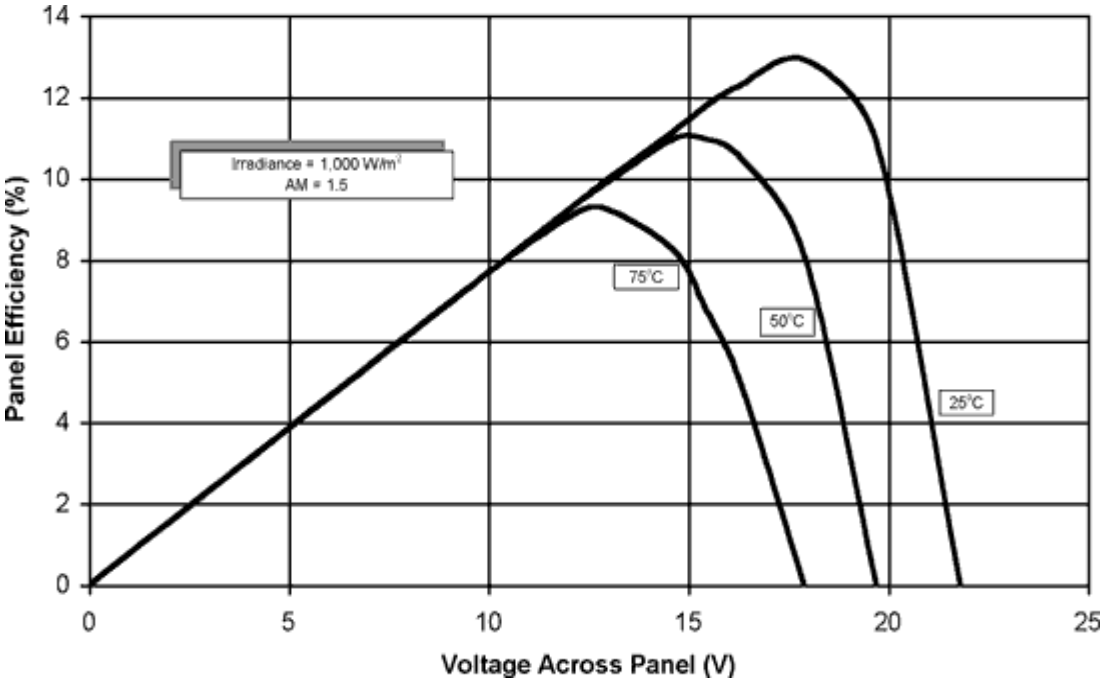

Figure 5.10 Photovoltaic panel efficiency at 1,000 W/m² for different cell temperatures. Data shown are for an air mass of 1.5.

Model - All of the factors discussed above must be included in a photovoltaic panel or collector performance model. The performance of a photovoltaic panel is a function of the solar irradiation level, the temperature of the cell and the air mass which affects the spectral distribution of the incident irradiance as discussed in Chapter 2, section 2.2.2 and demonstrated on Figure 2.5. One such model for photovoltaic collector efficiency is

$$\eta_{col} = \eta_{std}\left(\frac{\eta_G}{\eta_{std}}\right)\left(\frac{\eta_{G,T}}{\eta_G}\right)\left(\frac{\eta_{G,E(\lambda)}}{\eta_G}\right) \qquad (5.26)$$

where: η_{std} η_{std} - efficiency of panel at standard irradiance, cell temperature and air mass.

η_G / η_{std} - ratio of efficiency of panel at specified irradiance level to efficiency at standard irradiance.

$\eta_{G,T} / \eta_G$ - efficiency of panel at specified cell temperature to its efficiency at the specified irradiance level.

$\eta_{G,E(\lambda)} / \eta_G$ - efficiency of panel at a specified air mass to its efficiency at the specified irradiance level.

5.5 Measuring Collector Performance

To use a collector performance model data with some degree of confidence, it is important to understand the way in which such data are obtained and what limitations this might impose on how the data can be used. Below we describe the three most common methods of measuring collector performance. There are collector test standards available that specify both the experimental setup and the testing procedure. The most commonly accepted standards are listed in the References and Bibliography at the end of this chapter.

Testing is performed only on clear days when the solar irradiance level is high and constant. Prior to taking measurements, hot heat-transfer fluid is circulated through the absorber or receiver to bring it up to the test temperature. For a flat-plate collector, the test flow rate is generally specified by the test procedure in use. In the case of parabolic trough testing, turbulent flow is maintained within the receiver tube to ensure good heat transfer between the fluid and the wall of the receiver tube. A measurement is made only when the collector is at steady state, which is indicated by a constant rise in heat transfer fluid as it flows through the receiver.

5.5.1 Thermal Performance Measurements

In a typical test to determine solar collector efficiency, the collector aperture is aligned as close as possible to normal to the incident direct (beam) solar irradiance. This is done to eliminate any uncertainties due to off-normal incidence angle effects. Figure 5.11 is a photograph of a turntable at Sandia National Laboratory, Albuquerque used to align the aperture of a parabolic trough collector normal to the incident direct (beam) solar irradiance. Once data are obtained with the aperture normal to the sun, testing is repeated, usually only at one temperature, to determine the effect of varying angles of incidence on collector performance.

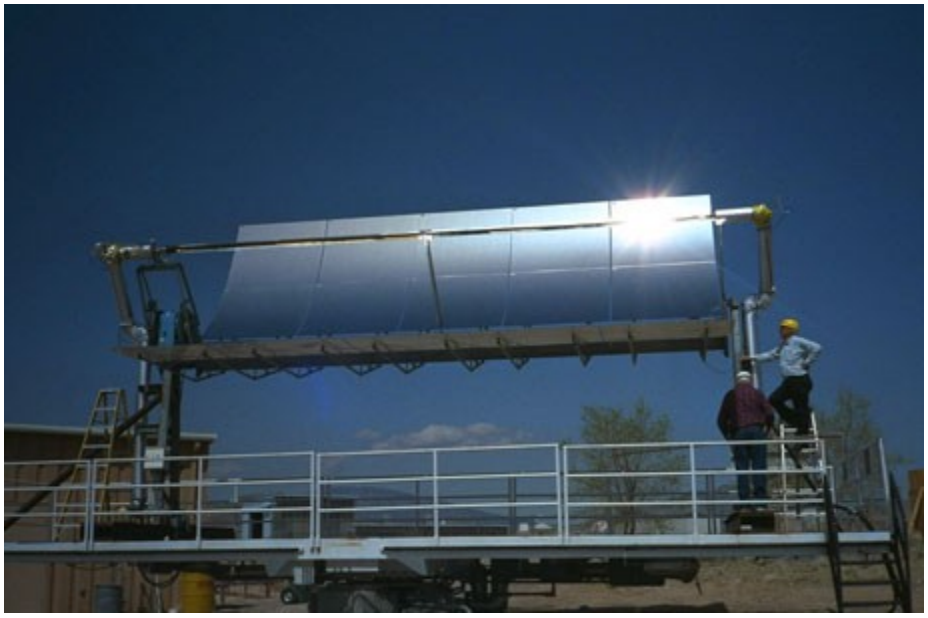

Figure 5.11 Collector module test facility at Sandia National laboratories. Courtesy of Sandia National Laboratories.

Three procedures for measuring the performance of thermal collectors are used, depending on the type of collector system being tested and the experimental apparatus available. We shall briefly describe each method; collector balance, system balance and heat loss measurement methods below. Figure 5.12 depicts the test setup used in these tests graphically.

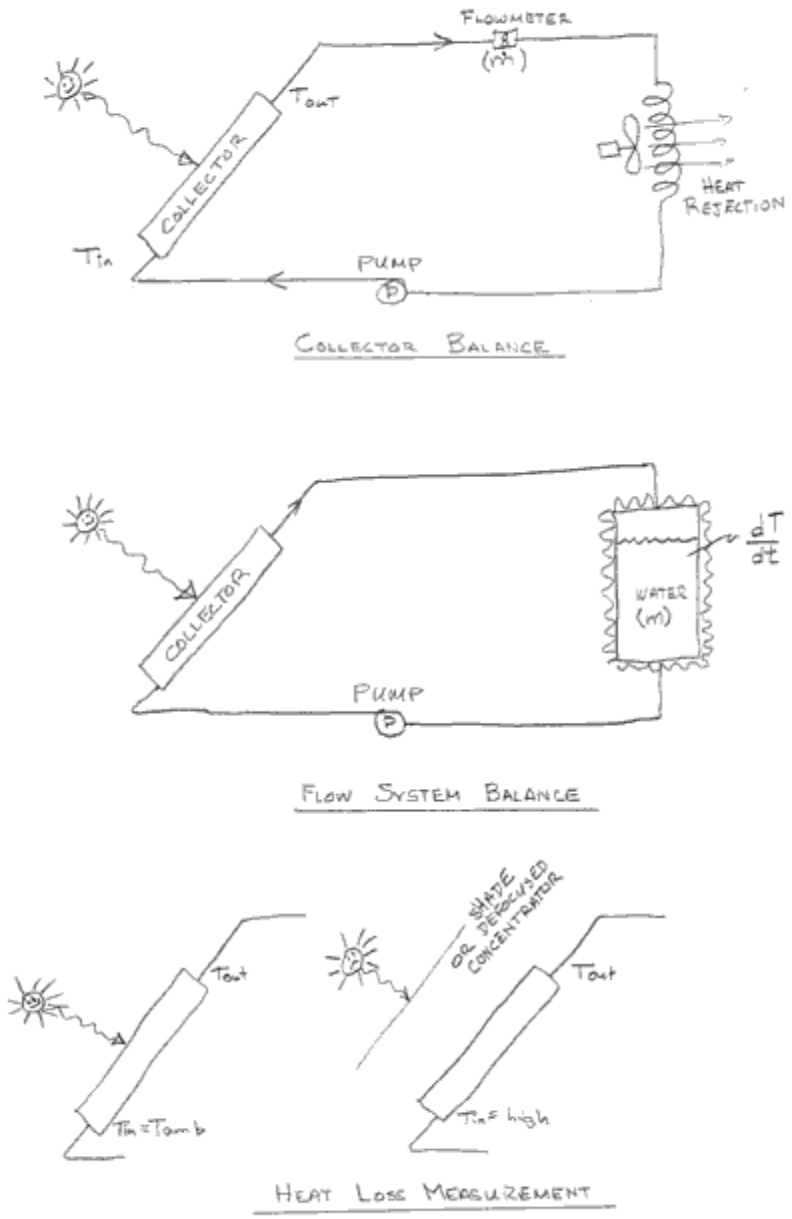

Figure 5.12 Three experimental methods for measuring collector efficiency.

Collector Balance - The most common test method used for flat-plate and parabolic trough collectors is that depicted in Figure 5.12 a). This flow loop must incorporate accurate measurement capabilities for the fluid inlet and outlet temperatures, and the mass flow rate of the heat transfer fluid. It must also include a temperature controller connected to auxiliary heating and cooling devices so that a constant fluid inlet temperature can be maintained. The rate of energy being transferred to the heat transfer fluid under steady state conditions is given in Equation (5.2)

Single collector modules are typically used in these tests, the temperature increase across a single module, especially a parabolic trough module, can sometimes be small (e.g., 1 to 5ºC in a parabolic trough) since these modules are designed to be connected in series in applications. Therefore, extreme care must be taken in making accurate temperature rise measurements. Dudley et al. (1982) describe, in general, the test procedures developed at Sandia National Laboratories for testing parabolic trough collectors.

Flow System Balance - In some cases, it is not easy to accurately measure the fluid inlet or outlet temperatures or the mass flow rate. Instead of performing the energy balance on the collector module itself, an insulated flow loop and tank can be used as illustrated in Figure 5.12 b). The energy balance for the system using this apparatus would be:

$$\dot{Q}_{useful} = m c_p \frac{dT}{dt} - \dot{W}_{pump} \qquad (W) \qquad (5.27)$$

where:

m - mass of fluid in entire system (kg)

dT/dt - the rate of increase of fluid in the tank (K/s)

$\dot{W}_{pump}$ - rate of pump work entering the insulated system (W)

For this method to work, the amount of fluid must be large enough so that the bulk temperature of the fluid (and therefore the collector fluid inlet temperature) does not increase too rapidly in order to obtain an approximate steady state temperature condition.

Heat Loss Measurement - A third method is often used on concentrating collector systems and involves two tests to obtain a single performance data point. This procedure is illustrated schematically in Figure 5.12 c). First the rate of optical energy collected defined in Equation (5.4) is measured. Operating the collector with heat transfer fluid close to ambient temperature does this. Since heat loss from the collector, as shown in Equation (5.9), is proportional to the difference between fluid and ambient temperature, there should be no heat loss when they are the same temperatures.

The second test is to operate the collector at normal operating temperatures (a heater is required) without solar input. Usually defocusing the concentrator attains this test condition. Under these conditions, heat will be lost from the receiver because of the temperature difference between it and ambient. If this test is performed at different temperatures, the non-linear relationship between

heat loss and temperature difference can be determined. The rate of useful energy out of the collector at any given temperature then is:

$$\dot{Q}_{useful} = \dot{m}c_p (T_{out} - T_{in})\Big|_{T_{fluid}=T_{amb}} - \dot{m}c_p (T_{out} - T_{in})\Big|_{I_a=0} \qquad (W) \qquad (5.28)$$

As with any test method, there are a number of inaccuracies that can affect the results obtained with this test procedure. Probably the most important discrepancy is from the fact that, due to the temperature difference needed to conduct heat through the absorber wall and transfer it into the working fluid, the absorber surface will be hotter than the heat transfer fluid, under normal operating conditions. However, when heat is being lost from a defocused or shaded collector during the second test above, the absorber surface will be cooler than the heat transfer fluid. This will result in the test measurement indicating heat losses that are lower than actually occur during normal operation.

Incident Angle Modifier - Most solar collector testing is performed using a two-axis tracking device that places the collector aperture normal to the sun such as shown in Figure 5.11. In actual installations, flat-plate collectors are usually mounted in a fixed position with the sun making different incident angles to the collector aperture over the day as described in Section 4.1.1.

Parabolic troughs likewise usually track about a single axis and have incident angles as described in Section 4.1.2. A non-zero angle of incidence not only changes the amount of irradiation incident on the collector aperture (already accounted for in the definitions of aperture solar irradiance), but also changes collector performance due to, among other things, variation of surface properties with incident angle and internal shading.

If total energy recovery from a collector field over a period of time is to be estimated from collector performance data, definition of the collector's performance at other than zero incident angles is necessary. The ratio of collector efficiency at any angle of incidence, to that at normal incidence is called the '*incident angle modifier', K_i*.

It is measured experimentally by varying the angle of incidence under noontime solar irradiance conditions with ambient temperature heat transfer fluid passing through the collector. Changes in this optical efficiency measurement give the incident angle modifier. Usually it is expressed as a polynomial curve fit as:

$$K_i \equiv \frac{\eta_{opt,\theta}}{\eta_{opt,n}} = a\theta_i + b\theta_i^2 \qquad (5.29)$$

where a and b are coefficients from a polynomial curve fit.

To predict the performance of a solar collector in a system, the collector normal incidence efficiency predicted by either the linear or the non-linear 'delta-T-over-I' experimental data correlation model described below, is multiplied by the incident angle modifier to obtain collector efficiency:

$$\eta_{col} = K_i \times \eta_{col,n} \qquad (5.30)$$

Optical Efficiency - Optical efficiency, as defined in Equation (5.14) is generally determined by one of two methods. The first method, easily performed on tracking collectors, involves operating the collector at constant inlet temperature, first with the concentrator focused 'on-sun' and then with it 'defocused'. The efficiency of the collector 'on-sun' is added to the rate of heat loss divided by the same irradiance and aperture area with the result being the optical efficiency.

This same type of test can be performed on a flat-plate collector by covering and uncovering the absorber with a sheet of opaque material.

5.5.2 Photovoltaic Performance Measurements

Due to the rapid response rate of the photovoltaic cell, testing of photovoltaic panels and concentrating photovoltaic collectors does not have many of the difficulties addressed above for thermal collectors. A detailed outline of performance testing procedures for photovoltaic panels is contained in ASTM 1036.

Generally all that is required is a variable load resistance and measurements of current through the load and voltage across the panel. A thermocouple should be placed adjacent to the photovoltaic cells to ascertain their temperature. An alternative to using a variable resistance is to connect the photovoltaic panel across a large capacitor. Taking simultaneous transient data of both voltage and current will provide the data necessary to plot an I-V curve.

Significantly more equipment is involved to determine the output at different cell temperatures and air mass.

Summary

Table 5.1 Summary of Collector Performance Models

Flat-plate Thermal Collectors:

Aperture Irradiance:

$$I_a = I_{t,a}$$

Receiver Temperature Approximation:

$$T_r = T_{in}$$

Performance Model:

$$\eta_{col,n} \equiv \frac{\dot{Q}_{useful}}{I_{t,\beta} A_a} = F_R \tau\alpha - F_R U_L \left[\frac{\left(T_{in} - T_a\right)}{I_{t,\beta}} \right]$$

Parabolic Troughs

Aperture Solar irradiance:

$$I_a = I_{b,a} = I_{b,n} \cos\theta_i$$

Receiver Temperature Approximation:

$$T_r = \overline{T}_f$$

Performance Model:

$$\eta_{col} \equiv \frac{\dot{Q}_{useful}}{I_{b,n} \cos\theta_i K A_a} = K_i \eta_{opt} - a \frac{\left(\overline{T}_f - T_a\right)}{I_{b,n} \cos\theta_i} - b \frac{\left(\overline{T}_f - T_a\right)^2}{I_{b,n} \cos\theta_i}$$

Parabolic Dish and Central Receiver

Aperture Solar irradiance:

$$I_a = I_{b,n}$$

Receiver Temperature Approximation:

T_r= best approximation

Performance Model:

$$\eta_{col} \equiv \frac{\dot{Q}_{useful}}{I_{b,n} A_a} = \eta_{opt} - \frac{const.}{I_{b,n}}$$

Flat-Plate Photovoltaic Panels

Aperture Irradiance:

$$I_a = I_{t,a}$$

Performance Model

$$\eta_{col} = \frac{i \times v}{I_{t,a} A_a} = \eta_{std} \left(\frac{\eta_G}{\eta_{std}} \right) \left(\frac{\eta_{G,T}}{\eta_G} \right) \left(\frac{\eta_{G,E(\lambda)}}{\eta_G} \right)$$

Concentrating Photovoltaic Collectors

Aperture Irradiance:

$$I_a = I_{b,a}$$

Performance Model

$$\eta_{col} = \frac{i \times v}{I_{b,a} A_a} = \eta_{std} \left(\frac{\eta_G}{\eta_{std}} \right) \left(\frac{\eta_{G,T}}{\eta_G} \right) \left(\frac{\eta_{G,E(\lambda)}}{\eta_G} \right)$$

References and Bibliography

Paitoonsurikarn, S, T. Taumoefolau and K. Lovegrove (2003) "Investigation of Natural Convection Heat Loss from a Solar Concentrator Cavity Receiver at Varying Angle of Inclination" to be presented at the 2003 ASME International Solar Energy Conference.

Stine, W. B. and C. G. McDonald (1989) "Cavity Receiver Convective Heat Loss" proceedings of the International Solar Energy Society Solar World Congress 1989 Kobe, Japan, September 4-8, 1989.

ANSI/ASHRAE Std. 93-1986 (RA 91) (1986) *Methods of Testing to Determine the Thermal Performance of Solar Collectors,* American Society of Heating and Refrigeration Engineers, Atlanta, GA (www.ashrae.org).

ANSI/ASHRAE Std. 95-1981 (1981) *Methods of Testing to Determine the Thermal Performance of Solar Domestic Water Heating Systems,* American Society of Heating and Refrigeration Engineers, Atlanta, GA (www.ashrae.org).

ANSI/ASHRAE Std. 96-1980 (RA 89) (1980) *Methods of Testing to Determine the Thermal Performance of Unglazed Flat-Plate Liquid-Type Solar Collectors* American Society of Heating and Refrigeration Engineers, Atlanta, GA (www.ashrae.org).

ANSI/ASHRAE Std. 109-1986 (RA 96) (1986) *Methods of Testing to Determine the Thermal Performance of Flat-Plate Liquid-Type Solar Collectors Containing Boiling Liquid,* American Society of Heating and Refrigeration Engineers, Atlanta, GA (www.ashrae.org).

ASTM E1036M-96e2 *Standard Test Methods for Electrical Performance of Nonconcentrator Terrestrial Photovoltaic Modules and Arrays Using Reference Cells*, American Society for Testing of Materials (www.astm.org)

6 Flat-Plate Collectors

Flat-plate collectors are in wide use for domestic household hot-water heating and for space heating, where the demand temperature is low. Many excellent models of flat-plate collectors are available commercially to the solar designer. A discussion of flat-plate collectors is included here because of their use in industrial systems either to supply low-temperature demands or to preheat the heat transfer fluid before entering a field of higher-temperature concentrating, collectors. Detailed descriptions of flat-plate collector design, performance and system design using these collectors may be found in the following sources: Duffie and Beckman (1980), Lunde (1980), and Kreider and Kreith (1982). The interested reader is referred to these for further information.

The emphasis of this chapter is to develop an understanding of both the attributes of different design features and the performance characteristics of this class of collector. This understanding will permit the system designer to evaluate whether flat-plate collectors should be considered in a system design. Also, the information required to select an appropriate commercial unit is presented here.

This development will follow the outline below:

6.1 Collector Description

The construction of a flat-plate collector is shown in Figure 6. 1. The basic parts noted are a full-aperture absorber, transparent or translucent cover sheets, and an insulated box. The absorber is usually a sheet of high-thermal-conductivity metal with tubes or ducts either integral or attached. Its surface is painted or coated to maximize radiant energy absorption and in some cases to minimize radiant emission. The cover sheets, called *glazing,* let sunlight pass through to the absorber but insulate the space above the absorber to prohibit cool air from flowing into this space. The insulated box provides structure and sealing and reduces heat loss from the back or sides of the collector.

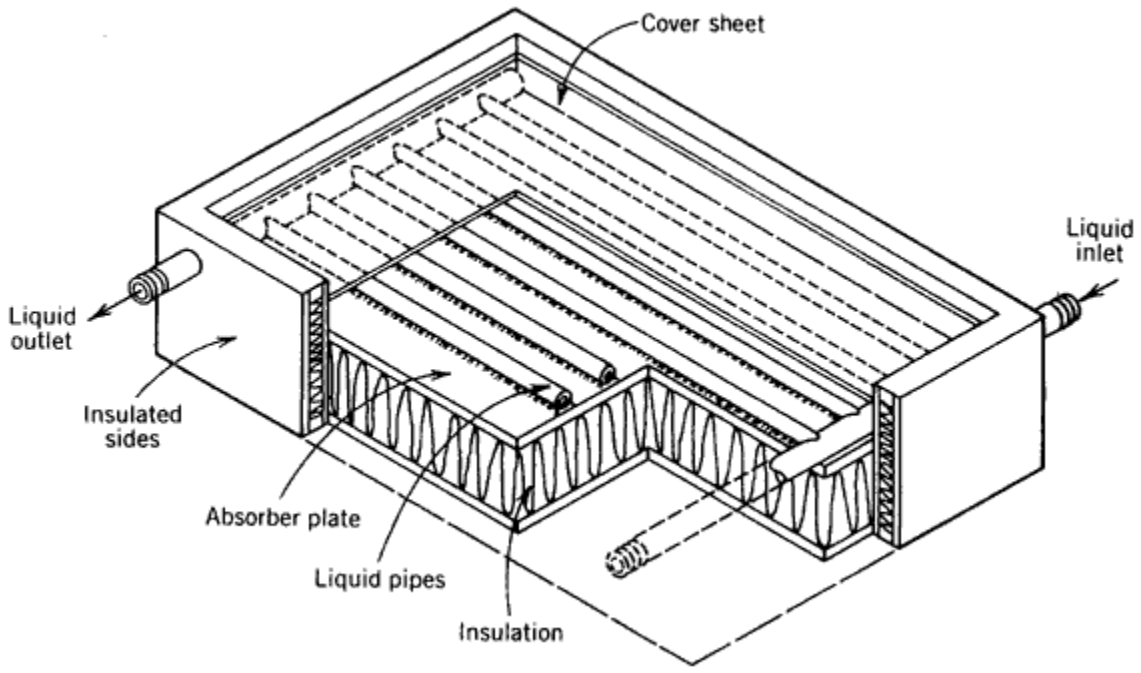

Figure 6.1 A typical liquid flat-plate collector.

6.1.1 Absorber Plate

The main element of a flat-plate collector is the absorber plate. It covers the full aperture area of the collector and must perform three functions: absorb the maximum possible amount of solar irradiance, conduct this heat into the working fluid at a minimum temperature difference, and lose a minimum amount of heat back to the surroundings.

Absorption. Solar irradiance passing through the glazing is absorbed directly on the absorber plate without intermediate reflection as in concentrating collectors. Surface coatings that have a high absorptance for short-wavelength (visible)

light, are used on the absorber. Usually these coatings appear dull or "flat," indicating that they will absorb radiation coming from all directions equally well. Either paint or plating is used, and the resulting black surface will typically absorb over 95 percent of the incident solar radiation.

Fin Heat Removal. The second function of the absorber plate is to transfer the absorbed energy into a heat-transfer fluid at a minimum temperature difference. This is normally done by conducting the absorbed heat to tubes or ducts that contain the heat-transfer fluid. The heat-transfer fluid may either be a liquid (water or water with antifreeze) or gas (air). The important design criterion here is to provide sufficient heat transfer capability that the difference between the temperature of the absorber surface and the working fluid is not excessive; otherwise, the heat loss from the absorber would be excessive. High heat-transfer rates are usually accomplished at the expense of pumping power and absorber plate material.

When a liquid is used as the heat-transfer fluid as is most often the case, special problems occur in transferring the heat absorbed on the absorber surface into the fluid. Liquid collector absorber plates often consist of a flat sheet of metal with tubes spaced 10-25 cm (4-10 in.) apart and attached to it in some fashion (integral, brazed or press fitted). The sheet of metal absorbs most of the solar irradiance and acts as a fin to bring the absorbed heat into the fluid. The following are important points in designing a good ‘tube and sheet’ absorber:

1. The fin (absorber sheet) must he made of a material with high thermal conductivity.
2. The fin should be thick to minimize the temperature difference required to transfer heat to its base (tube).
3. Tubes should not be spaced too far apart; otherwise, a higher temperature difference between the tip of the fin (midway between the tubes) and the base will result.
4. Tubes should be thin-walled and of a high-thermal -conductivity material.
5. The tube should be brazed or welded to the absorber sheet to minimize thermal contact resistance.
6. The tube and absorber sheet should be of similar material to prevent galvanic corrosion between them.

When air is the heat-transfer fluid, often the back side of the absorber plate usually forms one surface of a duct and heat is transferred through the absorber sheet to the air over the entire back surface of the absorber. A thin, rather than thick, absorber sheet of high-thermal-conductivity material will enhance this heat-transfer process. The internal air passage must be designed to provide a sufficiently high airflow velocity past the back of the absorber to give adequate heat transfer without producing a high pressure drop across the collector. Low heat-transfer rates cause the absorber plate to become significantly hotter than the heat-transfer fluid, which increases heat loss. On the other hand, a large

pressure drop across the collector causes high pumping power consumption by the fans supplying the air.

Emittance. Because the temperature of the absorber surface is above ambient temperature, the surface re-radiates some of the heat it has absorbed back to the surroundings. This loss mechanism is a function of the emittance of the surface for low-temperature, long-wavelength (infrared) radiation. The dilemma is that many coatings that enhance the absorption of sunlight (short-wavelength radiation) also enhance the long wavelength radiation loss from the surface. This is true for most dull black paints.

A class of coatings, mostly produced by metallic plating processes, will produce an absorber surface that is a good absorber of short-wavelength solar irradiance but a poor emitter of long-wavelength radiant energy. The function of these coatings, called selective surfaces, was described in detail in Chapter 5. Flat-plate absorbers that have selective surfaces typically lose less heat when operating at high temperature, as will be seen in Section 6.3.3. However, the absorptance of selective coatings is seldom as high as for non-selective coatings, and a tradeoff must be made based on whether the increased high-temperature performance overshadows the reduced low-temperature performance and expense of the selective coating.

6.1.2 Cover Sheets

The absorber is usually covered with one or more transparent or translucent cover sheets to reduce convective heat loss. In the absence of a cover sheet, heat is lost from the absorber as a result of not only forced convection caused by local wind, but also natural convective air currents created because the absorber is hotter than ambient air. The cover sheet forms a trapped air space above the absorber, thereby reducing these losses. However, convective loss is not completely eliminated because a convective current is set up between the absorber and the cover sheet, transferring heat from the absorber to the cover sheet. External convection then cools the cover sheet, producing a net heat loss from the absorber. In addition, heat loss is reduced because of the thermal resistance of the added air space.

Number of Covers. The number of cover sheets on commercial flat-plate collectors varies from none to three or more. Collectors with no cover sheet have high efficiencies when operated at temperatures very near ambient temperature. This is because incoming energy is not lost by absorption or reflection by the cover sheet. When no cover sheet is used, however, a considerable amount of the incident energy is lost during operation at temperatures much above ambient or at low solar irradiance levels. A typical application for an uncovered flat-plate collector is for swimming pool heating, where temperatures less than 10ºC (18ºF) above ambient are required.

Increases in the number of cover-sheets increases the temperature at which the collector can operate (or permits a given temperature to be reached at lower solar irradiance). One or two cover sheets are common, but triple glazed collectors have been designed for extreme climates. In addition to the added expense, each added cover sheet increases the collection efficiency at high temperature by reducing convection loss but decreases the efficiency at low temperatures because of the added absorption and reflectance of the cover.

In regions of average mid-latitude temperatures and solar radiation, collectors with no glazing are generally used for applications to 32ºC (90ºF), single-glazed collectors are used for applications to 70ºC (158º F), and double-glazing is used in applications above 70ºC (158ºF). As discussed in Chapter 5, collector efficiency increases with increasing solar irradiance level but decreases with increasing operating temperature. In regions of low average solar irradiance or extremely low temperatures, therefore, double-glazed collectors are used in applications where single-glazed collectors should be used normally and single-glazed collectors for unglazed applications. Also, selective absorber surfaces become more worthwhile.

Materials. Because of its superior resistance to the environment, glass is used as the outer cover sheet on most commercial collectors. Usually the glass is tempered, with a low iron content and 3.2-6.4 mm (0.12-0.25 in.) thick. The surface may be either smooth, making the glass transparent, or with a surface pattern, making it translucent. Both types have a transmittance of around 90 per cent.

Plastic cover sheets are sometimes used for the second cover sheet when two sheets are required. Installation of the plastic sheet beneath the glass protects the plastic from the environment. Glass also does not transmit UV radiation and thus protects the plastic, which is usually sensitive to this portion of the solar spectrum. Rigid sheets of acrylic-or fiberglass-reinforced polymers are in use, as are stretched films of polyvinyl fluoride. Some of these plastic cover sheets have a transmittance approaching that of low iron glass. A major draw back of this scheme is the potential for overheating the plastic sheet at collector stagnation (no-flow) temperatures.

6.2 Advantages

Flat-plate collectors will absorb energy coming from all directions above the absorber (both beam and diffuse solar irradiance). Because of this characteristic, flat-plate collectors do not need to track the sun. They receive more solar energy than a similarly oriented concentrating collector, but when not tracked, have greater cosine losses.

6.2.1 Non-tracking Option

Since tracking is not required, flat-plate collectors may be firmly fixed to a mounting structure, and rigid plumbing may be used to connect the collectors to the remainder of the system. Moving structure, motors, and tracking control systems are eliminated, thereby reducing the complexity of the system. As discussed in Chapter 5, however, because of the cosine effect, less total energy falls on a fixed surface over the period of a day than on a surface that tracks the sun about one or two axes.

In order to increase their output, flat-plate collectors may be repositioned at intervals or placed on a single- or two-axis tracking mechanism. Either of these options increases the output of the collector but eliminates the advantage of fixed piping and mounting structure.

6.2.2 Diffuse Solar Radiation Utilization

A flat-plate collector absorbs both the direct and the diffuse components of solar radiation. This partially compensates for the fact that fixed surfaces receive less energy because of the cosine effect. Although the diffuse solar irradiance is only about 10 percent of the direct normal solar irradiance on a clear day, on a cloudy day almost all of the available solar irradiance is diffuse.

A comparison between the energy falling on a fixed and a fully tracking flat-plate collector and on a fully tracking concentrating collector is shown in Table 6.1. The data are yearly average values taken from SERI (1981b). The comparison is location dependent because of the latitude effects on the incidence angle and the difference in cloud cover.

Table 6.1. Collectible Solar Radiation Comparison Between Flat-Plate and Concentrating Collectors

	Annual Average Daily Solar Radiation (MJ/m^2)	
Collector	Albuquerque	Madison
Two-axis tracking flat-plate collector (direct plus diffuse)	31	19.5
Fixed, latitude-tilt flat-plate collector (direct plus diffuse)	23	15
Two-axis tracking concentrator	26.5	14

(direct only)		

For both locations, the two-axis tracking flat-plate collector receives more energy. However, in the dry, high desert climate of Albuquerque, a fixed flat-plate collector loses more energy from the cosine effect than it gains by being able to collect diffuse energy. In the Midwestern climate of Madison, Wisconsin, the energy lost by fixing the flat-plate collector approximately equals that gained over a concentrator by its ability to collect the diffuse component of solar irradiance. It should be noted that Table 6.1 only indicates the relative amounts of energy available for collection. The choice of collector type or whether to track a flat-plate collector is generally based on system cost and energy output rather than energy input.

6.2.3 Cost

Currently, flat-plate collectors cost less than concentrating collectors. Part of reason is the lack of need for a complex tracking system. However, part of the reason is because many more flat-plate than concentrating collectors are being produced today. At large production rates, however, it is still not clear whether it is less expensive to cover an aperture area with an absorber plate or with reflective material.

Because of their potential to produce more low-temperature energy for a given cost, flat-plate collectors have been considered for use as pre-heaters for concentrating collectors in high-temperature industrial process heat systems. The major prototype of this system configuration is at Campbell Soup Company in Sacramento, California and is shown in Figure 6.2. The decision of whether to include flat -plate collectors as pre-heaters ultimately is based on the balance between performance and cost.

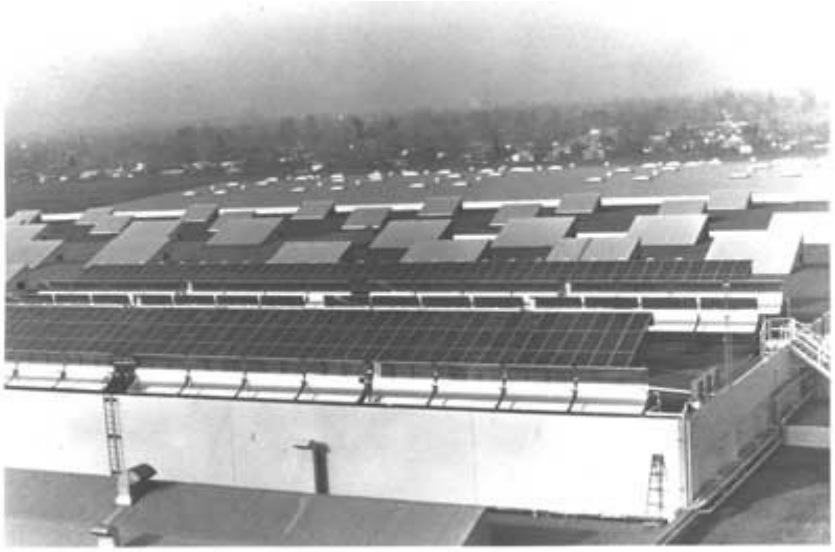

Figure 6.2 The Campbell Soup Company industrial process heat installation in Sacramento, CA. Flat-plate collectors are used to preheat water before entering the parabolic trough concentrators. Courtesy of Sandia National Laboratories.

6.3 Collector Performance

6.3.1 Orientation

The orientation of a flat-plate collector is a concern in system design. The designer must decide on both the collector azimuth and tilt angles or to install the collectors horizontally.

Azimuth. The most obvious azimuth for a fixed surface in the northern hemisphere is south facing. This will give equal amounts of energy before and after noon and usually the maximum daily total energy collected. There are a number of reasons why the system designer may not select this azimuth. It may be simply that the building or land orientation makes it desirable to rotate the azimuth axis to fit the installation conditions. Other performance related factors can affect the collector field orientation.

If the industrial demand is greater in the morning and there is no overnight thermal storage in the system , the azimuth may be rotated to the east. This would make the peak energy collection occur earlier in the morning but give a slightly lower daily total. A similar westerly rotation would provide more after noon energy if desired.

Another factor causing the collectors not to be oriented toward the south is the presence of a blockage (mountain or building) that shades morning or after noon sunlight. In this case the optimum orientation may call for rotation away from the blockage. Likewise, either persistent morning or afternoon cloud cover may cause the designer to orient the field azimuth for optimum energy collection.

It is generally accepted that the azimuth of a fixed field may be rotated up to 15 degrees from south and not make a significant difference in .the overall energy collection. With the information presented in Chapters 2 through 4, however, a simple average cloudy-day model can be easily coded and a comparison made between design alternatives.

Tilt. The most logical tilt angle for the fixed flat-plate collector is to tilt the surface from horizontal by an angle equal to the latitude angle. At this tilt, if the collector is facing south, the sun will be normal to the collector at noon twice a year (at the equinoxes). Also, the noontime sun will only vary above and below this position by a maximum angle of 23.5 degrees.

However, there are some system design considerations that may encourage the designer to tilt the collector's above or below this angle. For instance, if the slope of the roof where the collectors are to be installed is within 15 degrees of the

latitude tilt, one would probably choose a flush roof mounting. If the demand is greater in the winter months as with space heating, the designer may choose to tilt the collectors toward the horizon more and accept the summer energy loss. Similarly, the reverse may be true for a heavy summer demand (i.e., cooling).

As with collector azimuth orientation, shadowing objects may be considered and the collector tilted less because of blockage of solar irradiance when the altitude of the sun is low. Another factor that may affect the tilt orientation is the climate. If the particular region has considerable cloud cover during the winter, the collectors would be tilted to maximize summer energy collection. One final factor that could influence the approximate tilting of the collector is the systems operating threshold. If the system needs a high value of solar irradiance to begin operation, tilting the collectors closer to vertical may provide more energy to the system during start-up.

Again, in order to predict these effects, an analysis should be made using solar radiation data and sun angle computations to predict the exact effects of a particular set of circumstances

The yearly average data for two sites are shown on Figure 6.3. Plots for the other sites would be similar. Note that for both sites shown, the maximum yearly irradiation is obtained by surfaces tilted slightly less than the latitude angle. This is because of the greater cloud cover in the winter for both sites. Also note that a wide variation in tilt angle makes little difference in the irradiation received. This implies that the collector tilt optimization is not critical and that even horizontal surfaces may be an appropriate design choice if the cost of installation is considerably less for this orientation.

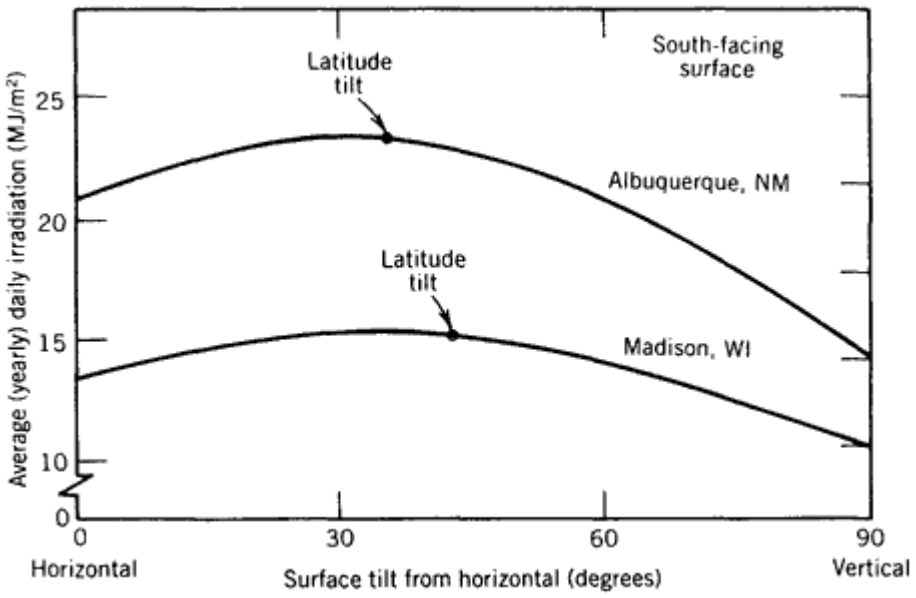

Figure 6.3 Total (global) irradiation on a south-facing tilted surface. Average ground reflectance was assumed to be 0.20

6.3.2 Efficiency Measurement

The energy collection efficiency is normally determined by testing. As discussed in Chapter 5, collector performance test data are correlated with a parameter comprised of the collector temperature rise above ambient divided by the solar irradiance. For flat-plate collector performance, the collector temperature and the solar irradiance used in this correlation are different from those used for concentrating collectors.

The collector temperature used for flat-plate collector performance correlation is normally the temperature of the heat-transfer fluid entering the collector, not the average fluid temperature, as is common for concentrating collectors.

Although the use of fluid inlet temperature makes application of the performance correlation easier in design studies, it also makes the correlation considerably more dependent on the flow rate of the heat-transfer fluid. Therefore, every correlation using fluid inlet temperature must specify the fluid flow rate at which the measurements were made. Deviation from this flow in a particular design requires that a different correlation be used. The recommended test flow rate (ASHRAE, 1977) for a liquid collector is 0.02 kg/hr (14.7 lb/hr ft^2) and for an air collector, 0.01 $m^3/s\ m^2$ (1.97 cfm/ft^2) at atmospheric pressure.

Because a flat-plate collector can collect both beam (direct) and diffuse solar radiation, the global (total) solar irradiance is used as the basis for flat-plate collector performance correlations. In testing the collector, the aperture irradiance is the global (total) solar irradiance measured in the plane of the collector, which includes the cosine loss of the beam component and some ground reflection if the collector is tilted from the horizontal as is usually the case.

A dilemma arises with the use of this performance correlation because the global (total) solar irradiance on a tilted aperture $I_{t,a}$ is used as input into the correlation. This value must include ground reflection. Equation (4.6) gives the designer a means of predicting the global (total) aperture irradiance when the aperture is tilted from the horizontal by an angle β .

The appropriate collector performance correlation for a flat-plate collector is Equation (5.7) modified for a non-concentrating collector:

$$\eta_{col} = F_R \eta_{opt} - F_R U_l \left(\frac{T_{in} - T_a}{I_{t,a}} \right) \qquad (6.1)$$

where the optical efficiency η_{opt} and the overall heat loss coefficient U_L were discussed in Chapter 5, and the total aperture irradiance $I_{t,a}$ in Chapter 4, Equation 4.29. The term F_R is the collector heat removal efficiency factor and is dependent on the absorber plate tube spacing and the flow rate of heat transfer fluid through these tubes. The analytical development of this factor is described in Duffie and Beckman (1980).

6.3.3 Typical Performance

Figure 6.4 gives typical performance for a number of different types of flat-plate collectors. These range from an unglazed absorber as is used for very low temperature applications to double-glazed, selective-surface collectors. Also included on this plot is an evacuated tube-type collector, which is discussed in the following paragraphs.

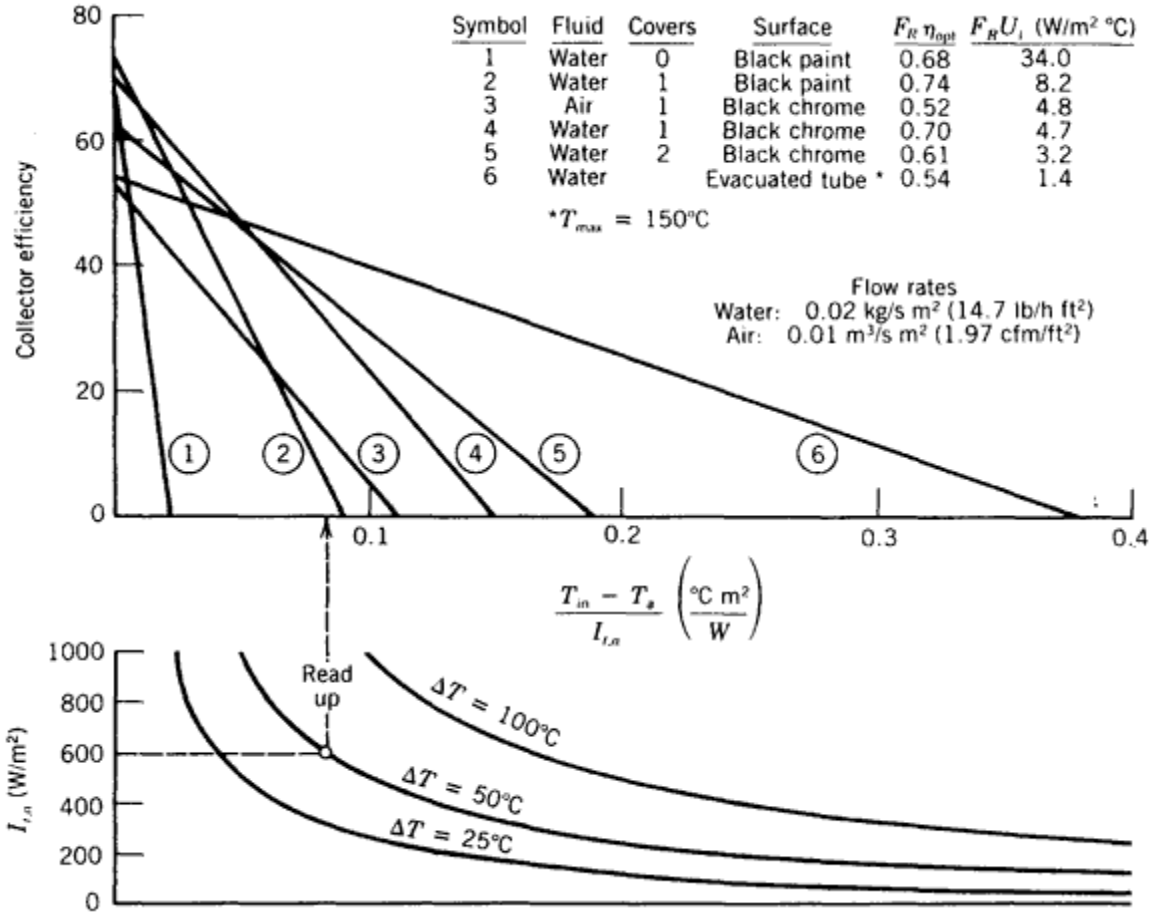

Figure 6.4 Performance of typical commercial flat-plate solar collectors.

A second abscissa scale has been included on this plot to aid in rapid interpretation. Since the abscissa is the temperature difference divided by the total solar irradiance, these parameters may be separated in nomogram style with a separate abscissa.

Although flat-plate collectors may be operated at fairly high temperatures when solar irradiance or ambient temperature is high, as solar irradiance or ambient temperature decreases or the angle of incidence increases, the efficiency falls. An example is shown in Figure 6.4 for a temperature difference of 50ºC (90ºF), where the solar irradiance has decreased to 600 W/m^2 (190 $Btu/hr\ ft^2$), and the efficiencies of the first three collectors have dropped below usable levels. This curve supports the conclusion made previously that flat-plate collectors are adequate for applications where the temperature rise above ambient is less than about 50ºC (90ºF). An exception to this conclusion is the evacuated-tube collector, which appears to be operable at twice that temperature rise. However, there are few high-temperature applications of the evacuated-tube collector to confirm their reliability at these temperatures.

6.3.4 Comparison with Parabolic Troughs

Treadwell (1979) used TMY (Typical Meteorological Year) weather data to compare the long-term performance of flat-plate collectors with parabolic trough collectors to determine at what collector operating temperature the parabolic trough collects more energy than the flat-plate collector on an annual basis.

A field of single glazed flat-plate collectors with selective absorber surfaces was compared with a field of commercial parabolic trough concentrators. Both horizontal and latitude-tilt south-facing orientations for the flat-plate collectors were considered, and both north-south and east-west tracking axis orientations were considered for the parabolic trough collectors. Typical Meteorological year (TMY) solar radiation data were used from the 26 original SOLMET sites.

It was found that the amount of diffuse energy collected by flat-plate collectors in most regions of the contiguous United States was not sufficient to compensate for the tracking capability of the troughs. Also that the typically higher optical efficiency of the flat-plate collector compensates only partially for the higher thermal efficiency of the concentrators. Over a full year's operation, the north-south trough orientation and the latitude-tilt flat-plate orientations provided the most energy. It was also found that for a 71ºC (168ºF) demand, flat-plate collectors outperform troughs only in Florida and southern Louisiana.

The break-even temperatures for the most efficient configurations (north south troughs and latitude-tilt flat-plates) are shown in Figure 6.5. This figure shows that troughs and flat-plate collectors have equivalent performance at about 49ºC (120ºF) in the southwestern region, whereas flat -plates and troughs may be

considered equivalent in terms of performance, for applications at 66ºC (150ºF) in most of the southeastern region.

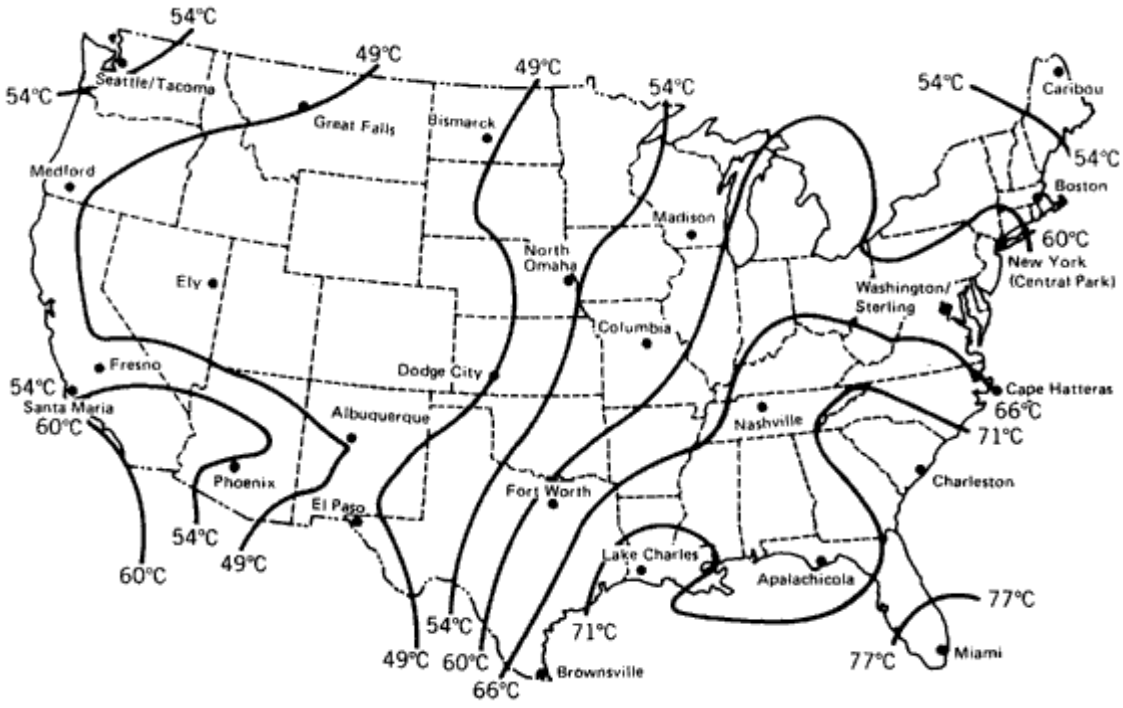

Figure 6.5 Break-even temperature for comparison between flat-plate collectors tilted at the latitude angle and parabolic troughs with the tracking axis oriented in the north-south direction. From Treadwell (1979).

6.4 Applications

In addition to the numerous applications of flat-plate collectors for domestic hot-water heating and space heating for both homes and business, there are a number of industrial process heat applications of flat-plate collectors. Table 6.2 summarizes many of these. The information was extracted from Kutscher et al. (1982) and shows a wide variety of applications. Note that all the demand temperatures are under 100ºC (212ºF).

The Campbell Soup Company process heat system in Sacramento, California is the singular example of the use of flat-plate collectors to preheat water before it enters a field of parabolic trough concentrators. The field, shown in Figure 6.2, incorporates 371.6 m^2 (4000 ft^2) of flat-plate collectors connected in series to 278.7 m^2 (3000 ft^2) of parabolic trough concentrators. The industrial demand for this system is for 91ºC (195ºF) hot water, which is used in a can washing process.

Table 6.2. Industrial Process Heat Systems in the United States Using Flat-Plate Collectors

Company	Location	Process Application	Temperature (ºC)	Area (m^2)
Hot- Water Systems				
Anhauser-Busch, Inc.	Jacksonville, FL	Beer pasteurization	60[a]	427
Aratex Services, Inc.	Fresno, CA	Heat process water	50 -70	624
Berkeley Meat Co.	S. Lake Tahoe, CA	Sanitation	82	232
Campbell Soup Co.	Sacramento, CA	Preheat can wash water	91	372
Coca-Cola Bottling Co.	Jackson, TN	Bottle washing	NA[a]	881
Easco Photo	Richmond, VA	Film processing	46	NA
General Extrusion, Inc.	Youngstown, OH	Solution heating	71-82[a]	409
Iris Images	Mill Valley, CA	Film processing	24-38	59
Jhirmack Enterprises, Inc.	Redding, CA	Preheat boiler water	71-93	622
Mary Kay Cosmetics	Dallas, TX	Sanitizing	60	305
Riegel Textile Corp.	LaFrance, SC	Heat dye-beck water	88[a]	621
Spicer Clutch (Dana)	Auburn, IN	Parts washing	54	87
Hot-Air Systems				

Gilroy Foods, Inc.	Gilroy, CA	Preheat drier air/ boiler feedwater	90	553
Gold Kist, Inc.	Decatur, AL	Preheat drier air [b]	82	1217
LaCour Kiln Services	Canton, MS	Lumber drying	82	234
Lamanuzzi & Pantaleo	Fresno, CA	Raisin drying	62	1951

[a]Evacuated tube type

[b]Water collector fluid/hot-air demand

6.5 Other Types

6.5.1 Evacuated-Tube Collectors

In an attempt to design higher-performance flat-plate collectors with mass production capability, collectors are being manufactured that are made from glass tubes with the enclosed space sealed and evacuated. Called evacuated-tube collectors, these have very low overall heat loss when operated at high temperatures. This is because they are essentially single glazed collectors with the space between the glazing and absorber evacuated, thereby eliminating convective loss. This leaves re-radiation as the only major loss mechanism. The results of this low heat loss can be seen in the exceptional high-temperature, low-solar irradiance performance of this collector design (Figure 6.4).

Figure 6.6 shows two evacuated-tube designs. In Corning Glass Company's design, a flat absorber plate with an attached water tube is sealed into a glass tube that is then evacuated. Solar energy is absorbed on the absorber plate and is extracted by water or other heat-transfer fluid flowing through the attached tube.

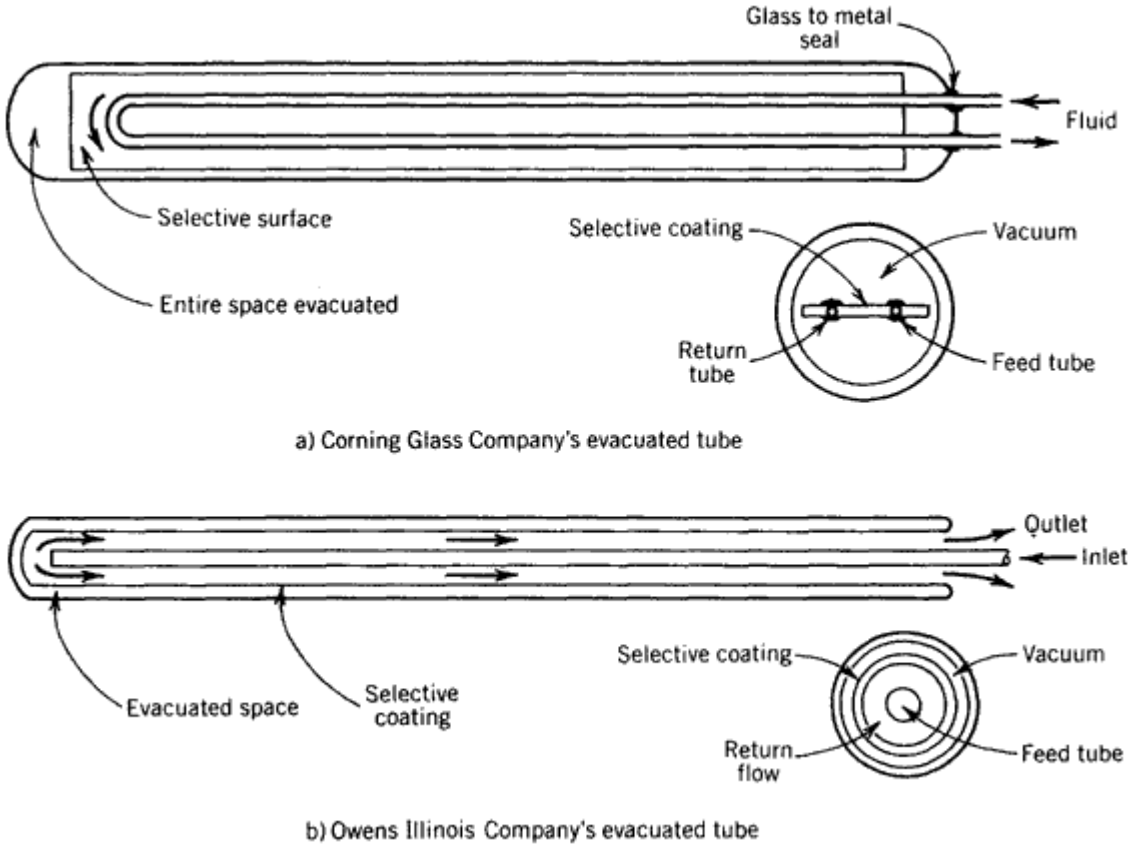

Figure 6.6 Designs of evacuated-tube collectors. Tubes are normally 5-10 cm (2-4 in.) in diameter.

In the Owens-Illinois design, concentric glass tubes are used with the inner tube surface becoming the absorber by coating it with a selective absorbing coating. The space between these tubes is evacuated. Heat-transfer fluid flows in through a third, inner, concentric feeder tube and flows out in the annulus outside the feeder tube in contact with the absorber tube surface.

The evacuated tube collector has the potential for developing high efficiencies at high temperatures. However, as a result of degradation of elastomeric seals, differential thermal expansion, and coating limitations, these collectors are limited to temperatures considerably below their maximum potential at noontime isolation levels. This means not only that applications cannot be planned for temperatures beyond these temperature limits, but also that under stagnation conditions (no heat removal ____ i.e., the zero-efficiency conditions) the collectors can exceed these limits. System designs must incorporate provisions to circumvent this possibility. An extensive review of the status of evacuated tube collector technology may be found in Window and Harding (1984).

6.5.2 Solar Ponds

It appears that the least expensive type of solar collector is a large solar pond. However, they have been considered primarily for large industrial applications because their cost decreases considerably with increases in size. There are two basic types of solar ponds: the shallow pond and the salt-gradient pond. Both are equivalent to horizontal flat-plate collectors, since they are non-concentrating, accept both direct and diffuse solar energy, and are limited to low temperature applications.

Shallow Ponds. A shallow solar pond consists of a group of collectors made of black plastic liners lying on top of insulation that has been laid on flat graded ground. Above the water bag is at least one translucent cover sheet, supported by side curbs. When there is adequate sunshine, water is pumped into the collectors from an underground storage tank. The water inside the collectors is heated by solar radiation absorbed by the pond liner and can attain temperatures of up to 60ºC (140ºF). Once heated, the water in the collectors may be pumped to an industrial demand or a hot storage tank for later use. At night or during periods of low solar irradiance, the water in the collectors may be drained back into the underground tank, thereby conserving the heat collected. A design guide for shallow ponds has been prepared by Casamajor and Parsons (1979).

Figure 6.7 shows a shallow pond collector design proposed by Dickenson et al. (1976) for use in a low-temperature solar thermal power system. The collector modules are 4 m (14 ft) wide and 200 m (656 ft) long. The width was determined by the width of commercially available unseamed, weatherable plastic sheets.

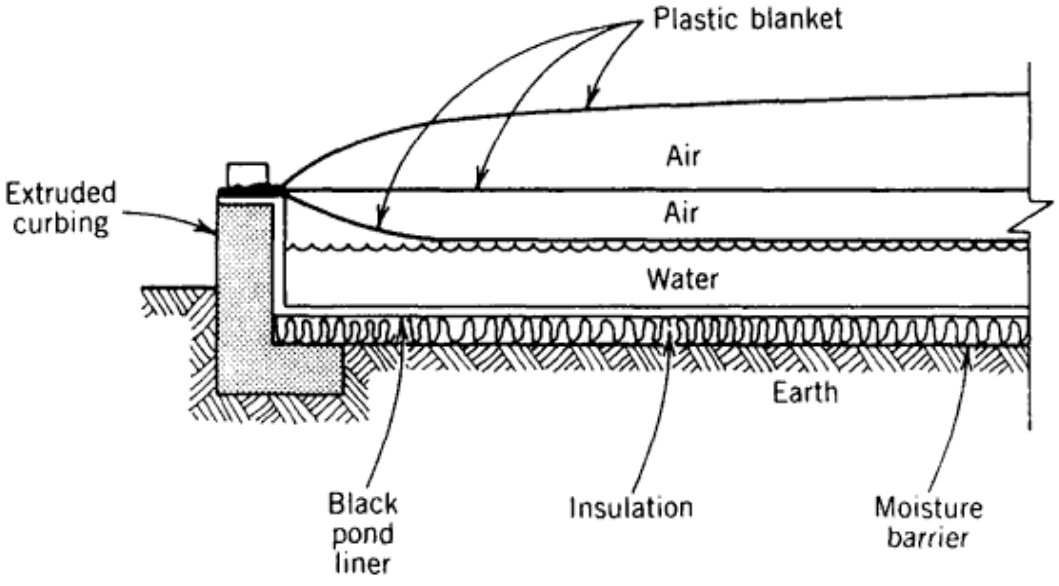

Figure 6.7 A shallow solar pond collector. Modules are 4 m ×200 m (13 ft × 656 ft). From Dickenson et al. (1976).

Salt-Gradient Ponds. When an open body of water absorbs solar energy, convection currents are created. As the sunrays that pass through the surface layer are absorbed in lower layers, this water is heated and rises to the surface, where heat is transferred away by convection to ambient air. Once the water cools, the density increases and the surface water moves downward. This movement of water equalizes the temperature throughout the body of water.

A salt-gradient solar pond employs a salt concentration gradient to suppress natural convection. Heated water holds more dissolved salt than does cooler water. The salty, heated water is also heavier and thus remains at the bottom of the solar pond. Sunlight penetrating through the top layers of the pond is absorbed at the bottom and trapped by the non-convecting gradient layer, which acts as an effective thermal insulator against convection.

In practice, salt-gradient solar ponds consist of three layers, or zones: (1) a surface convecting zone of low-salinity water, typically 0.2-0.4 m (8-16 in.) thick; (2) a non-convecting or salinity-gradient zone beneath the surface zone, in which salt concentration increases with depth, typically 1.0-1.5 m (3.3-5 ft) thick; and (3) a storage zone at the bottom of the pond of uniformly high salt concentration that stores heat and is typically 1-3 m (3.3-10 ft) thick..

For utilization of the heat stored at the bottom of the pond, hot brine is drawn from the storage zone (bottom layer) of the pond and pumped through a heat exchanger and back to the bottom of the storage zone. For power production applications where a Rankine cycle is used, condenser cooling water is drawn off the top of the pond and passed through the condenser and back to the surface, where it cools.

Construction of economical solar ponds requires the availability of inexpensive, flat land; accessibility to water; and an inexpensive source of salt or brine. A typical arrangement for this process is shown in Figure 6.8.

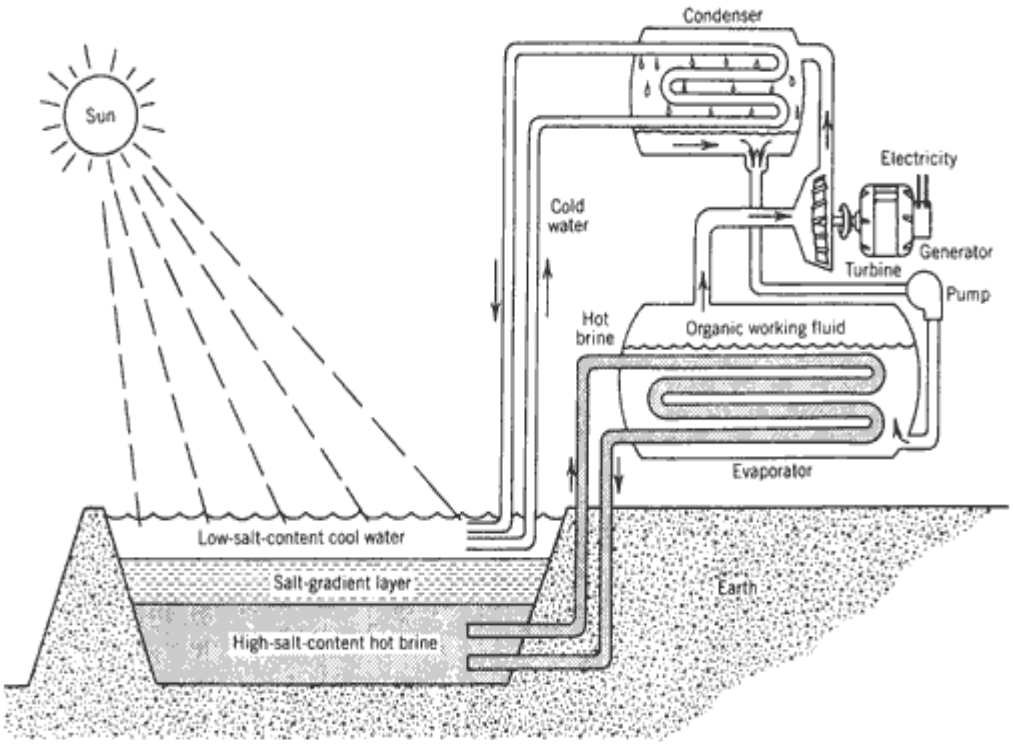

Figure 6.8 Electrical power production concept using salt-gradient ponds.

A salt-gradient solar pond can provide heat at temperatures in excess of 90ºC (194ºF). Such a pond provides built-in thermal storage of such large volume that heat can be collected in the summer and stored for use during the winter. Pioneering work on salt-gradient solar ponds has been done in Israel. Tabor (1981) gives an extensive review of the status and problems in this field [see also Tabor (1983)]. An extensive bibliography on the subject has been published in SERI (1981a).

The basic physical principles of salt-gradient ponds were defined by Weinberger (1964). Rabl and Nielsen (1975) subsequently presented a model that included a convective bottom layer. A computational procedure for determination of the thermal efficiency of a pond with a diffusely reflecting bottom may be found in Hull (1982) and a parametric analysis of various design considerations in Wang and Akbarzadeh (1983).

References and Bibliography

ASHRAE (1977), "Methods of Testing to Determine the thermal Performance of Solar Collectors," ASHRAE Standard 93-77, American Society for Heating, Refrigeration, and Air -Conditioning Engineering, New York.

Casamajor, A. B., and R. E. Parsons (1979), "Design Guide for Shallow Solar Ponds," Lawrence Livermore Labs Report UCRL 52385 (Rev. 1), January.

Dickenson, W. C., A. F. Clark, J. A. Day, and L. F. Wouters (1 976), "The Shallow Solar Pond Energy Conversion System," Solar Energy 18 (1), 3.

Duffie, J. A., and W. A. Beckman (1980), Solar Engineering of Thermal Processes, John Wiley & Sons, New York, 1980.

Huil, J. R. (1982), "Calculation of Solar Pond Thermal Efficiency with a Diffusely Reflecting Bottom," Solar Energy 29 (5), 385.

Kreider, J. F., and F. Kreith (1982), Solar Heating and Cooling, 2nd ed., McGraw-Hill, New York.

Kutscher, C. F., R. L. Davenport, D. A. Dougherety, R. C. Gee, P. M. Masterson, and E. K. May (1982), "Design Approaches for Solar Industrial Process Heat Systems," SERI Report SERI/ TR-253-1356, August.

Lunde, P. J. (1980), Solar Thermal Engineering, John Wiley & Sons, New York.

Rabl, A., and C. E. Nielsen (1975), "Solar Ponds for Space Heating," Solar Energy 17 (1), 1.

SERI (198la), "Solar Ponds: A Selected Bibliography," SERI Report SERI/TR-752-711, November.

SERI (1981b), "Solar Radiation Energy Resource Atlas of the United States," SERI Report SERI/SP-642-1037, October.

Smith, J. H. (1980), "Handbook of Solar Energy Data for South-Facing Surfaces in the United States," Jet Propulsion Laboratory Report DOE/JPL-1012-25, Vol. 1, January.

Tabor, H. (1981), "Solar Ponds," Solar Energy 27(3), 181.

Tabor, H. (1983), "Solar Ponds-Corrections," letter to the editor, Solar Energy 30(1).

Treadwell, G. W. (1979), "Low-Temperature Performance Comparisons of Parabolic -Trough and Flat -Plate Collectors Based on Typical Meteorological Year Data," Sandia National Labs, Report SAND78 -0965, February.

Wang, Y. F., and A. Akbarzadeh (1983), "A Parametric Study on Solar Ponds," Solar Energy 30(6), 555.

Weinberger, H. (1964), "The Physics of the Solar Ponds," Solar Energy 8(2), 45.

Window, B., and G. L. Harding (1984), "Progress in the Materials Science of All-Glass Evacuated Collectors," Solar Energy 32 (5), 609.

8. Concentrator Optics

To this point, we have developed an understanding of how solar energy is collected by flat-plate collectors…those where the entire area that the sun's radiation falls, absorbs the incident energy. Concentrating collectors, on the other hand, use large reflectors to ´concentrate´ the incident solar energy onto a smaller receiver. The main goal for doing this is to increase the temperature of the heat collected from the sun. Increased temperature is a benefit for many industrial process uses, and is directly connected to the efficiency at which electricity can be produced from thermal sources.

In the following sections we will develop the analytical tools necessary to understand the basic concepts of concentration of solar energy, in parabolic trough, parabolic dish, central receivers and Fresnel lens solar collection systems. These tools will be presented with the following outline:

- Conclusions

8.1 Why Concentration?

The operation of any solar thermal energy collector can be described as an energy balance between the solar energy absorbed by the collector and the thermal energy removed or lost from the collector. If no alternative mechanism is provided for removal of thermal energy, the collector receiver heat loss must equal the absorbed solar energy.

The temperature of the receiver increases until the convective and radiation heat loss from the receiver equals the absorbed solar energy. The temperature at which this occurs is termed the *collector stagnation temperature.*

For control of the collector temperature at some point cooler than the stagnation temperature, active removal of heat must be employed. This heat is then available for use in a solar energy system. The rate at which heat is actively removed from the collector determines the collector operating temperature. For removal of a large fraction of the absorbed solar energy as useful heat, the amount of heat lost from the receiver must be kept small.

Receiver heat loss can be reduced by operating the collector near the ambient temperature (such as with low-temperature flat-plate collectors) or by constructing the collector such that heat loss at elevated temperature is reduced. The most common way of reducing receiver heat loss at elevated temperatures is to reduce the size of the hot surface (i.e., the receiver) since heat loss is directly proportional to area of the hot surface. Concentrating collectors reduce the area of the receiver by reflecting (or refracting) the light incident on a large area (the collector aperture) onto an absorber of small area. With reduced heat loss, concentrating collectors can operate at elevated temperatures and still provide significant quantities of useful thermal energy.

A second reason for using concentration in the design of solar collectors is that, in general, reflective surfaces are usually less expensive than absorbing (receiver) surfaces. Therefore, large amounts of inexpensive reflecting surface area can placed in a field, concentrating the incident solar energy on smaller absorbing surfaces. However, concentrating collectors must track the sun´s movement across the sky, adding significant cost to the construction of a concentrating collector system.

8.1.1 Concentration Ratio

The term "*concentration ratio*" is used to describe the amount of light energy concentration achieved by a given collector. Two different definitions of

concentration ratio are in general use. They are defined briefly here so that the terms may be used.

Optical Concentration Ratio (CR_o). The averaged irradiance (radiant flux) (I_r) integrated over the receiver area (A_r), divided by the insolation incident on the collector aperture.

$$CR_o = \frac{\frac{1}{A_r}\int I_r dA_r}{I_a} \qquad (8.1)$$

Geometric Concentration Ratio (CR_g). The area of the collector aperture A_a divided by the surface area of the receiver A_r

$$CR_g = \frac{A_a}{A_r} \qquad (8.2)$$

Optical concentration ratio relates directly to lens or reflector quality; however, in many collectors the surface area of the receiver is larger than the concentrated solar image.

Thermal losses in such situations are larger than might be inferred from examination of the optical concentration ratio. Since geometric concentration ratio refers to receiver area, it is most commonly used because it can be related to collector heat loss [e.g., see Chapter 5] . Note that if the aperture insolation and receiver irradiance are both uniform over the entire area, the optical and geometric concentration ratios are equal.

Perhaps the simplest solar concentrator is a concentrating flat-plate collector. An example of such a collector is shown in Figure 8.1. This type of concentrator is a flat-plate collector surrounded by mirrors that reflect sunlight incident outside the normal perimeter of the flat plate onto the absorber plate of the collector. This type of collector is usually constructed to reduce the cost of a flat-plate collector by reducing the area of the absorber and cover plates, which are frequently expensive. A concentrating flat-plate collector such as that shown in Figure 8.1 is typically limited to geometric and optical concentration ratios of 2-3.

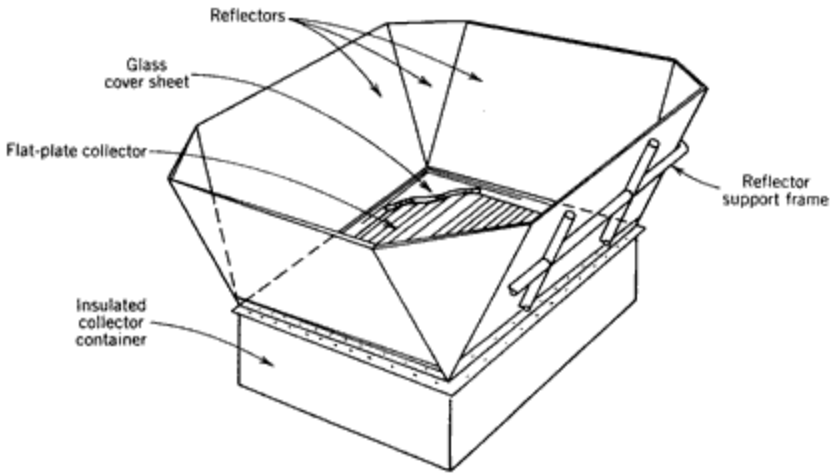

Figure 8.1 A concentrating flat-plate collector

If higher concentration ratios are desired, curved mirrors or lenses are used. Circular and parabolic mirror optics are described in Section 8.3, and Fresnel lenses are examined in Section 8.7.

8.2 Parabolic Geometry

8.2.1 The Parabola

A parabola is the locus of a point that moves so that its distances from a fixed line and a fixed point are equal. This is shown on Figure 8.2, where the fixed line is called the *directrix* and the fixed point F, the focus. Note that the length FR equals the length RD. The line perpendicular to the directrix and passing through the focus F is called the *axis of the parabola.* The parabola intersects its axis at a point V called the *vertex,* which is exactly midway between the focus and the directrix.

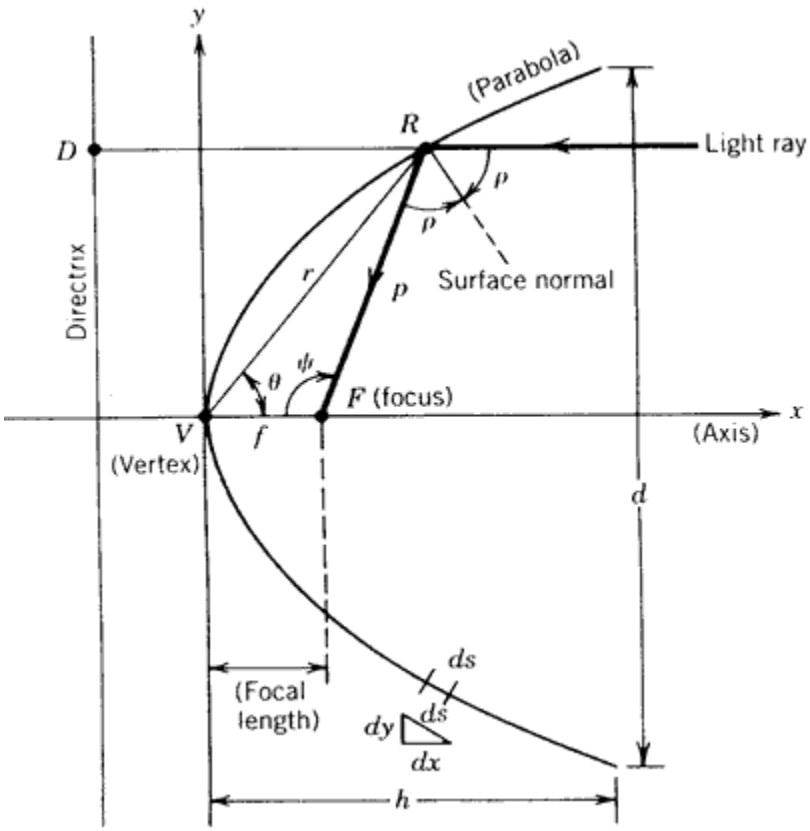

Figure 8.2 The parabola.

If the origin is taken at the vertex V and the *x*-axis along the axis of the parabola, the equation of the parabola is

$$y^2 = 4fx \qquad (m^2) \qquad (8.3)$$

where f, the focal length, is the distance VF from the vertex to the focus. When the origin is shifted to the focus F as is often done in optical studies, with the vertex to the left of the origin, the equation of a parabola becomes

$$y^2 = 4f(x + f) \qquad (m^2) \qquad (8.4)$$

In polar coordinates, using the usual definition of r as the distance from the origin and θ the angle from the *x*-axis to r, we have for a parabola with its vertex at the origin and symmetrical about the *x*-axis

$$\frac{\sin^2\theta}{\cos\theta} = \frac{4f}{r} \qquad (8.5)$$

Often in solar studies, it is more useful to define the parabolic curve with the origin at F and in terms of the angle ψ in polar coordinates with the origin at F . The angle ψ is measured from the line VF and the parabolic radius p, is the distance from the focus F to the curve. Shifting the origin to the focus F, we have

$$p = \frac{2f}{1+\cos\psi} \quad (m) \qquad (8.6)$$

The parabolic shape is widely used as the reflecting surface for concentrating solar collectors because it has the property that, for any line parallel to the axis of the parabola, the angle p between it and the surface normal is equal to the angle between the normal and a line to the focal point. Since solar radiation arrives at the earth in essentially parallel rays and by Snell's law the angle of reflection equals the angle of incidence, all radiation parallel to the axis of the parabola will be reflected to a single point F, which is the focus. Careful inspection of the geometry described in Figure 8.2 will show that the following is true:

$$\psi = 2\rho \qquad (8.7)$$

The general expressions given so far for the parabola define a curve infinite in extent. Solar concentrators use a truncated portion of this curve. The extent of this truncation is usually defined in terms of the rim angle ψ_{rim} or the ratio of the focal length to aperture diameter *f/d.* The scale (size) of the curve is then specified in terms of a linear dimension such as the aperture diameter *d* or the focal length *f.* This is readily apparent in Figure 8.3, which shows various finite parabola having a common focus and the same aperture diameter.

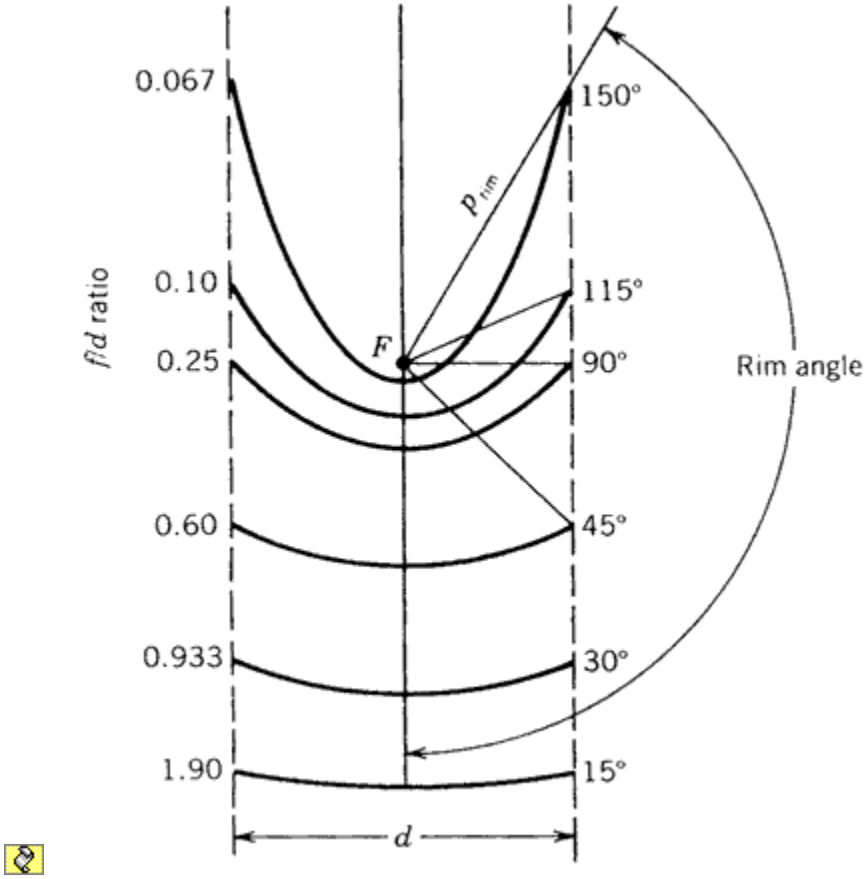

Figure 8.3 Segments of a parabola having a common focus *F* and the same aperture diameter.

It can be seen that a parabola with a small rim angle is relatively flat and the focal length is long compared to its aperture diameter. Once a specific portion of the parabolic curve has been selected, the height of the curve, h may be defined as the maximum distance from the vertex to a line drawn across the aperture of the parabola. In terms of focal length and aperture diameter, the height of the parabola is

$$h = \frac{d^2}{16f} \qquad (m) \qquad (8.8)$$

In a like manner, the rim angle ψ_{rim} may be found in terms of the parabola dimensions:

$$\tan\psi_{rim} = \frac{1}{(d/8h) - (2h/d)} \qquad (8.9)$$

Another property of the parabola that may be of use in understanding solar concentrator design is the arc length *s*. This may be found for a particular

parabola from Equation (8.3) by integrating a differential segment of this curve and applying the limits $x = h$ and $y = d/2$ as pictured in Figure 8.2. The result is

$$s = \left[\frac{d}{2}\sqrt{\left(\frac{4h}{d}\right)^2 + 1}\right] + 2f \ln\left[\frac{4h}{d} + \sqrt{\left(\frac{4h}{d}\right)^2 + 1}\right] \qquad (m) \tag{8.10}$$

where d is the distance across the aperture (or opening) of the parabola as shown in Figure 8.2 and h is the distance from the vertex to the aperture. The cross sectional area of the space enclosed between a parabola and a line across its aperture and normal to the axis is given by

$$A_x = \frac{2}{3} d \cdot h \qquad (m^2) \tag{8.11}$$

this area should not be confused with the reflecting surface area of a parabolic trough or dish or their aperture areas, the equations for which are given in the following section.

Often in evaluating parabolic geometry and related optical derivations, the casual reader becomes confused with the many forms used to represent the geometry of a particular parabolic shape. The following equivalencies are given for the convenience of the reader:

$$\tan\psi_{rim} = \frac{(f/d)}{2(f/d)^2 - \frac{1}{8}} \tag{8.12}$$

$$\tan\left(\frac{\psi_{rim}}{2}\right) = \frac{1}{4(f/d)} \tag{8.13}$$

$$\frac{f}{d} = \frac{1 + \cos\psi_{rim}}{4\sin\psi_{rim}} \tag{8.14}$$

$$\frac{f}{d} = \frac{1}{4\tan(\psi_{rim}/2)} \tag{8.15}$$

8.2.2 Parabolic Cylinder

The surface formed by moving a parabola along the axis normal to its plane is called a *parabolic cylinder.* Solar concentrators with this type of reflecting surface are often called parabolic *troughs* because of their appearance, or *line focus*

concentrators because the foci of the parabola describe a line in this geometry. When the plane containing the axes of the parabola is aligned parallel to the rays of the sun, the rays are focused on this focal line. For a parabolic cylinder of length l and having the cross-sectional dimensions shown in Figure 8.2, the collector aperture area is given by

$$A_a = l \cdot d \qquad (m^2) \qquad (8.16)$$

The reflective surface area is found by using the arc length developed in Equation (8.10):

$$A_s = l \cdot s \qquad (m^2) \qquad (8.17)$$

The focal length f and the rim angle ψ_{rim} for the parabolic cylinder are given in Equations (8.8) and (8.9).

8.2.3 Paraboloid

The surface formed by rotating a parabolic curve about its axis is called a *paraboloid* of *revolution.* Solar concentrators having a reflective surface in this shape are often called *parabolic dish* concentrators. The equation for the paraboloid of revolution as shown in Figure 8.4, in rectangular coordinates with the z-axis as the axis of symmetry, is

$$x^2 + y^2 = 4fz \qquad (m^2) \qquad (8.18)$$

where the distance f is the focal length VF. In cylindrical coordinates, where a is the distance from the z-axis, this becomes

$$z = \frac{a^2}{4f} \qquad (m) \qquad (8.19)$$

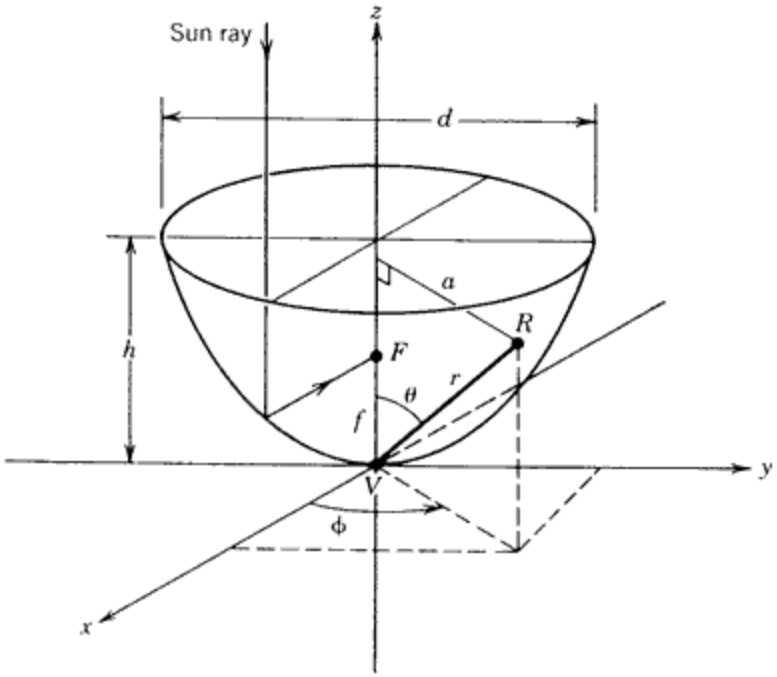

Figure 8.4 Paraboloid of revolution.

In spherical coordinates, the equation of a paraboloid of revolution with its vertex V at the origin and r, ϕ and θ defining the location of point R on the paraboloid, is

$$\frac{\sin^2\theta}{\cos\theta} = \frac{4f}{r} \qquad (8.20)$$

The surface area of the paraboloid may be found by integrating Equation (8.19) over the appropriate limits. We can define a circular differential area strip on the paraboloid as shown in Figure 8.5 as

$$dA_s = 2\pi \; a\sqrt{dz^2 + da^2} \qquad \left(m^2\right) \qquad (8.21)$$

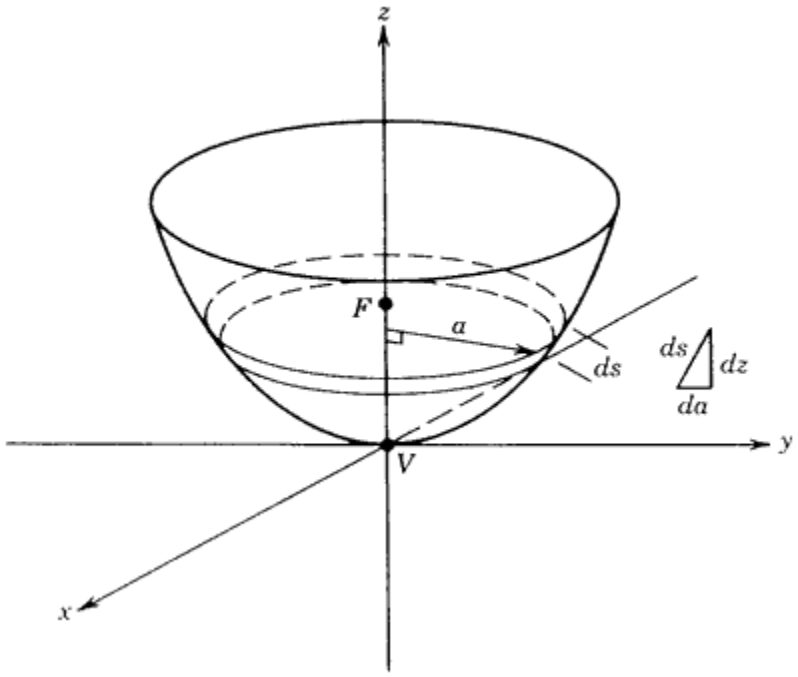

Figure 8.5 Parameters defining a circular strip of differential area.

Note that the differential element of arc ds is cast in terms of the height dz and the radial distance da. Finding the derivative of z with respect to a using Equation (8.19), we express the differential area band as

$$dA_s = 2\pi \; a\sqrt{\left(\frac{a}{2f}\right)^2 + 1} \quad da \qquad \left(m^2\right) \tag{8.22}$$

The full surface area A_s of a paraboloid having a focal length f and an aperture diameter d may be found by integrating Equation (8.22). The result is

$$A_s = \int_0^{d/2} dA_s = \frac{8\pi \; f^2}{3}\left\{\left[\left(\frac{d}{4f}\right)^2 + 1\right]^{3/2} - 1\right\} \qquad \left(m^2\right) \tag{8.23}$$

The concentrator aperture area, of most importance to the solar designer for prediction of solar concentrator performance, is simply the circular area defined by the aperture diameter d and is given by

$$A_a = \frac{\pi \; d^2}{4} \qquad \left(m^2\right) \tag{8.24}$$

An equation for the aperture area may also be cast in terms of the focal length and the rim angle. Using Equation (8.6), which is the polar form of the equation of a parabola, we have

$$A_a = \frac{\pi}{4}\left(2p\sin\psi_{rim}\right)^2$$

$$= 4\pi\ f^2 \frac{\sin^2\psi_{rim}}{\left(1+\cos\psi_{rim}\right)^2} \qquad \left(m^2\right) \qquad (8.25)$$

Note: Equation (8.26) has been renumbered and moved to another chapter.

(8.26)

8.3 Parabolic and Spherical Optics

Both spherical and parabolic geometries are represented in solar thermal concentrators. In some concentrators, however, a spherical (or more usually cylindrical) geometry is used as an approximation to a true parabola. As will be shown in Chapter 9, spherical optics allow for fixed- aperture (i.e., non-tracking) concentrators. Since parabolic geometries strongly dominate solar concentrators, a rather thorough examination of the analytical description of parabolic geometry is presented in this chapter.

In order to facilitate a discussion of spherical and parabolic optics, it is convenient to define the term ‘plane of curvature’, as illustrated for a parabolic trough in Figure 8.6.

The plane of curvature (i.e., cross section) can be considered as a two-dimensional slice normal, in the case of a parabolic trough, to the linear axis of the concentrator. For a spherical or a parabolic dish, the plane of curvature is rotated to generate the dish geometry. The optical principles of spherical and parabolic mirrors are examined below through ray trace diagrams and by initially restricting the discussion to the plane of curvature. The impact of translation or rotation of the plane of curvature is then discussed in order to evaluate the optical characteristics of actual concentrator geometries.

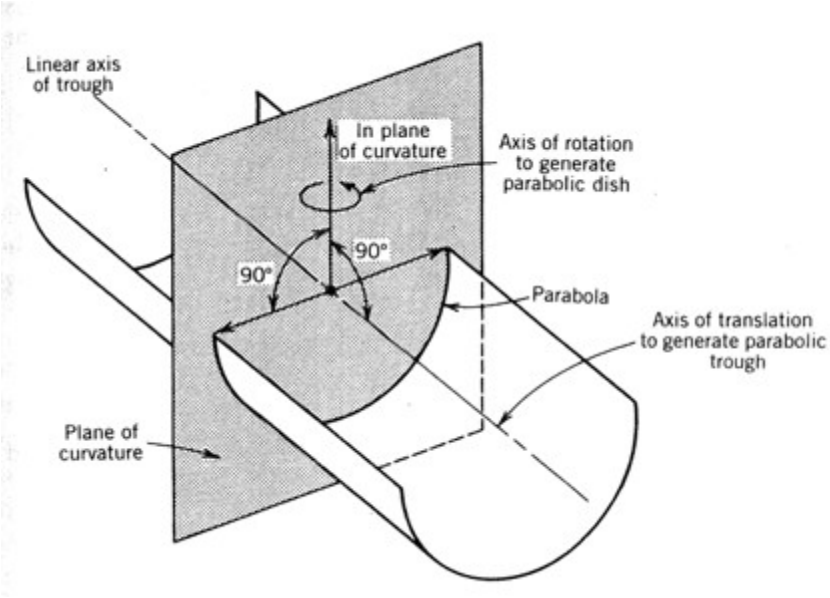

Figure 8.6 Definition of plane of curvature

The purpose of a general discussion at this point, prior to examining individual concentrator concepts, is to develop an understanding of the basic limitations imposed by spherical and parabolic geometries and how these limitations impact basic concentrator design.

The equation of a circle as drawn in Figure 8.7a in Cartesian coordinates with its center at a, b and radius r is

$$(x-a)^2+(y-b)^2=r^2 \qquad (m^2) \qquad (8.27)$$

which reduces to the familiar form

$$x^2+y^2=r^2 \qquad (m^2) \qquad (8.28)$$

when the circle is centered at $(0,0)$. The equation for a line tangent to this circle at the point (x_1, y_1) is

$$x_1x+y_1y=r^2 \qquad (m^2) \qquad (8.29)$$

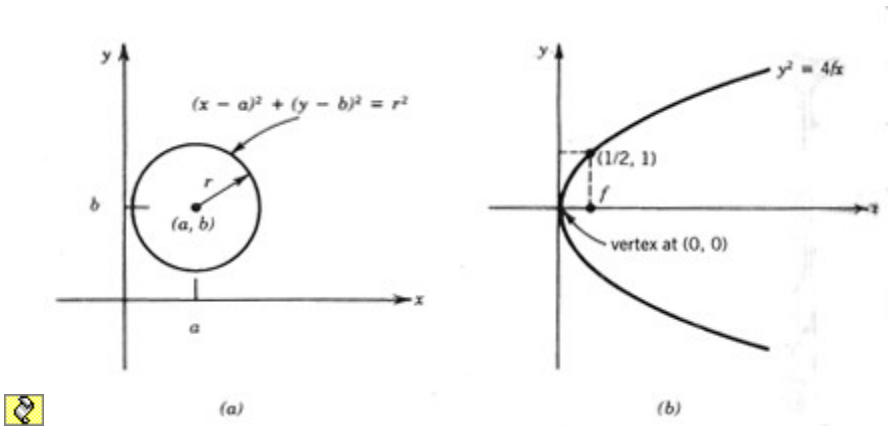

Figure 8.7 Definition of *(a)* circle and *(b)* parabola

A parabola (see Figure 8.7b) can be defined as any section of a right circular cone resulting from a plane slicing through the cone parallel to, but not including, the axis of the cone. The equation for a parabola, with focal length *f*, in the Cartesian coordinates is

$$y^2 = 4fx \qquad (m^2) \qquad (8.30)$$

The vertex of a parabola having this form will be at $(0,0)$. The equation of the tangent to this parabola at (x_1, y_1) is

$$y_1 y = 4f(x_1 + x) \qquad (m^2) \qquad (8.31)$$

These basic equations are useful in examination of the optical properties of spherical and parabolic mirrors.

Another characteristic useful in discussing parabolic or spherical mirrors is the *rim angle*. Rim angle (ψ_{rim}) is defined graphically in Figure 8.8 for a parabolic trough. A similar definition holds for parabolic dishes and mirrors based on spherical geometry.

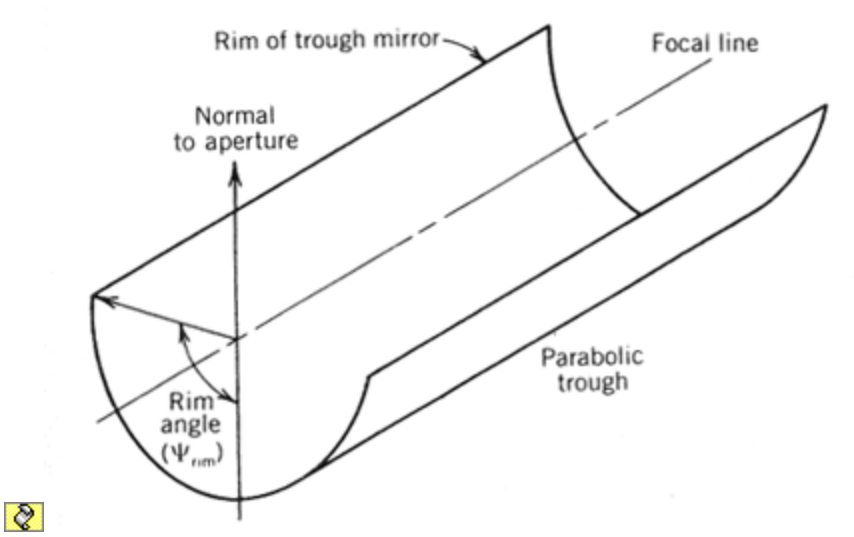

Figure 8.8 Definition of rim angle

8.3.1 Two -Dimensional Ray Trace Diagrams

The reflections of parallel rays of sunlight from both two dimensional circular and parabolic mirrors are shown in the ray trace diagrams in Figures 8.9 and 8.10, respectively. The characteristics of these two mirrors in concentrating parallel rays of incident light which are normal to the reflector aperture are:

- All parallel rays reflected from a circular mirror pass through a line drawn through the center of the circle and parallel to the incident rays (see Figure 8.9*a*).

2. All parallel rays reflected from a parabolic mirror, when they are parallel to the axis of symmetry, intersect at a point (see Figure 8.10*a*).

In addition, a circular mirror is symmetrical with respect to rotations about its center. This means that if the sun's rays (assumed to be parallel for this discussion) are not normal to the mirror's aperture as in Figure 8.9*a*, the pattern of reflected rays looks the same but is rotated (see Figures 8.9*b* and 8.9*c*).

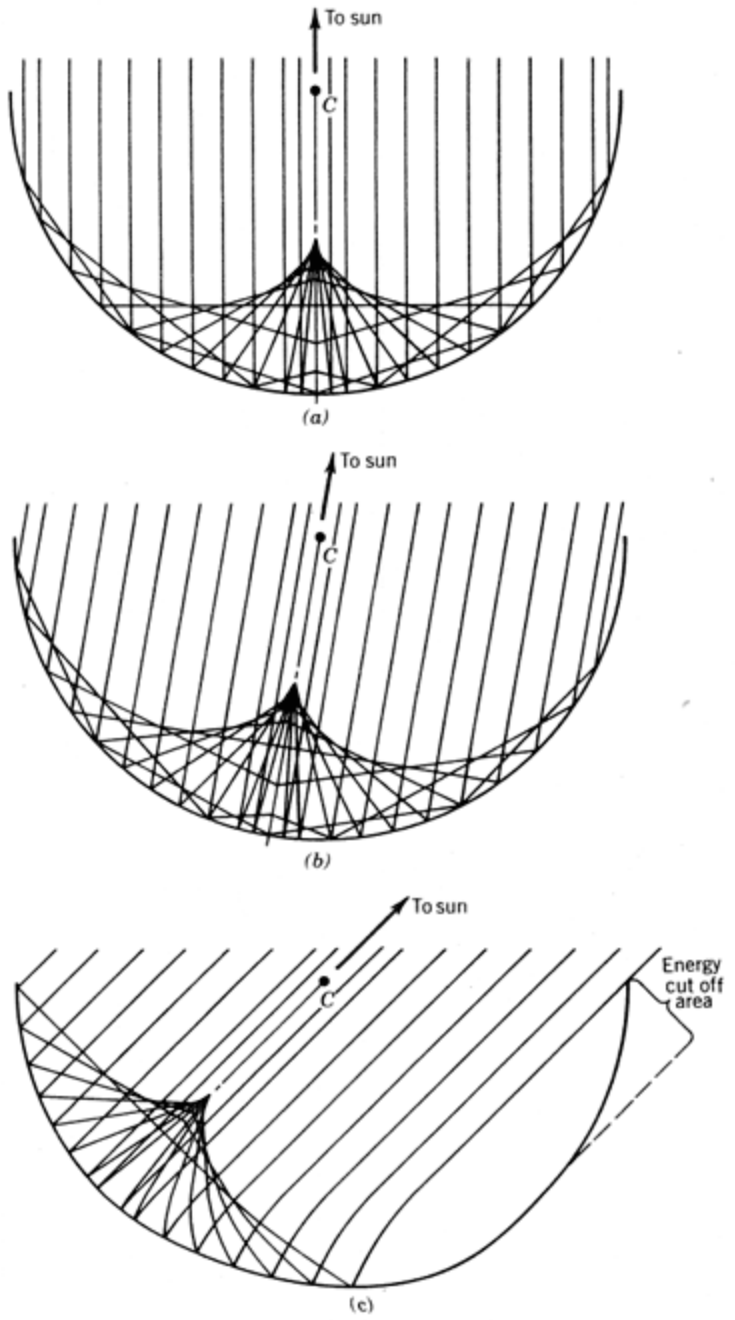

Figure 8.9 Characteristics of spherical optics (C = center of circle).

A parabolic mirror, on the other hand, is not symmetrical to rotations about its focal point. As shown in Figure 8.10, if the incident beam of parallel rays is even slightly off normal to the mirror aperture, beam dispersion occurs, resulting in spreading of the image at the focal point. For a parabolic mirror to focus sharply, therefore, it must accurately track the motion of the sun to keep the axis (or plane) of symmetry parallel to the incident rays of the sun.

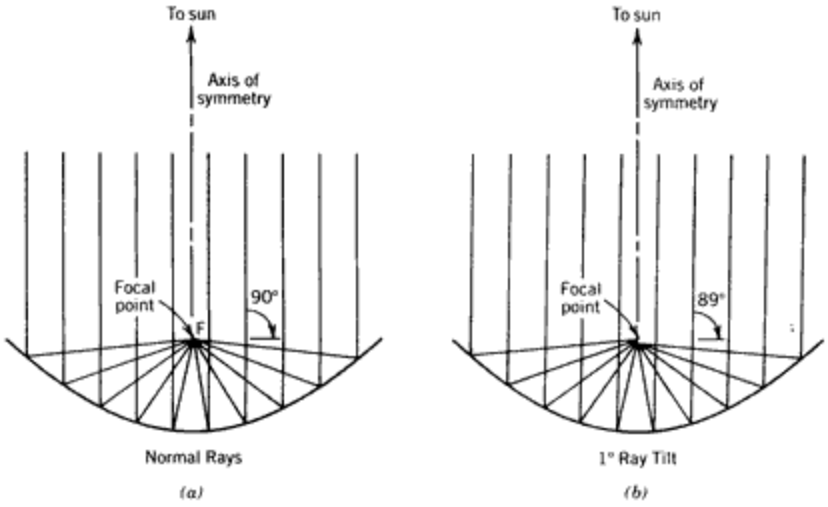

Figure 8.10 Characteristics of parabolic optics, (a) for rays parallel to the axis of symmetry, (b) for rays 1◦ off of the axis of symmetry.

8.3.2 Line Focus Troughs

To form either a cylindrical or parabolic trough, the two-dimensional mirrors shown in Figures 8.9 and 8.10 must be translated normal to the plane of curvature as illustrated in Figure 8.11. Tracking requirements of the linear troughs are similar to that of the two-dimensional mirrors discussed above.

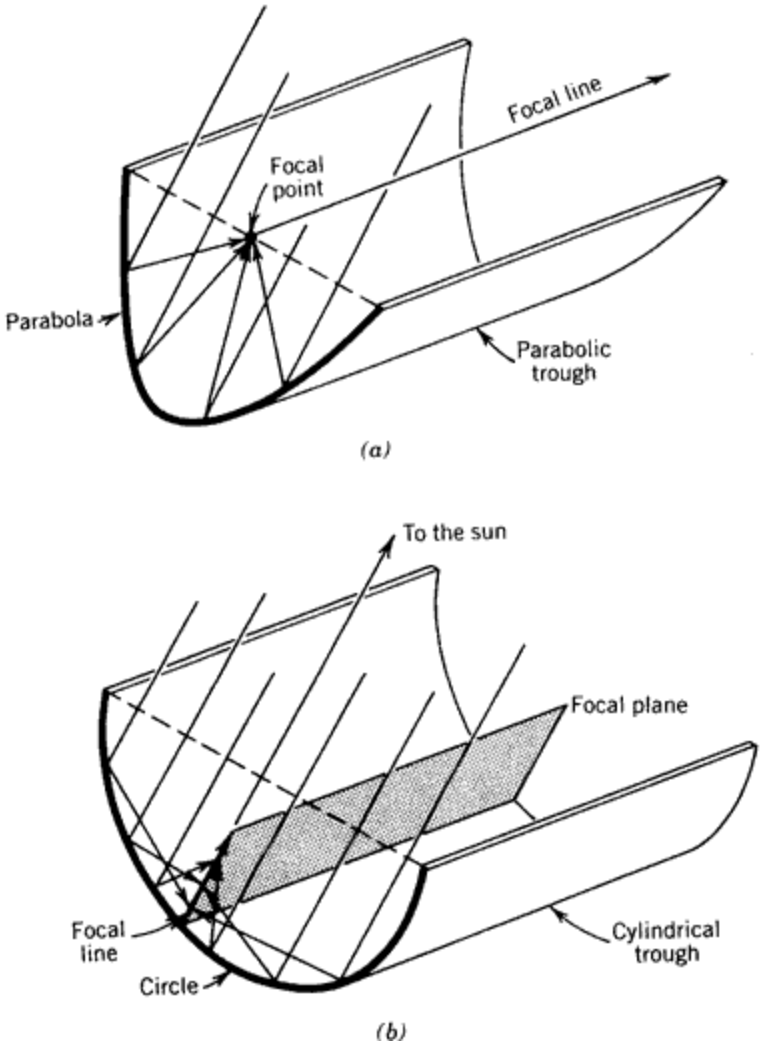

Figure 8.11 Formation of linear troughs: *(a)* parabolic trough; *(b)* cylindrical trough.

A parabolic trough as shown in Figure 8.11*a* has a line focus and must be tracked about its linear axis in order to maintain focus. The proper tracking angle is defined by the orientation of the trough relative to the sun's position. Analytical expressions for the proper tracking angle of parabolic troughs are developed in Chapter 4. Basically, a parabolic trough must track about its linear axis so that when the sun's rays are projected onto the plane of curvature, they are normal to the trough aperture.

Since linear translation does not introduce curvature along the translation axis, the trough need not be tracked in this direction in order to maintain focus. Just as reflection from a plane mirror does not defocus parallel rays of light, neither is the component of the incident beam (direct) insolation in the plane of translation defocused by a linear translation. The net effect of a non-normal incidence angle (θ_i) in a parabolic trough (assuming that the trough has been tracked to

satisfy focusing requirements) is that the reflected beam is simply translated along, but still focused on, the receiver tube.

Figure 8.12 shows a photograph of a receiver tube illuminated by direct insolation entering the trough aperture with a non-normal incidence angle. In this case, the trough has been tracked about its linear axis as indicated by the highly focused beam image on the receiver tube. As a result of the non-normal incidence angle, however, the reflected beam is translated down the receiver tube; note that the right end of the receiver tube is dark. At the far end of the parabolic trough some of the incident insolation is reflected past the end of the receiver tube. This is illustrated in Figure 8.13 for another collector. Note that some concentrated light is failing on the flexible hose and not on the receiver. This energy is lost to the collector and is called the collector *endloss.*

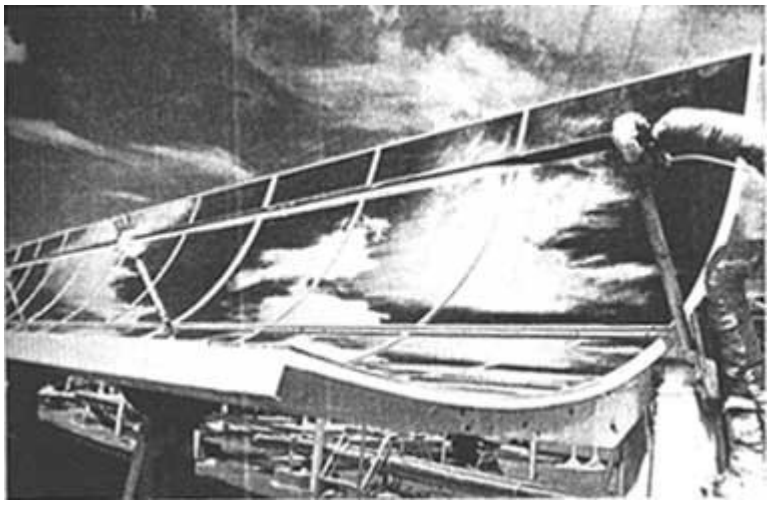

Figure 8.12 Translation of focused radiation along receiver tube due to non-normal incident insolation. Courtesy of Sandia National Laboratories.

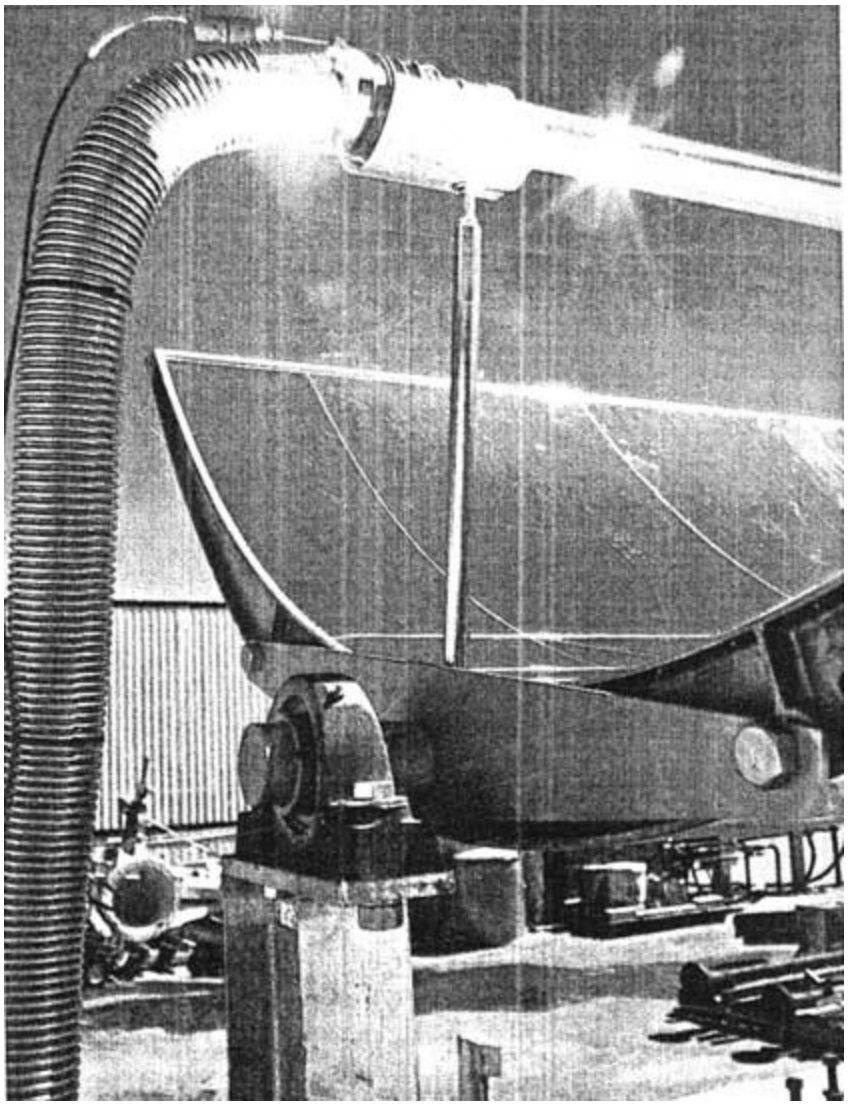

Figure 8.13 Parabolic trough endloss. Courtesy of Sandia National Laboratories.

Since linear translation does not introduce defocusing of the concentrated radiation, the aperture of a cylindrical trough need not track at all to maintain focus. However, as indicated in Figure 8.11*b*, a high-rim angle cylindrical trough would have a focal plane not a focal line. To avoid a dispersed focus, cylindrical troughs would have to be designed with low rim angles in order to provide an approximate line focus. The advantage of a cylindrical mirror geometry is that it need not track the sun in any direction as long as some means is provided to intercept the moving focus.

The effect of rim angle ψ_{rim} on the focus of a cylindrical trough can be seen by observing the path of an individual ray as it enters the collector aperture.

Figure 8.14 shows the angles involved. At the mirror surface the incident ray will undergo reflection. Since, by definition, a radius of a circle is normal to the tangent to the circle at all points, it follows that $\theta_1 = \theta_2$ (solid lines). In addition, since the incident ray is assumed parallel to the axis of curvature, $\theta_3 = \theta_1 = \theta_2$. Thus the triangle *C-PF-M* is an isosceles triangle with the characteristics that *C-PF* is equal to *r/2* for small values of θ_3.

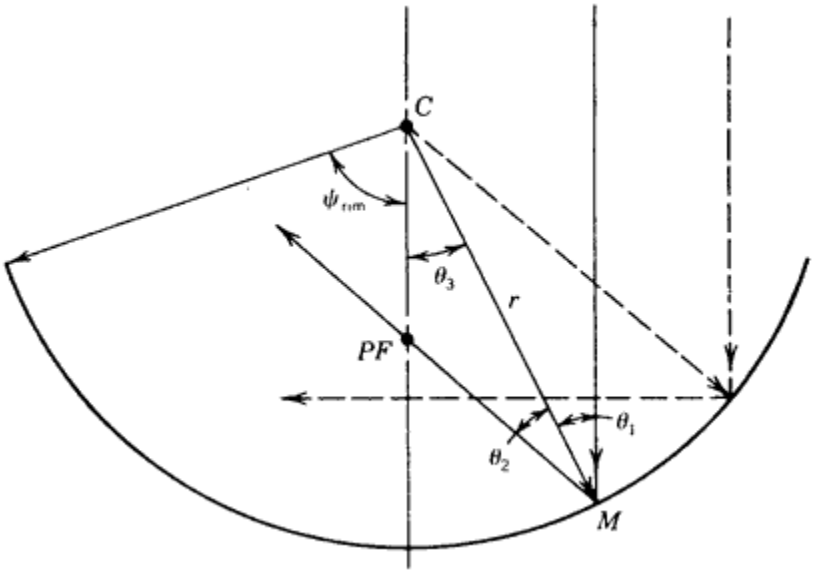

Figure 8.14 Definitions of angles for reflection from a cylindrical (or spherical) mirror.

Point *PF* is termed the *paraxial focus.* As θ_3 increases, the reflected ray crosses the line below *PF* as illustrated by the dashed lines shown in Figure 8.14. The spread of the reflected image as θ_3 increases, is termed *spherical aberration*.

For practical applications, if the rim angle of a cylindrical trough is kept low (e.g., <20-30 degrees), spherical aberration is small and a virtual line focus trough is achieved. Figure 8.15 shows the focusing of circular mirrors with various rim angles.

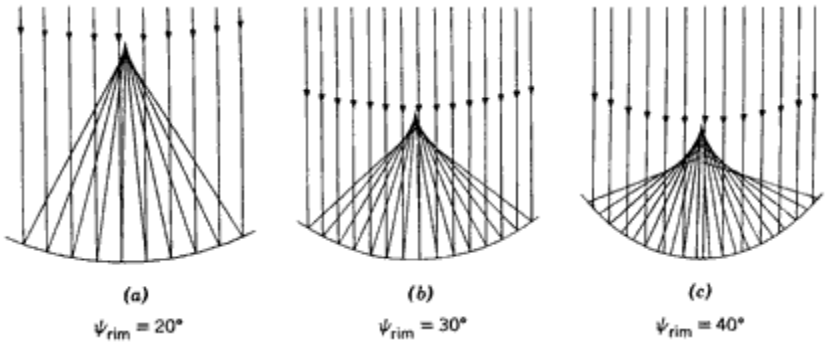

Figure 8.15 Focusing of parallel rays of light using circular mirrors with different rim angles.

8.3.3 Point Focus Dishes

If the two-dimensional curved mirrors shown in Figures 8.9 and 8.10 are rotated rather than translated, the resulting geometric figures are spherical and parabolic dishes, respectively. A parabolic dish must be tracked in two dimensions in order to maintain the incident beam insolation normal to the dish aperture at all times to allow focusing. As with the cylindrical trough, however, the aperture of a spherical dish need not be tracked because of the symmetry of a sphere (circle) as discussed earlier. However, a linear receiver that tracks the moving focal line (see Figure 8.9) must be provided. A prototype parabolic dish concentrator is described in Chapter 9 along with a prototype non-tracking aperture spherical dish.

8.4 Reflection of Energy to the Receiver

Although the design details of any one parabolic collector may differ from those of another parabolic collector, optical constraints define the basic configuration of all parabolic concentrators. This section reviews these constraints and examines the process of supplying concentrated optical energy to the receiver. Heat-loss considerations are addressed in Section 9.2. The basic logic flow followed in this review is summarized in Figure 8.16. The reflection of parallel rays of light, normal to the collector aperture, is reviewed. The goal is to develop an analytical equation that shows the contribution of light reflected to the focus as a function of rim angle.

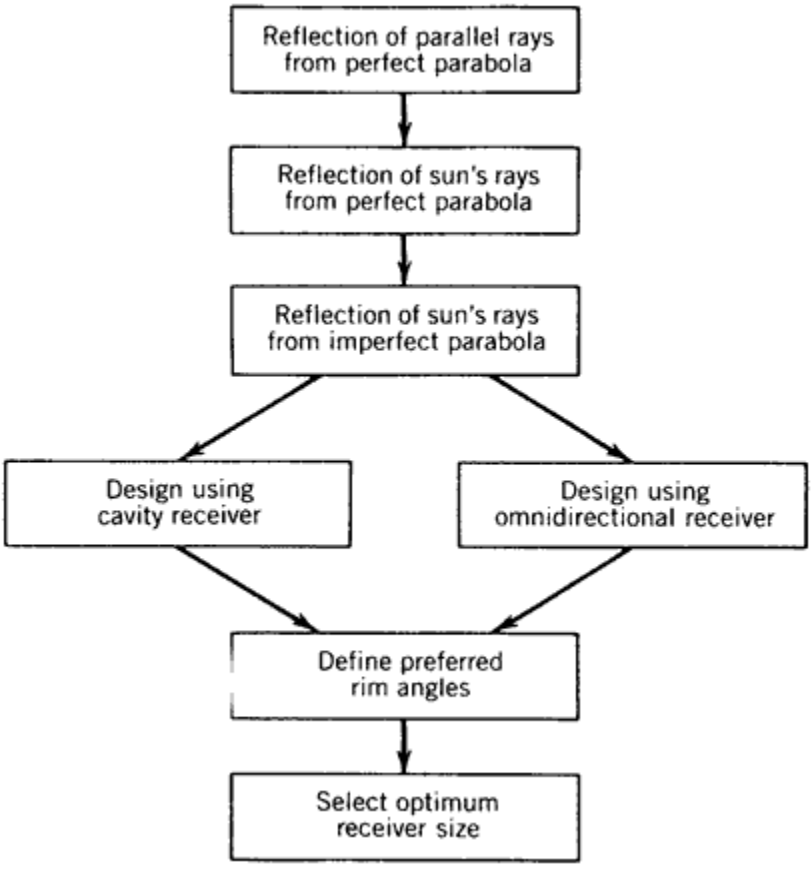

Figure 8.16 Optical analysis of parabolic concentrators.

This analysis is then modified to account for the fact that the sun's rays are not truly parallel. Angular errors (e.g., slope errors) in the conformity of the reflector surface to a true parabolic shape are incorporated at this stage. The spread of the reflected beam due to errors in mirror surface slope, tracking, and nonparallel solar rays provides the information needed to examine the principles used in selecting the size of the receiver.

An examination of the resulting concentration ratios yields information about the approximate rim angle for a parabolic collector. Heat-loss considerations discussed in Section 9.2 will further constrain the design of the receiver.

8.4.1 Reflection of Parallel Rays

Consider the parabolic mirror illustrated in Figure 8.17. A ray of light, with intensity of I_b incident parallel to the axis of the parabola, will be, as shown, reflected to the focus F of the parabola. Since we will want to discuss the total quantity of light reflected by the entire mirror surface, it is convenient to first

consider a differential area dA_s that can, in turn, be integrated over the entire surface of the mirror if desired . The differential surface area dA_s is defined as

$$dA_s = l\, ds \qquad \left(m^2\right) \qquad (8.32)$$

where

ds = differential arc length of the parabola shown in Figure 8.17

l = either length of a differential strip on the surface of a parabolic trough along the direction of the focal line, or circumference of the differential ring on the surface of a parabolic dish.

An expanded view of Figure 8.17*a* shows the angles associated with ds.

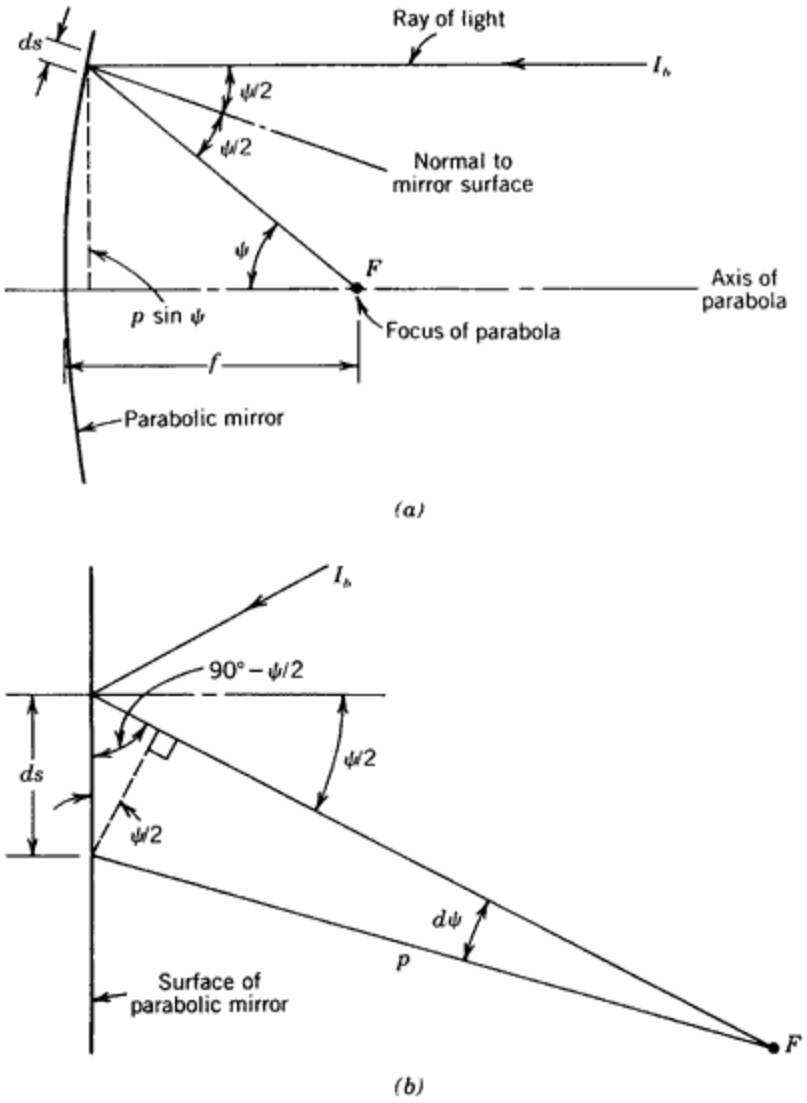

Figure 8.17 Reflection of a light ray from a parabolic mirror.

Application of Figure 8.17*b* yields

$$ds = \frac{p \sin(d\psi)}{\cos(\psi/2)} \qquad (m) \qquad (8.33)$$

Since the angle $(d\psi)$ is small, $\sin(d\psi) = d\psi$, and Equation (8.33) reduces to

$$ds = \frac{p(d\psi)}{\cos(\psi/2)} \qquad (m) \tag{8.34}$$

Thus

$$dA_s = \frac{l\ p\ d\psi}{\cos(\psi/2)} \qquad (m^2) \tag{8.35}$$

The total radiant flux $(d\Phi)$ reflected from this differential area (assuming no reflectance loss) to the point of focus is

$$\begin{aligned} d\Phi &= dA_s\ I_b \cos(\psi/2) \\ &= l\ p\ I_b\ d\psi \qquad (W) \end{aligned} \tag{8.36}$$

Substitution of equation 8.6 for p (see Section 8.2) results in

$$d\Phi = \frac{2fl\ I_b d\psi}{(1+\cos\psi)} \qquad (W) \tag{8.37}$$

Equation (8.37) is the general form of the equation and holds for both parabolic troughs and dishes. However, for a parabolic dish we can substitute for l in Equation (8.37). Introducing the subscripts PT and PD to signify parabolic trough and parabolic dish, respectively, we can rewrite Equation (8.37) as

$$d\Phi_{PT} = \frac{2fII_b d\psi}{(1+\cos\psi)} \qquad (W) \tag{8.38a}$$

and

$$d\Phi_{PD} = \frac{8\pi\ I_b f^2 \sin\psi\ d\psi}{(1+\cos\psi)^2} \qquad (W) \tag{8.38b}$$

where the following substitution was used (see Figure 8.17).

$$l = 2\pi p \sin\psi$$
$$= \frac{4\pi f \sin\psi}{(1+\cos\psi)} \quad (m) \qquad (8.39)$$

8.4.2 Reflection of Nonparallel Rays

The preceding discussion is based on the incident light rays being parallel. This is not true for solar applications. Because of the finite angular size of the sun's disc (about 33 minutes of arc or 9.6 mrad), the sun's rays reaching the concentrator are not parallel. Thus, rather than all the incident rays being reflected to the focal point (or line in the case of a trough), the reflected rays form an "image" of finite size centered about the focus. The geometry involved is illustrated in Figure 8.18, where the angular size of the sun's disc is denoted by (ε).

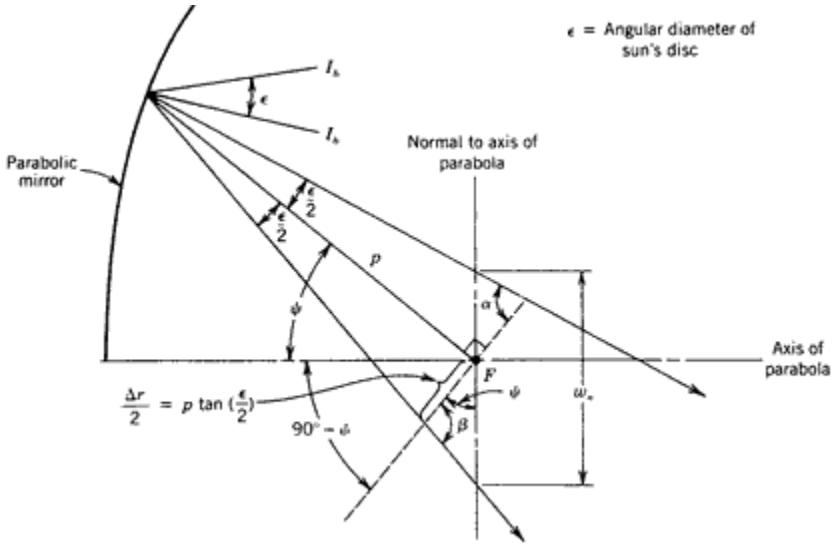

Figure 8.18 Reflection of nonparallel rays from a parabolic mirror.

The width (beam spread) of the reflected sun's image Δr on a plane normal to p and passing through the focus F is, as indicated

$$\Delta r = 2p\tan\left(\frac{\varepsilon}{2}\right) \quad (m) \qquad (8.40)$$

This is the minimum beam spread that will occur. Any errors in, for example, the trueness of the mirror slope will cause additional spreading of the image size.

8.4.3 The Contribution of Errors

In addition to the finite angular size of the sun, independent errors in the conformity of the mirror to a true parabolic shape (i.e., slope errors), non-specular reflection of the incident light beam, tracking errors, and receiver alignment errors all contribute to further apparent spreading of the reflected light beam. Typically, these errors are assumed to be random and are reported in standard deviation units. Their combined effect is statistically determined. Although the sun's intensity is not normally distributed across its disc, it may be approximated as a standard distribution so that it can be treated similarly to the concentrator errors.

Harris and Duff (198l) have evaluated the use of a normal distribution to describe the sun's intensity. They found that the approximation does not introduce significant errors for parabolic troughs and dishes. Table 8.1 shows a typical list of concentrator errors along with the equivalent width of the sun. These errors are for one standard distribution unit (1σ), which means that approximately 68 percent of all measurements of the errors fall within the angular deviations noted.

Table 8.l Typical Parabolic Concentrator Errors

Type and Source	Effective Magnitude (1σ)	σ^2
One-Dimensional (σ_{1D})		
Structure (σ_{slope})	2.5 mrad × 2 = 5 mrad	25
Tracking:		
Sensor (σ_{sensor})	2 mrad	4
Drive Non-uniformity (σ_{drive})	2 mrad	4
Receiver:		

Alignment, etc. (σ_{rec})	2 mrad	4
		$\sum \sigma_{1D}^2$ = 37
		σ_{1D} = 6.1 mrad

Two-Dimensional (σ_{2D})

Mirror specular reflectance (σ_{refl})	0.25 mrad × 2 = 0.50 mrad	0.25
Sun 's width (σ_{sun})	2.8 mrad	7.84
		$\sum \sigma_{2D}^2$ = 8.09
		σ_{2D} = 2.8 mrad

Total Effective Error

$\sigma_{tot} = \sqrt{\sigma_{1D}^2 + \sigma_{2D}^2} = 6.7\,(\text{mrad})$

Note that the 1σ sun width (2.8 mrad) reported in Table 8.1 is smaller than the usually reported sun width of 9.6 mrad. This is a result of forcing a standard distribution on the solar disc. As discussed in the following paragraphs, the usual process during analysis will be to use multiples of one standard distribution.

Note also that Table 8.1 is divided into two main parts: one-dimensional errors, and two-dimensional errors. One-dimensional errors are those errors that contribute to beam spreading in the plane of curvature. They are combined as

$$\sigma_{1D} = \sqrt{\left(2\sigma_{\text{slope}}\right)^2 + \left(\sigma_{\text{sensor}}\right)^2 + \left(\sigma_{\text{drive}}\right)^2 + \left(\sigma_{\text{rec}}\right)^2} \qquad (mrad) \tag{8.41}$$

Note that the slope error is multiplied by 2. This is a result of Snell's law (Equation 8.54) and the fact that with a slope error, the mirror surface direction is changed whereas the receiver position is not (see Figure 8.19).

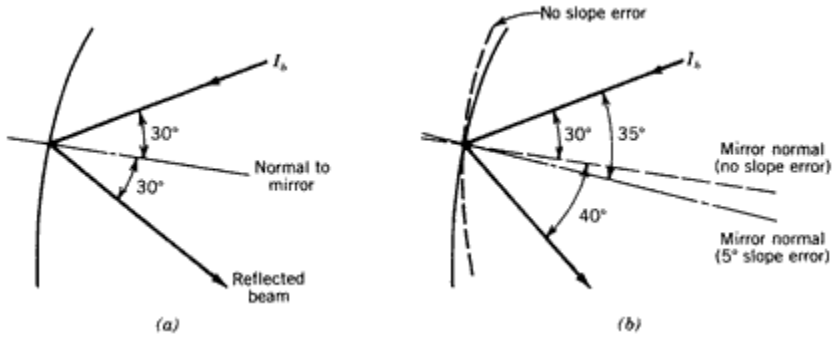

Figure 8.19 Impact of slope error on beam deflection.

Figure 8.19*a* shows the reflection of the beam with no slope error. If, as illustrated in Figure 8.19*b*, there is a slope error of 5 degrees, the reflected beam is misdirected by an amount of 10 degrees from the original reflected path. In the case of a tracking error, for example, the receiver moves together with the mirror surface so that the factor of 2 does not appear for this type of error in Equation (8.41). The factor of 2 appears only when an error is the result of a movement on the mirror surface and not the receiver.

Two-dimensional errors (σ_{2D}) occur in parabolic troughs when an incident ray does not lie within the plane of curvature. The angular width of the sun and non-specular reflectance fall into this category. These errors are combined as

$$\sigma_{2D} = \frac{\left(\sigma_{sun}^2 + \sigma_{refl}^2\right)^{1/2}}{\cos\theta_i} \qquad (mrad) \tag{8.42}$$

where (θ_i) is the solar angle of incidence. The total 1σ error is then

$$\sigma_{tot} = \sqrt{\left(\sigma_{1D}^2 + \sigma_{2D}^2\right)} \qquad (mrad) \tag{8.43}$$

Note that at normal incidence $(\theta_i = 0)$. For a parabolic dish therefore, (θ_i) is always equal to 0. Incorporation of these error considerations into the

above equation for Δr is accomplished by replacing $(\varepsilon/2)$ with some multiple of $(\sigma_{tot}/2)$. Equation (8.40) can then be rewritten as

$$\Delta r = 2p\tan\left(n\frac{\sigma_{tot}}{2}\right) \qquad (m) \qquad (8.44)$$

where n is the number of standard deviations being considered.

One can expect 68 percent of the energy incident on that part of the reflecting surface (defined by p) to fall on line Δr when n is chosen to be equal to 2 (i.e. $\pm 1\sigma_{tot}$). It is common to use ± 2 to ± 3 times σ_{tot} in solar analyses to ensure that 95 percent or more of all possible energy is captured.

Table 8.2. Percent of Measurements of Flux Falling Within Multiples of a Given Standard Deviation (σ)

Multiples of Standard Deviation (σ)	n	Percent Within Limits
±l	2	68.27 %
±2	4	95.45 %
±3	6	99.73 %

8.5 Reflection to a Fixed Point (the Power Tower)

With central receiver systems, the sun 's rays that hit a field of movable mirrors (heliostats) are reflected to a single fixed point in space (the receiver). The tracking angles for the reflector surface, along with the angle of incidence to this surface, may be derived using the vector techniques developed in Chapter 4.

The appropriate geometry can be best described by using zenith, east, and north *(z, e, n)* coordinates with their origin O at the base of the aim point *A* as shown in Figure 8.20. The location of a reflecting surface *B* can be defined as z_1, e_1 and n_1 and the aim point located at a distance z_{00} above the origin.

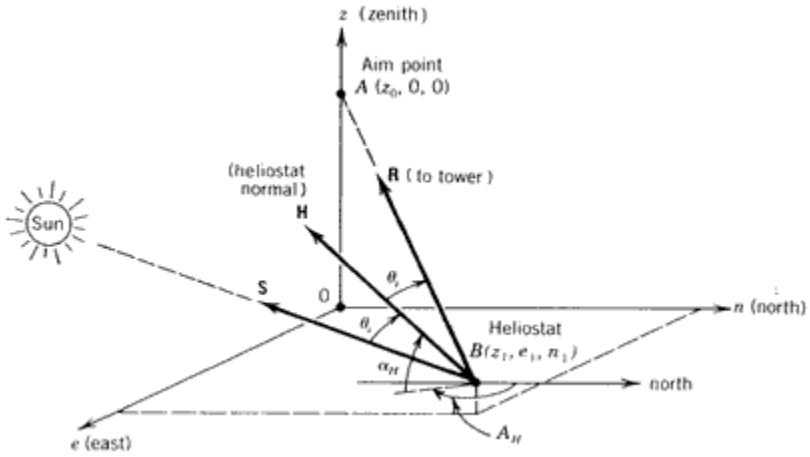

Figure 8.20 Coordinates defining the reflection of the sun's rays by a heliostat to a single aim point. Vector $\mathbf{H}$ is normal to the heliostat reflecting surface

To predict the reflector (heliostat) altitude (α_H) and azimuth (A_H) angles, we must describe three unit vectors. A central sun ray unit vector $(\mathbf{S})$ pointing toward the sun has been described in Equation (3.9). A unit vector pointing from the reflector toward the aim point (A) is defined as

$$\mathbf{R} = \frac{(z_0 - z_1)\mathbf{i} - e_1\mathbf{j} - n_1\mathbf{k}}{\sqrt{(z_0 - z_1)^2 + e_1^2 + n_1^2}} \qquad (8.45)$$

where ***i, j,*** and ***k*** are unit vectors in the z, e, and n directions, respectively. Defining Equation (8.45) in terms of direction cosines, we have

$$\mathbf{R} = R_z\mathbf{i} + R_e\mathbf{j} + R_n\mathbf{k} \qquad (8.46)$$

The third vector of interest is a unit vector normal to the reflector surface. This is defined as

$$\mathbf{H} = H_z\mathbf{i} + H_e\mathbf{j} + H_n\mathbf{k} \qquad (8.47)$$

Table 8.3 summarizes the sign conventions used to develop the angles related to heliostat design.

Table 8.3 Sign Convention for Important Heliostat Angles

Title	Symbol	Zero	Positive Direction	Range	Equation No.	Figure No.
Heliostat Angles						
Angle of Incidence		perpendicular to surface	toward surface	0 to 90°	8.49	8.20
Surface Altitude		horizontal	up	0 to 90°	8.51	8.20
Surface Azimuth	A_H	due north	clockwise	0 to 360°	8.52 or 8.53	8.20

Since the laws of specular reflection require that the angle of incidence (θ_i) is equal to the angle of reflection, an expression for this angle can be written in terms of the central sun ray unit vector (**S**) and the aim point unit vector (**R**) as

$$\cos 2\theta_i = \mathbf{S} \cdot \mathbf{R} \qquad (8.48)$$

Using Equations (3.9) and (8.46), we have

$$\cos 2\theta_i = R_z \sin\alpha + R_e \cos\alpha \sin A + R_n \cos\alpha \cos A \qquad (8.49)$$

from which the angle of incidence or reflection can be obtained, if we know the position of the sun and the position of the aim point relative to the reflection surface.

The reflection surface unit normal (**H**) can be found by adding the incidence and reflection vector and dividing by the appropriate scalar quantity. This gives

$$\mathbf{H} = \frac{\mathbf{R}+\mathbf{S}}{2\cos\theta_i} = \frac{(R_z+S_z)\mathbf{i}+(R_e+S_e)\mathbf{j}+(R_n+S_n)\mathbf{k}}{2\cos\theta_i} \qquad (8.50)$$

Substituting Equation (3.9) and describing the altitude and azimuth of the reflecting surface (α_H) and (A_H) respectively, in terms of the orthogonal coordinates in a manner similar to that shown in Figure 3.6, we have

$$\sin\alpha_H = \frac{R_z + \sin\alpha}{2\cos\theta_i} \qquad (8.51)$$

and

$$\sin A_H = \frac{R_e + \cos\alpha \sin A}{2 \cos\theta_i \cos\alpha_H} \qquad (8.52)$$

The third expression is redundant but is written here for completeness:

$$\cos A_H = \frac{R_n + \cos\alpha \cos A}{2 \cos\theta_i \cos\alpha_H} \qquad (8.53)$$

When the reflector azimuth is found by using the arc sine and arc cosine functions, the problem of quadrant ambiguity must again be recognized. It could be handled analytically by solving both Equations (3.52) and (3 .53) or with simpler logic i.e. it is obvious that the angle of incidence (θ_i) cannot exceed 90 degrees.

EXAMPLE: As an example of the use of these equations, take the case where the aim point A (receiver) is 200 m above a reflector (heliostat) that is located 100 m east and 50 m north of the base of the tower. If the solar altitude angle is 50 degrees with a solar azimuth of 180 degrees, solutions of Equations (3.49), (3.51), and (3.52) give an angle of incidence (θ_i) of 18 degrees, and the reflector's altitude and azimuth are 59.5 and 206.88 degrees, respectively.

8.6 Principles of Reflection and Refraction

The basic processes that take place when light encounters the surface of a transparent material are shown in Figure 8.21. A portion of the incident ray may be reflected from the surface as shown, with an angle equal to the angle (θ_i) the incident light makes with the surface normal. Some of the incident light will pass through the surface and enter the material. In so doing, the direction of the light is changed (i.e., refracted) in accordance with Snell's law:

$$N_1 \sin\theta_i = N_2 \sin\theta_{refr} \quad \text{(Snell's law)} \qquad (8.54)$$

where the symbols are defined as in Figure 8.21.

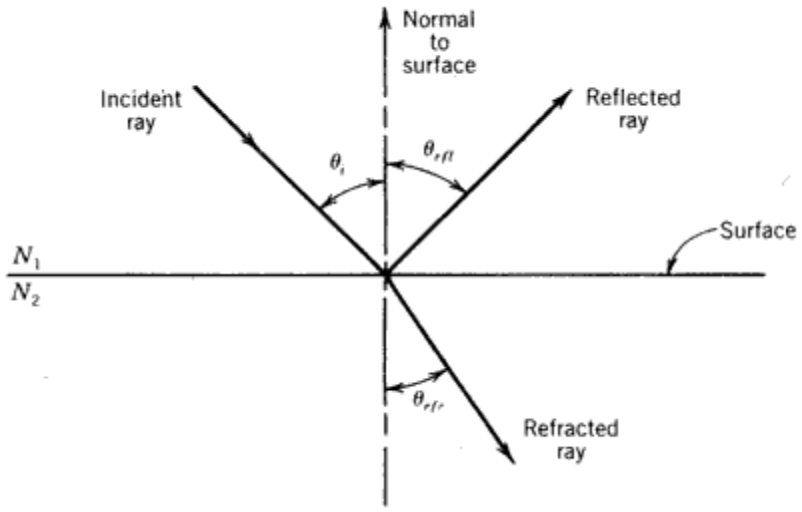

Figure 8.21 Interaction of light with a material. N_1, index of refraction of material 1; N_2, index of refraction material 2.

As the light passes through the material, some of it may be absorbed, thus decreasing the energy content of the refracted light. The ability of material to pass light is reported as transmittance (τ) or transmissivity. The physical properties reflection, refraction, and transmittance define the optical behavior of concentrating solar collectors and are examined in the following sections.

8.6.1 Mirrors

All reflector surfaces follow the basic principle shown in Figure 8.21, specifically, that the angle of incidence (θ_i) equals the angle of reflection (θ_{refl}). Thus, if the direction of the incoming solar radiation is known, a smooth reflector surface can be placed in the path of the incoming beam and the radiation reflected to some predetermined location. If the surface of the mirror is smooth over a large area so that the angle of the reflected light can be determined by the general contour of the surface, the reflection is termed *specular.* If small surface irregularities cause the incident light to be reflected at angles that cannot be determined by the general surface contour, the reflection is termed *non-specular.* Generally, both specular and non-specular reflection occur simultaneously to some extent. In evaluation of the ability of a reflector surface to reflect light, the term "reflectance" is typically used. On the basis of these observations, two definitions of reflectance are employed.

Specular Reflectance (ρ_s) The fraction of incident light that is reflected such that the angle θ_{rfl} of the reflected beam, with respect to the normal to the mirror surface, is equal (within some defined limit) to the angle θ_i that the incoming beam makes with the normal to the mirror surface.

Non-specular Reflectance (ρ_{ns}) The fraction of incident light energy that is reflected from a surface such that the angle (θ_{rfl}) of the reflected beam is not defined by the angle (θ_i) that the incoming beam makes with the normal to the average surface contour.

Specular reflectance is normally reported for specific acceptance angles (θ_{accept}) through which the measuring instrument will allow light to pass. Figure 8.22 illustrates the measurement of specular reflectance. Analytically, this relationship can be written as

$$\rho_s = \frac{I_{r,a}}{I_b} \qquad (8.55)$$

where $I_{r,a}$ is the reflected irradiance falling within the acceptance angle (θ_{accept}) and I_b is the irradiance of the incident beam.

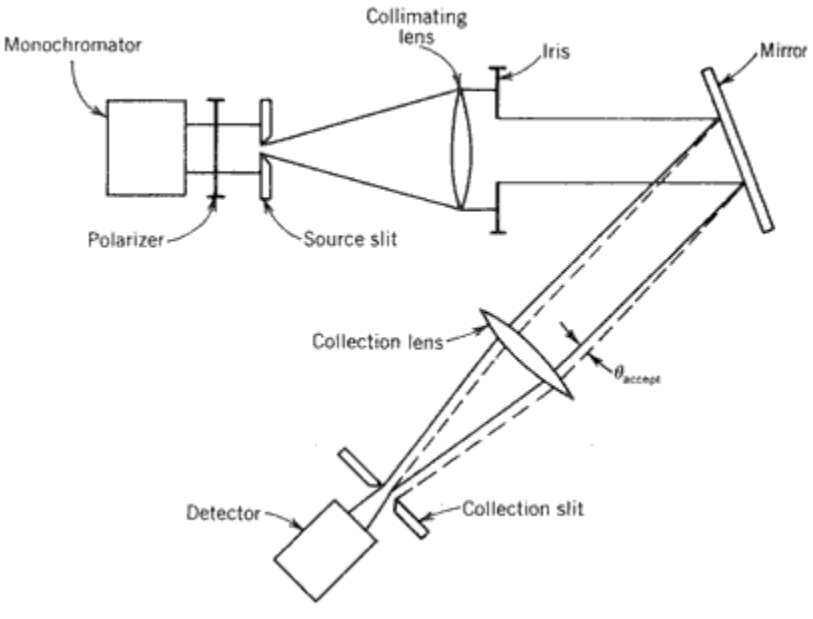

Figure 8.22 Measurement of specular reflectance

Non-specular reflectance is measured by use of a device that integrates the amount of light reflected by the surface in all directions.

An example of a specular reflector is a highly polished silver mirror that gives a clear undistorted reflected image. An example of a diffuse non-specular reflector is snow that yields no reflected image. The properties of curved mirrors to concentrate solar energy through specular reflection are examined in the following paragraphs.

It is important to recognize that, for a solar concentrator, specular reflection of the entire terrestrial solar spectrum is important. Not all materials exhibiting high specular reflectance reflect equally well at all wavelengths. The terrestrial solar spectrum is reported in Figure 2.10. Figure 8.23 shows the specular reflectance of several materials as a function of wavelength and illustrates why silver is widely used as a reflector material for solar collectors. Gold, for example, has a very high reflectance in the IR spectrum, which leads to its use as a radiation barrier in thermal insulation applications. However, it absorbs in the blue part of the visible spectrum (hence its color), decreasing its effectiveness as a solar reflector. The specular reflectance of several materials integrated over the entire solar spectrum are given in the Appendix.

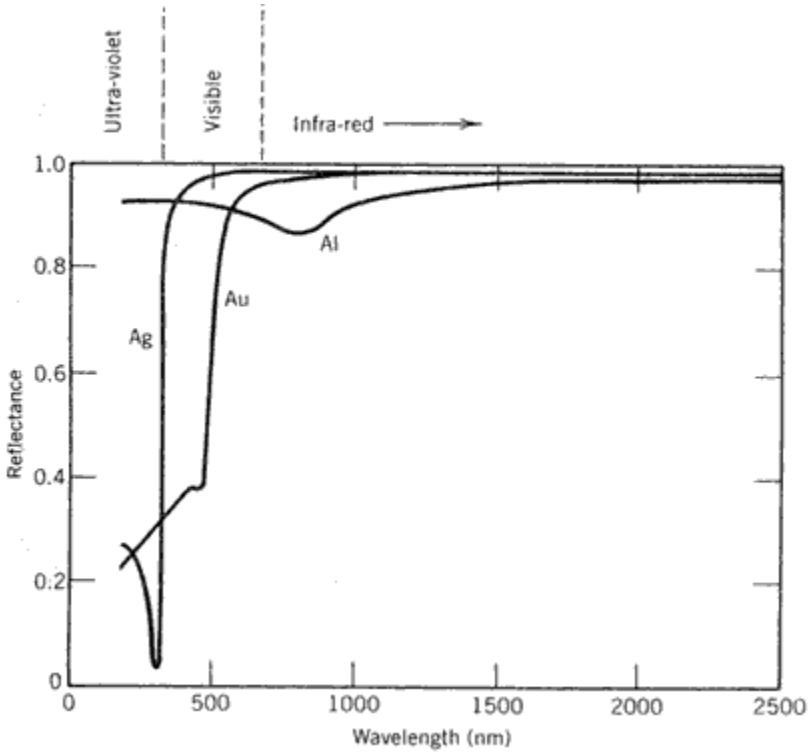

Figure 8.23 Specular reflectance of selected materials. Ag, silver; Al, aluminum; Au, gold

Mirrors used in solar concentrators are frequently back-surface or second surface mirrors (i.e., the reflector surface is behind a protective sheet of glass or

plastic). When light passes through a material, part of the light energy is absorbed. The absorption of light by transparent materials is an important factor in the design of the mirrors used in solar concentrators. Figure 8.24 is an example of a back-surface reflector. Since the light beam must traverse the thickness of the protective layer twice (once on incidence and again on reflection), any material that absorbs light can significantly reduce the solar energy reaching the receiver. The ability of a material to transmit light is characterized by its transmittance.

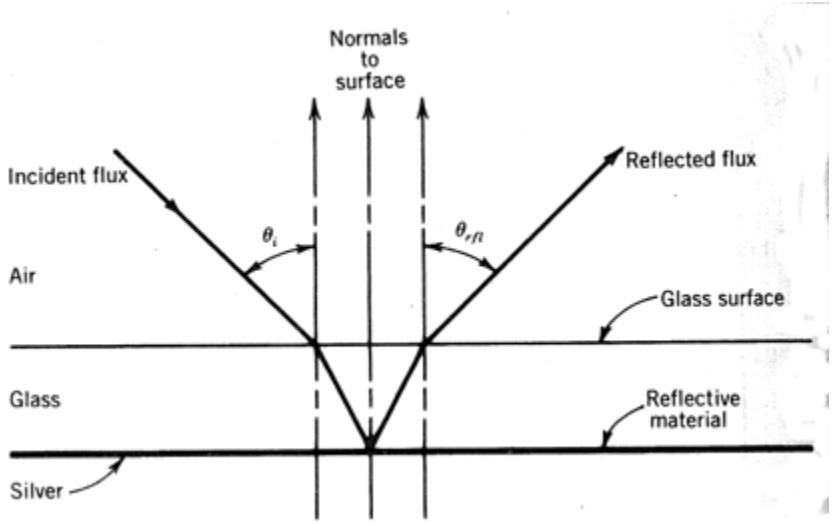

Figure 8.24 A back-surface reflector

Transmittance (τ). The ratio of the radiant flux transmitted (I_{tr}) by a material to the total incident radiant flux (I) is defined as its transmittance. Mathematically, this is expressed as

$$\tau = \frac{I_{tr}}{I} \qquad (8.56)$$

As in the case of reflectance, transmittance can be either specular or diffuse. Light transmission through a homogeneous material such as glass or clear plastic is typically specular in that the transmitted ray follows Snell's law (Equation (8.54). A translucent material such as fiberglass may have high transmittance but localized discontinuities (e.g. glass fibers) that scatter the light, giving rise to a diffuse non-specular transmittance. Since solar concentrators typically employ only materials having high specular transmittance, the term "transmittance" in this book refers only to specular transmittance unless specified otherwise.

The ability of a material to transmit light is frequently a function of the wavelength of the light. Figure 8.25 shows the reflectance of back-surface glass mirrors with

varying amounts of iron present as Fe^{2+}. Since Fe^{2+} absorbs light in the visible part of the spectrum, the transmittance of glass (reflectance of a mirror) for the solar spectrum decreases with increasing concentrations of Fe^{2+}. Thus, low-iron (i.e., 0.06 percent Fe^{2+} or less) glass and glass manufactured in a manner to convert Fe^{2+} to Fe^{3+}, which does not absorb strongly in the solar spectrum, is of growing interest. In addition, thin mirrors are of interest since reduction of the path length that the light must traverse through the glass will reduce losses that are due to light absorption by the glass.

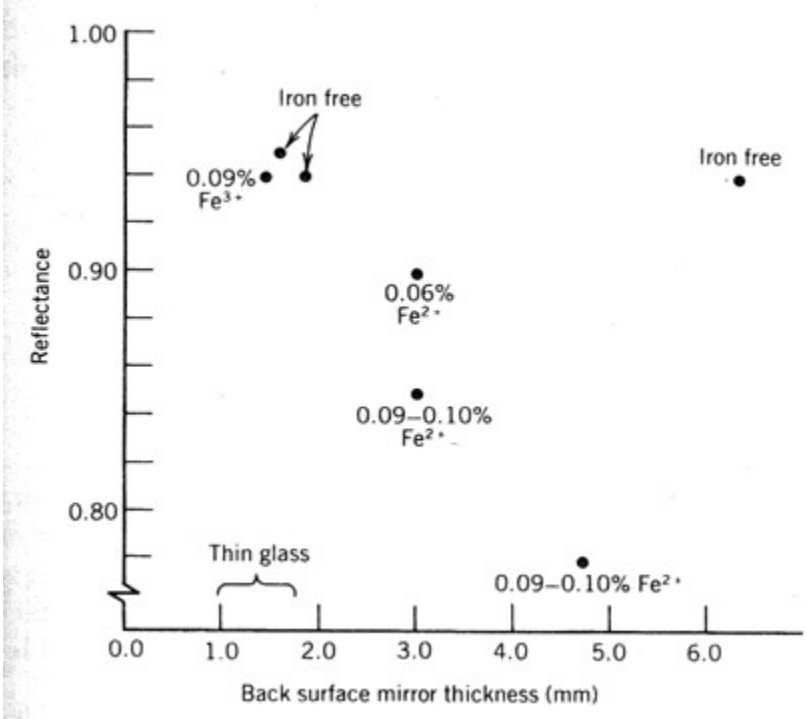

Figure 8.25 Effect of iron concentration on glass mirror reflectance (Clark, 1981).

8.6.2 Lenses

Lenses operate on the principle of Snell's Law. In particular, materials such as glass and clear plastics are used to refract the incident light, transmit the light specularly through the lens medium, and then refract the light again as it leaves the lens. Properly oriented, a curved lens is capable of refracting the parallel rays of the sun and concentrating the image on a receiver as shown in Figure 8.26. The optics of Fresnel lenses are discussed further in Section 8.7.

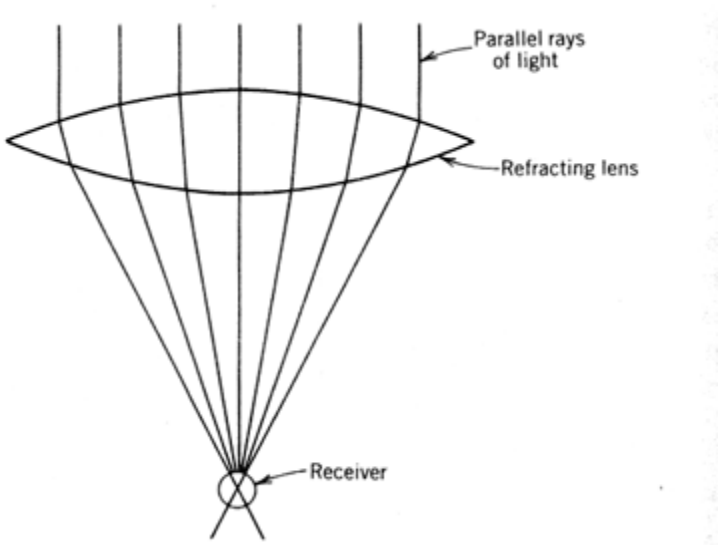

Figure 8.26 A concentrating lens.

8.6.3 Total Internal Reflection

An interesting consequence of Snell's law is the occurrence of total internal reflection. Total internal reflection can occur when light passes from a medium of high index of refraction to a medium of low index of refraction. Consider, for example, the passage of light from glass to air as shown in Figure 8.27. Total internal reflection occurs, as shown, when θ_{rfr} equals 90 degrees. Therefore, the incidence angle θ_i at which total internal reflection will occur can be calculated using Equation (8.54).

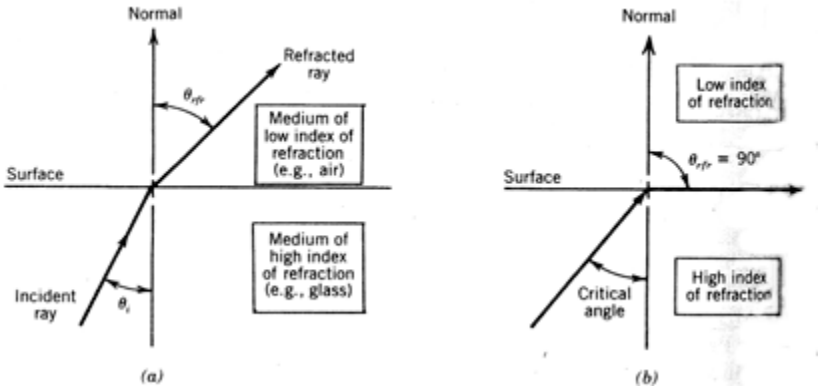

Figure 8.27 Total internal reflection: (*a*) refraction; (*b*) total internal reflection.

Example: Calculate the angle at which total reflection of light passing from glass to air occurs.

$$(N_{\text{glass}})(\sin\theta_i) = (N_{\text{air}})(\sin\theta_{rfr})$$

$$N_{\text{glass}} = 1.5, \quad N_{\text{air}} = 1.0, \quad \theta_{\text{rfr}} = 90°$$

$$\therefore \sin\theta_i = \frac{1}{1.5} = 0.67$$

$$\theta_i = 42°$$

Thus, for incidence angles equal to or greater than 42 degrees, light passing from glass, with an index of refraction of 1.5, to air, with an index of refraction of 1.0, will undergo total internal reflection. This is termed the *critical angle* of the glass-air interface. Note that there is no critical angle for light passing from a medium of low index of refraction to a medium of high index of refraction.

8.6.4 Dielectric Reflection and Antireflection Coatings

In the discussion of reflection given above, there was no discussion of reflection from, for example, an air-glass interface. Reflection does occur, of course, as we all have observed when looking at a glass window. This is called the *dielectric reflection.* Referring to Figure 8.28, the fraction of the incident beam that is reflected at the interface is given by (Smith , 1966)

$$\frac{I_{\text{rfl}}}{I_b} = \frac{1}{2}\left\{\left[\frac{\tan^2(\theta_i - \theta_{\text{rfr}})}{\tan^2(\theta_i + \theta_{\text{rfr}})}\right] + \left[\frac{\sin^2(\theta_i - \theta_{\text{rfr}})}{\sin^2(\theta_i + \theta_{\text{rfr}})}\right]\right\} \qquad (8.57)$$

where the angles (θ_i) and (θ_{rfr}) are as defined in Figure 8.28.

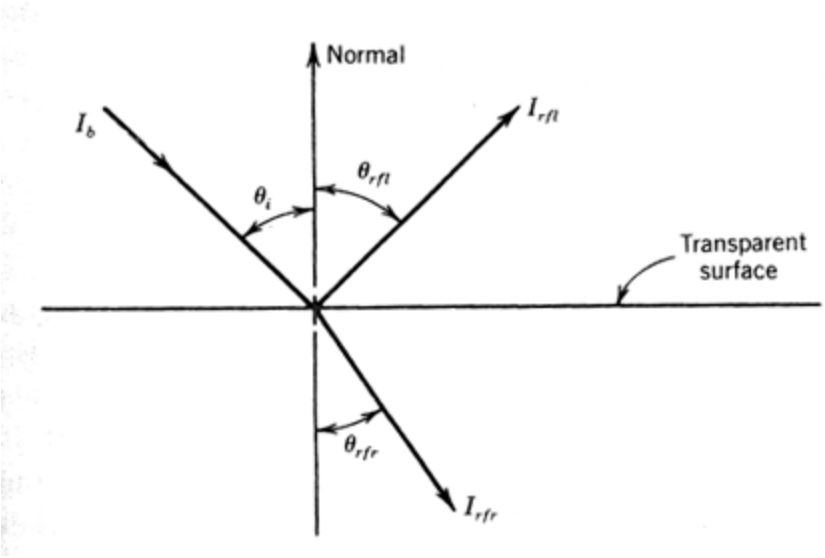

Figure 8.28 Dielectric reflection - definition of angles.

The first term in Equation (8.57) gives the fraction of the incident beam polarized in the plane of incidence, and the second term gives the fraction polarized in the plane normal to the plane of incidence. Figure 8.29 is a plot of the reflection from a single air-glass interface as a function of incidence angle. Note that at (θ_i) equal to about 57 degrees, the component of the surface reflection polarized normal to the plane of incidence goes to zero. This is called the *polarizing angle* since the reflected light is plane polarized in one direction only. At normal incidence Equation (8.57) reduces to (Smith, 1966)

$$\frac{I_{\mathrm{rfl}}}{I_b} = \frac{\left(N_1 - N_2\right)^2}{\left(N_1 + N_2\right)^2} \qquad (8.58)$$

where N_1 and N_2 are the refractive indices of the two media.

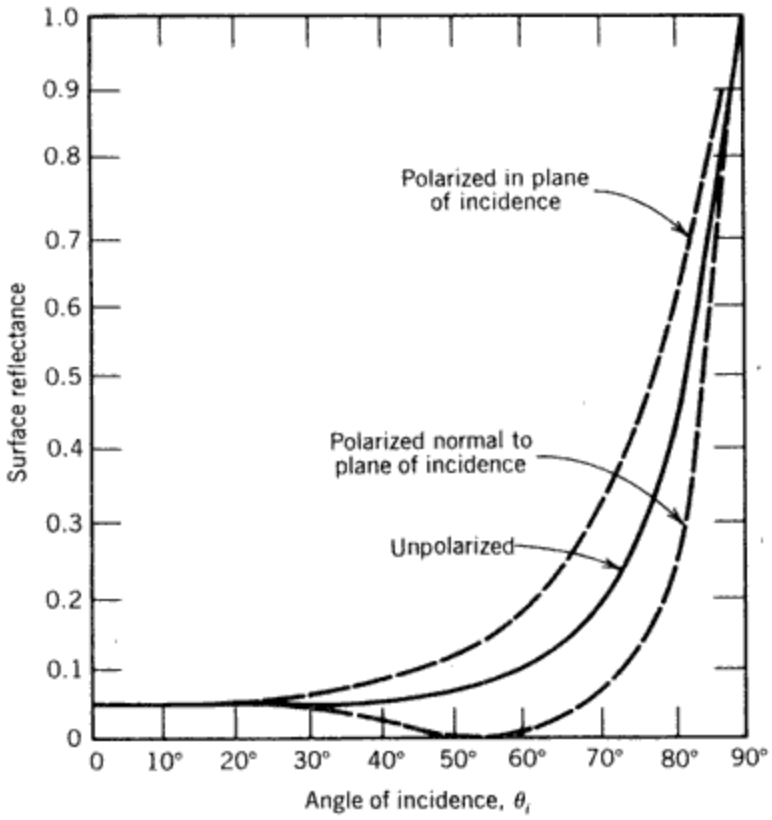

Figure 8.29 Effect of incidence angle on dielectric reflection from air-glass interface (Smith, 1966).

Optical coatings, so-called *antireflection coatings,* have been developed to reduce reflection from the air-glass interface in order to improve optical transmission. Such optical coatings have been used on the glass envelopes surrounding the receiver tubes of solar thermal concentrators.

One method of preparing antireflection glass surfaces is by etching the surface (Elmer and Martin, 1979). Antireflection surfaces on alkali-borosilicate glasses can be produced by exposing the glass surface to dilute acid solutions containing low concentrations of etchants, such as ammonium fluoride or ammonium bifluoride.

These solutions selectively extract soluble oxides within the surface layer, leaving a hydrated porous layer, largely silica, at the surface of the glass. The resulting surface layers are unique in that they maintain low reflectance losses in both the visible and the near-infrared. The reduction in dielectric reflectivity is attributable to a variable refractive index gradient caused by the interconnected pores of the silica-rich surface layer. The process is applicable to glasses that exhibit selective solubility in hot acid solutions. Etching has been used to produce an antireflection surface on the glass envelope surrounding the receiver in parabolic

troughs (Anonymous, 1981). Figure 8.30 shows the transmittance of borosilicate glass treated in this manner.

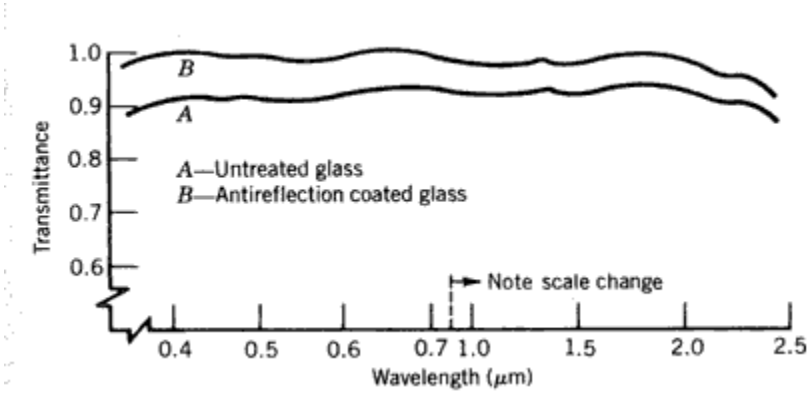

Figure 8.30 Transmittance of glass with antireflection coating (Elmer and Martin, 1979).

8.7 Fresnel Lens Optics

Fresnel (pronounced $Fr\bar{a}'nel'$ $Fr\bar{a}'nel' Fr\bar{a}'nel'$) lenses have been widely used in solar collectors that concentrate light by refraction. Since it is a flat approximation of a curved lens, a Fresnel lens has less material and weighs less than a corresponding curved lens. This results in lower cost and less optical transmission loss through the lens. An idealized Fresnel lens that focuses parallel rays of light to a point is illustrated in Figure 8.31. The Fresnel lens employs canted facets to approximate the curvature of a lens; the more facets, the better the approximation. Typically, a high-quality linear Fresnel lens will have more than 1000 facets per centimeter.

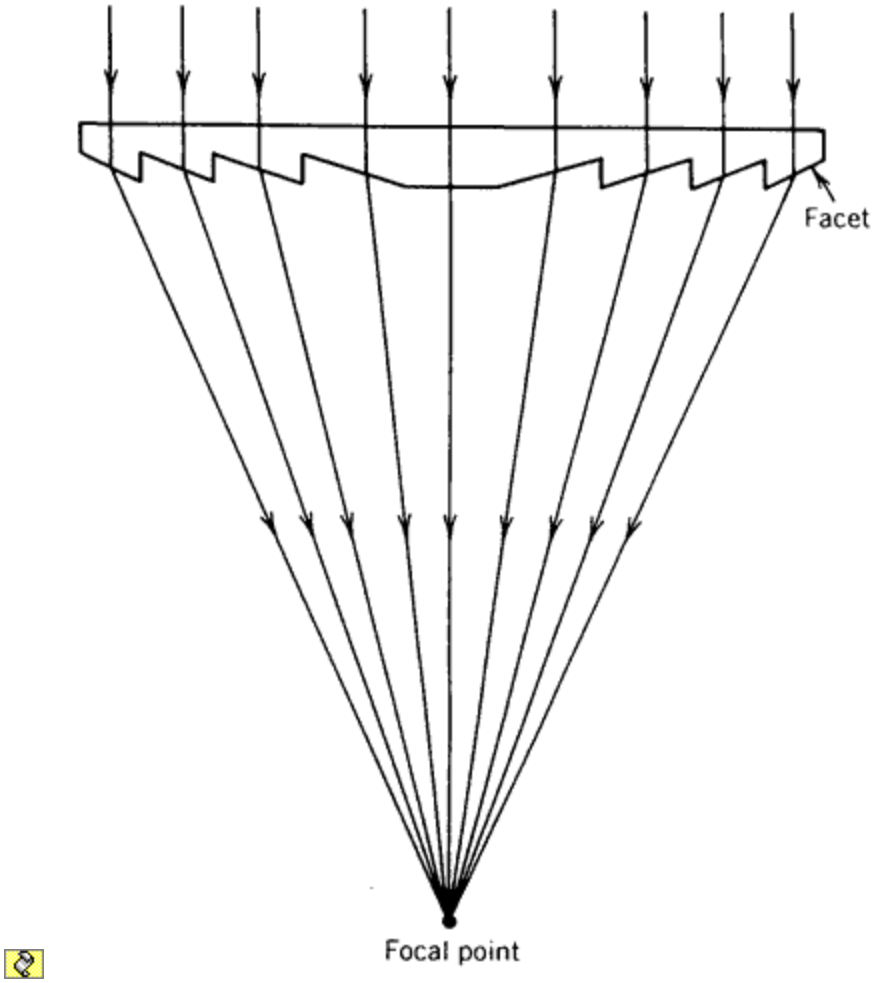

Figure 8.31 Idealized Fresnel lens.

Several factors limit the effectiveness of Fresnel lenses. The most serious is, perhaps, the sharpness of the facets that can be produced. Any manufacturing process will produce slightly rounded facets as shown in Figure 8.32. Any ray striking the back side of a facet (e.g., ray 1) or the tip or valley of a facet (e.g., rays 2 and 3, respectively), is not properly directed to the receiver. The total fraction of the aperture area represented by these features is ineffective and reduces the ability of a Fresnel lens collector to perform efficiently.

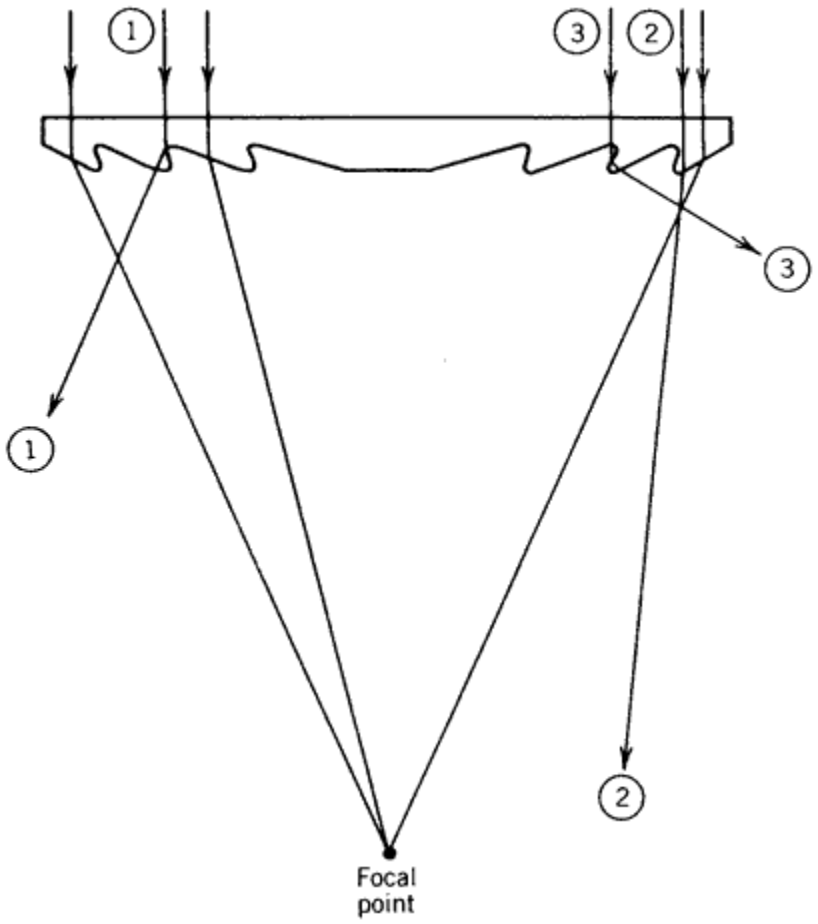

Figure 8.32 Problems associated with Fresnel lenses

Another feature that limits the performance of a Fresnel lens (or any other lens, for that matter) is dielectric and internal reflection (see Section 8.6). As the angle of incidence of light on a facet increases, the quantity of light reflected due to dielectric reflection increases. Figure 8.29 shows the reflection of light from an air-glass interface. Note that as the angle of incidence approaches 42 degrees, total internal reflection occurs for a glass lens. Thus the edge facets of a Fresnel lens are less effective than facets closer to the center of the lens. The effect is similar for plastic lenses since they have indices of refraction similar to glass (see Appendix D).

A more serious factor limiting the use of refractive optics is the need to track the lens about two axes. This is necessary to keep the concentrated image focused on a receiver that is fixed with respect to the lens. This is true even in the case of a linear lens. Figure 8.33*a* shows that as the incident rays are inclined (e.g., Ray l), in the plane of curvature, the refracted rays move. Thus, as would be expected, a minimum of single-axis tracking is required with a linear Fresnel collector.

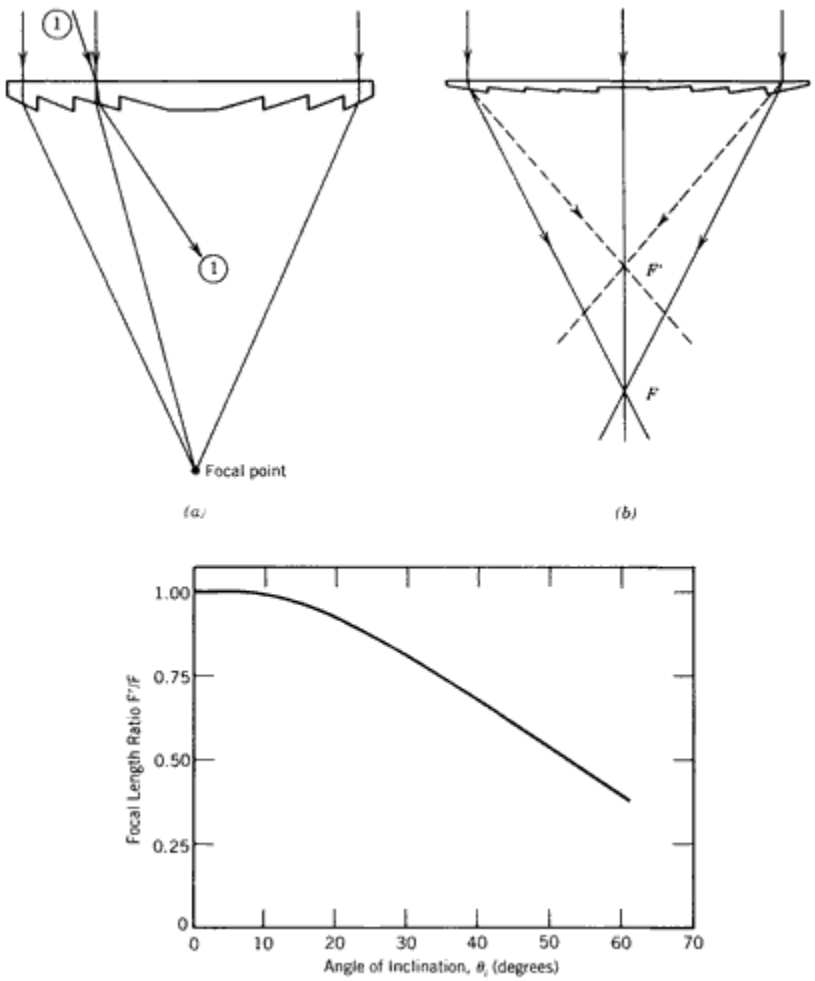

Figure 8.33 Two-axis tracking requirements for Fresnel lenses. (*a*) Effect on refracted beam inclined to lens aperture in the plane of curvature; (*b*) effect on refracted beam inclined along linear axis of lens. Solid line is in plane of paper (focus F). Dashed line is out of plane of paper (focus F'); (*c*) change in focal length of linear Fresnel lens when incident rays inclined at an angle along the linear axis of the lens. Reprinted with permission from Solar Energy Technology Handbook, Marcel Dekker, New York (1980).

However, a somewhat more subtle effect also due to refraction, occurs if the incident ray is inclined along the linear axis of the Fresnel lens. This is illustrated in Figure 8.33*b* and 8.33*c*. The net result, over the entire lens, is the creation of a new focal line for the lens that is above the normal focal line. To maintain the refracted image focused on a receiver that is fixed with respect to the lens, therefore, one must track a Fresnel lens collector (or any lens system) to maintain the incident light normal to the lens aperture. This requires two-axis tracking.

8.8 Conclusions

In summary, the impact of the geometric optics of cylindrical and parabolic mirrors is that parabolic optics allow construction of high rim-angle troughs that need track about only one axis, whereas low rim-angle cylindrical troughs may be constructed that need not track at all to maintain a moving linear focus. These discussions of tracking requirements involve only focusing considerations. Complete two-axis tracking of the collector aperture will, of course, increase the amount of insolation incident on the collector aperture by elimination of the cosine effect. The magnitude of this effect for the various tracking modes is discussed in Chapter 4.

References

Abramowitz and Stegun (1970), *Handbook of Mathematical Functions,* National Bureau of Standards, Washington D.C.

Anonymous (1981), "Solar Thermal Monthly Progress Report," Sandia National Laboratories, Albuquerque.

Bergeron, K. D., and J. M. Freese (1981), "Cleaning Strategies for Parabolic Trough Collector Fields; Guidelines for Decisions," SAND81-0385, Sandia National Laboratories Albuquerque.

Clark, N.H. (1981), "Material Design Considerations for Silvered Glass Mirrors," in Proceedings of the *Line-Focus Solar Thermal Energy Technology Development-A Seminar .for Industry,* p. 409, SAND80-1666, Sandia National Laboratories, Albuquerque.

Elmer, F. H., and F. W. Martin (1979), "Antireflection Films on Alkali-Borosilicate Glasses Produced by Chemical Treatments," *Am. Ceramic Society Bulletin* **58,** 1092.

Kutscher, C. T., and R. Davenport (1981), "Preliminary Results of the Operational Industrial Process Heat Field Tests," SERI/TR-632-385R, Solar Energy Research Institute, Golden, CO, June.

Harris, J. A. and W. S. Duff (1981), "Focal Plane Flux Distribution produced by Solar Concentrating Reflectors" *Solar Energy* **27** (5), 403.

Larsen, L. M., and J. M. Freese (198l), "Solar Collector Cleaning Study," in Proceedings of The Line-Focus Solar Thermal Energy Technology Development - A Seminar for Industry, p. 189, SAND80-1966, Sandia National Laboratories, Albuquerque.

Pettit, R. B., and E. P. Roth (1980), "Solar Mirror Materials: Their Properties and Uses in Solar Concentrating Collectors," in Solar Materials Science, L. E. Murr, ed., p. 171, Academic Press, New York.

Smith, W. J. (1966), Modern Optical Engineering, McGraw-Hill, New York.

Torkelson, L., and D. L. Larsen (1981), "1980 Annual Report of the Coolidge Solar Irrigation Project," SAND80-2378, Sandia National Laboratories, Albuquerque.